The variational multiscale method for mixed finite element formulations

A THESIS
SUBMITTED TO THE FACULTY OF THE GRADUATE SCHOOL
OF THE UNIVERSITY OF MINNESOTA
BY

Klaas Franciscus Stein Stoter

IN PARTIAL FULFILLMENT OF THE REQUIREMENTS
FOR THE DEGREE OF MASTER OF SCIENCE

Prof. Bernardo Cockburn

April, 2018

Abstract

In this thesis, the variational multiscale method is explored in the context of mixed formulations of partial differential equations. The domain decomposition variational multiscale method that has recently been introduced by the author is used as a basis. The function spaces of both the primary and the auxiliary variable are decomposed in a coarse-scale and a fine-scale space. The mixed weak formulations are then derived on a per-element basis. The same scale decomposition is used to rewrite the transmission conditions, which are then incorporated into the weak formulations to couple the elements. The result is a mixed finite element formulation that includes all the fine-scale terms that capture the exact scale interaction, irrespective of the order of continuity of the coarse-scale and fine-scale function spaces.

A closure model has to be substituted in place of the fine-scale terms. This closure model dictates the nature of the scale decomposition by imposing a constraint on the fine-scale solution. It is shown that, in the context of Poisson's equation, numerous existing discontinuous Galerkin formulations may be interpreted as particular choices of closure models. Due to the mixed origin of the formulation, a broad range of formulations may be retrieved. Also the Raviart-Thomas method, the Brezzi-Douglas-Marini method and hybridized formulations are investigated from this perspective. The associated fine-scale constraints are examined in depth. Similarly, an advection-diffusion problem is considered, and the fine-scale constraint associated with upwind finite element formulations are investigated.

Finally, the residual-based modeling of the fine-scale solution is explored in the context of mixed formulations. Incorporation of the model for the one-dimensional advection-diffusion problem leads to a significant accuracy improvement. In particular does it mitigate the overshoot and the oscillation problems that are observed at boundary layers which occur for advection dominated problems.

Table of contents

List of tables

List of figures

Glossary

Abbreviations

Acronym	Full form
BDM	Brezzi-Douglas-Marini
DDVMS	Domain decomposition variational multiscale
DG	Discontinuous Galerkin
GLS	Galerkin least-squares
IP	Symmetric interior penalty
NIPG	Nonsymmetric interior penalty Galerkin
NURBS	Non-uniform rational B-spline
PDE	Partial differential equation
PSPG	Pressure-stabilized Petrov-Galerkin
RT	Raviart-Thomas
RVMS	Residual-based variational multiscale
SUPG	Streamline-upwind Petrov-Galerkin
VMS	Variational multiscale

Subscripts and markings

Symbol	Description	Example
$\{\cdot\}_D$	Dirichlet boundary or data.	$\partial\Omega_D$, u_D
$\{\cdot\}_N$	Neumann boundary or data.	$\partial\Omega_N$, σ_N
$\{\cdot\}_h$	Mesh dependent function or variable.	u_h, V_h
$\{\bar{\cdot}\}$	Coarse-scale component.	$\bar{u}$, $\overline{U}$
$\{\cdot\}'$	Fine-scale component.	u', U'
$\{\hat{\cdot}\}$	Hybrid variable or numerical flux.	$\hat{u}$, $\widehat{u\,n}$
$\{\!\{\cdot\}\!\}$	Average operator.	Table 2.1
$[\![\cdot]\!]$	Jump operator.	Table 2.1

Latin symbols

Symbol	Description	Reference
$\mathcal{A}'$	Component of generalized fine-scale constraint equation.	Eq. (4.15)
$\mathcal{B}'$	Component of generalized fine-scale constraint equation.	Eq. (4.15)
$\mathcal{C}^n$	Continuity of order n.	-
$\mathbb{D}$	Dirac-layer operator.	Eq. (2.15)
$\mathcal{D}'$	Component of generalized fine-scale constraint equation.	Eq. (4.15)
D	Permeability tensor.	Eq. (3.1)
F	Element facet.	Eq. (5.18)
$\mathbb{H}$	Green's function boundary operator.	Eq. (5.8)
$\mathcal{H}'$	Component of generalized fine-scale constraint equation.	Eq. (4.16)
K	Unbounded element domain.	Eq. (2.17)
∂K	Element boundary.	Eq. (2.17)
$\mathcal{L}$	Differential operator.	Eq. (2.16)
$\mathcal{L}^*$	Adjoint differential operator.	Eq. (2.6)
$\mathcal{N}'$	Component of generalized fine-scale constraint equation.	Eq. (4.15)
$\mathcal{P}$	Projector onto coarse-scale space.	Eq. (2.22)
P	Piezometric head.	Eq. (3.1)
$\mathcal{R}$	Residual.	Eq. (2.8)
$\mathcal{T}$	Partitioning of domain into elements.	Eq. (2.17)
a	Advective velocity vector field.	Eq. (3.41)
d	(Spatial) dimension of the domain.	Eq. (2.16)
e	Facet or edge of the computational mesh.	Eq. (3.50)
f	Forcing/source function.	Eq. (2.16)
$g(x, y)$	Green's function.	Eq. (2.8)
h	Measure of element size.	Table 4.1
n	Normal vector.	Eq. (2.17)
p	Polynomial order of primal variable basis functions.	Eq. (3.22)
q	Polynomial order of auxiliary variable basis functions.	Eq. (3.23)
s	Required order of the Sobolev space.	Eq. (2.18)
t	Stabilization parameter in the Hybridizable DG scheme.	Eq. (4.55)
u	Primal solution variable. Exact solution.	Eq. (2.3)

Greek symbols

Symbol	Description	Reference
Γ	Set of element boundaries.	Table 2.1
Ω	Domain of definition of the PDE.	Eq. (2.16)
Ω_K	Set of unbound element interiors.	Table 2.1
$\partial\Omega$	Boundary of Ω.	Eq. (2.16)
$\partial\Omega_\mathrm{l}$	Left boundary of Ω for a one-dimensional domain.	Eq. (4.17)
$\partial\Omega_\mathrm{r}$	Right boundary of Ω for a one-dimensional domain.	Eq. (4.17)
β	Penalty parameter of Local DG method.	Table 4.1
η	Penalty parameter of the IP, Local DG or NIPG method.	Table 4.1
γ	Element averaged surface Green's function.	Eq. (5.20)
ν	Diffusion parameter.	Eq. (3.41)
φ	Flow field in porous medium.	Eq. (3.2)
σ	Auxiliary variable.	Eq. (3.17)
τ	Element averaged volumetric Green's function.	Eq. (5.19)

Chapter 1

Introduction

The variational multiscale (VMS) method was developed in the 1990s by Hughes and coworkers as a generalized tool for developing stabilized methods [1–3]. It was hypothesized that the unresolved fine-scale nature of the solution of the partial differential equation (PDE) is of key importance for the stability of finite element schemes. The VMS methodology offers a means to track the effect of the fine-scale solution onto the resolved finite element solution. Once the occurrences of the fine-scale effects are determined, they can be incorporated in the finite element formulation via fine-scale models.

One particular class of fine-scale models is the residual-based model [4]. Via inversion of the associated fine-scale problem, the fine-scale solution can be approximated as the residual of the coarse-scale finite element solution, multiplied by some factor. This factor depends on the problem at hand via the corresponding Green's function. Researchers have shown that the resulting stabilized formulation is closely related (and often equivalent) to stabilized methods, such as streamline-upwind Petrov-Galerkin (SUPG) [5], Galerkin least-squares (GLS) [6], and pressure-stabilized Petrov-Galerkin (PSPG) [7]. Nowadays, the residual-based modeling of the fine scales is used for more than developing stabilized methods. For instance, in the case of the Navier-Stokes equation it has proven to be an effective turbulence model that is currently widely used in finite element computational fluid mechanics applications [4, 8, 9].

The derivation proposed for the original VMS framework hinges on sufficient continuity of the finite element basis. Ad hoc solutions were proposed to make the theory applicable for typical $\mathcal{C}^0$ finite element basis functions, e.g. by assuming vanishing fine-scales on

element boundaries [1–4] or by treating the lack of continuity by incorporating inter-element Dirac-layers [10]. Recently, the author has proposed a modified framework to make the VMS theory applicable also when discontinuous basis functions are used [11–13]. This was achieved by writing the original PDE in a domain decomposition format. The approach is referred to as the domain decomposition variational multiscale (DDVMS) method. At the time, the focus of study was to develop suitable residual-based models to incorporate subgrid scale effects in discontinuous Galerkin (DG) formulations [12]. It was discovered that the proposed framework may actually serve as the basis for a reclassification of discontinuous Galerkin formulations. Specifically, it was shown that discontinuous Galerkin formulations are retrieved via the proposed DDVMS formulation when certain constraints are enforced on the fine-scale solution [13]. This perspective opens new avenues for interpretation of the behavior of these finite element schemes. In that earlier work, the DDVMS method was studied for primal formulations of the PDE. This meant that only a few discontinuous Galerkin formulations could be retrieved. These are the symmetric interior penalty method, the Bassi-Rebay method and the Local DG method. The latter two still require lifting operators to be interpreted in a primal form.

Usually, discontinuous Galerkin formulations originate from a mixed formulation of the PDE instead. Finite element methods based on mixed formulations (or "reduced order forms") of the PDE were first proposed in the 60s [14–16]. This requires the introduction of an auxiliary variable, such as the heat flux or the stress/strain. The original PDE is then rewritten as a system of lower order PDEs, involving the primal and auxiliary variables. An advantage of this approach is that the auxiliary variable, which is often the quantity of interest, can directly be obtained from the finite element computation. Also, splitting the PDE into a system of PDEs may capture the associated physical laws better, such as conservation laws. Finally, since the order of the PDE is reduced, basis functions that used to be unsuitable due to their lacking order of continuity can now once again be used. This is likely part of the reason for the use of mixed PDEs as a starting point for developing discontinuous Galerkin formulations. Hence, when the DDVMS framework was introduced, it was already recognized that choosing a mixed formulation of the PDE as the origin of the method was a natural pathway for further research, which is now presented in this work.

Earlier attempts at applying the VMS principles to mixed formulations have been made. In the early 2000s, the 'mixed multiscale finite element' method was developed in separate papers by Arbogast et al. [17, 18] and Aarnes et al. [19, 20]. In both works, suitable pairs of $H(\mathrm{div}, \Omega)$ and $L^2(\Omega)$ spaces are used for the coarse-scale solution. The fine scales are discretized explicitly with a separate set of fine-scale basis functions. These additional

basis functions are locally supported, making their incorporation computationally cheap. Both authors investigate porous media flow, a problem for which mixed finite elements are often employed. Many more researchers have investigated different angles of VMS/mixed method synergies, especially in the last decade. The work by Arbogast is built on by Larson et al. in 2009, where the authors analyze the methods performance in terms of parallelization, conservativity and convergence of certain error norms [21]. Masud et al. investigate a mixed advection-diffusion equation in [22], where they perform the function space decomposition only on the space of the primal variable with the aim of developing a residual-based fine-scale model to stabilize the mixed finite element formulation. More recently, a number of articles have been published that apply similar concepts for problems concerning solid mechanics. Mixed formulations are especially applicable in the case of nearly incompressible materials [23]. In 2014, the residual-based fine-scale models are used to stabilize the mixed conservation law formulation in fast solid dynamics in [24]. Their applications mainly involve impact models of nearly incompressible materials. In that article, the multiscale nature of the residual-based stabilization technique is mentioned, but it hardly plays a role in their research. This is different in the 2015 article by Cervera and coworkers [25], which focuses on the multiscale interpretation of residual-based stabilized methods in mixed finite element simulation of nearly incompressible solids.

The aforementioned papers focus mostly on numerical implementation. The issues that may arise due to the lack of continuity of the coarse-scale basis functions are disregarded. Also, none of these works consider the use of discontinuous basis functions for both the primal and auxiliary variable. These aspects will be the focus of the current work. With these goals in mind, the DDVMS methodology developed earlier will be extended to incorporate the use of a primary variable as well as an auxiliary variable. It is shown that this may serve as a singular perspective from which a wide variety of finite element formulations may be classified as special cases of scale decompositions. This is depicted in Figure 1.1 which illustrates that the DDVMS framework offers a generalized strategy for the development and understanding of many finite element methods, including mixed methods, hybrid methods and discontinuous Galerkin methods. Overall, the use of mixed formulations of partial differential equations has been a missing piece in the DDVMS framework developed thus far. With the current work, this piece is filled in. Thereby, the DDVMS procedure comes closer to an all-encompassing framework for obtaining, and interpreting, multiscale finite element formulations.

This thesis is structured as follows. First, in Chapter 2, a literature survey of the variational multiscale method is provided. This includes a historic overview of the original VMS framework as proposed in the 90s. Additionally, the DDVMS method is summarized, and

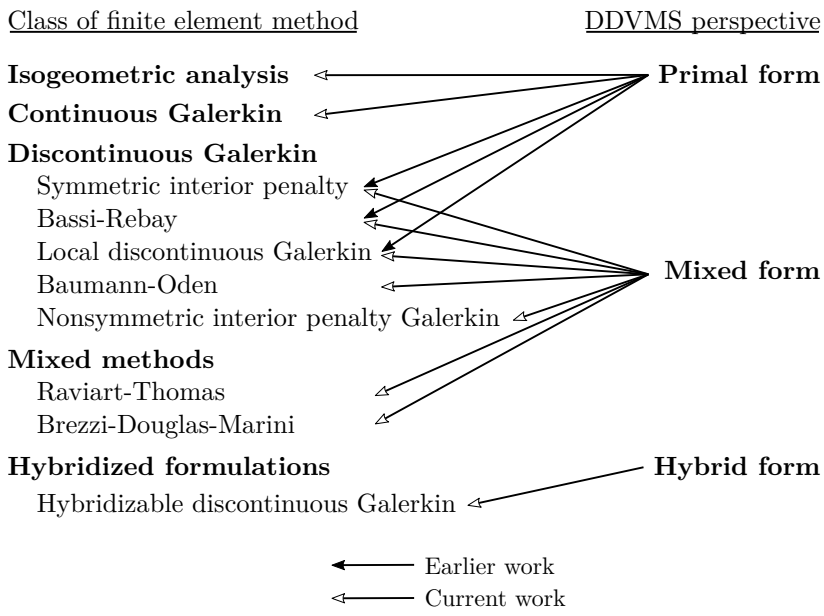

Fig. 1.1: *Overview of the different finite element formulations that can be retrieved based on a domain decomposition variational multiscale derivation, as developed in earlier work or in the current work.*

it is shown that this framework is suitable independent of the continuity of the basis functions. Once the reader is familiarized with the VMS methodology, it is extended to a mixed formulation setting in Chapter 3. Two model problems are considered: a Poisson equation and a steady advection-diffusion equation. In the next chapter, Chapter 4, it is shown that many existing finite element methods can be derived from the mixed multiscale formulation developed in Chapter 3 by choosing specific coarse-scale function spaces and fine-scale closure models. The interpretation of these closure models is also investigated. For advection based problems, the occurrence of certain fine-scale terms in the mixed multiscale formulations may prompt the use of additional fine-scale models. To this end, the theory of residual-based fine-scale models is incorporated into the mixed variational multiscale equations in Chapter 5. Finally, a summary and concluding remarks are provided in Chapter 6.

Chapter 2

The variational multiscale method

In this chapter, the variational multiscale method and the domain decomposition variational multiscale method principles are thoroughly reviewed. Since the aim later on will be to use discontinuous basis functions, the main challenges that have hindered the development of VMS formulations for low-order continuous basis functions are also addressed. The concepts and mathematics outlined here serve as the foundation on which the mixed formulation variant is built in the remainder of this thesis.

Starting with a historical overview in Section 2.1, the original objective that lead to the development of the VMS framework is reviewed. The developments that followed and its main current use are also discussed. Next, in Section 2.2, the fundamental mathematical concepts that make up the DDVMS method are addressed. These are outlined for the primal form of Poisson's equation. Since the continuity of the finite element basis is of key importance, the multiscale weak formulation is derived for three different classes of basis functions with decreasing order of continuity.

While the majority of this chapter is a literature review and a summary of previous work of the author, the generalized framework by which VMS formulations may be derived for *arbitrary* finite element basis functions (rather than the original focus purely on discontinuous basis functions) is, in fact, novel. Since it forms the basis of the VMS method as will be utilized in the remaining work, it is presented in this introductory chapter.

2.1 Historical overview

The success of finite element methods for dealing with solid mechanics problems lead researchers to explore its capabilities in the context of fluid mechanics in the 70s, see, for example, [26,27]. Soon, it became clear that similar advances were not so easily achieved. Where weak formulations associated to the mechanics of solid materials often originate from minimizing an energy functional, the same can not be said for those obtained for fluids. The stability of the obtained system of equation does thus not come naturally. The non-self-adjoint property of the sets of equation, and the resulting nonsymmetric system matrix, yields further difficulty. Techniques for stabilizing the finite element formulations were sought. The 'streamline-upwind Petrov-Galerkin' stabilization method was introduced by Brooks and Hughes in a seminal 1982 publication [5]. The idea combined artificial diffusion with the use of upwind test functions to yield a scheme that is both stable and consistent. While hugely successful, one of the authors hypothesized that there was a more sophisticated physical interpretation to the effectiveness of the added stabilization terms. Over ten years later, in 1995, Hughes started exploring the fine-scale nature of the solution as a potential candidate [1]. This would lead to the development of the variational multiscale method.

In that early paper, the focus was on weak formulations that could be obtained from minimization of certain functionals. Generally speaking, a solution u is sought that is an item of the space $\mathcal{Q}(u_D)$ and minimizes the functional J. The space $\mathcal{Q}(u_D)$ is constructed such that all members of the space satisfy the Dirichlet boundary condition. The functional J is often an integral expression of its arguments on the domain Ω. The problem may then be expressed as:

Find $u \in \mathcal{Q}(u_D)$ s.t.:

$$J(u, \nabla u, \nabla^2 u, \cdots) = \inf_{v \in \mathcal{Q}(u_D)} J(v, \nabla v, \nabla^2 v, \cdots) = \inf_{v \in \mathcal{Q}(u_D)} \int_\Omega I(x, v, \nabla v, \nabla^2 v, \cdots)\, \mathrm{d}x \tag{2.1}$$

Problems of this nature range from path optimization, to solid mechanics, and even to image analysis [28]. The solution of such problems can be found by equating the functional derivative (or Gâteaux derivative) to zero. In this functional setting, the Gâteaux derivative may be obtained according to:

$$\frac{\mathrm{d}}{\mathrm{d}\epsilon} \int_\Omega I(x, u + \epsilon w, \nabla(u + \epsilon w), \nabla^2(u + \epsilon w), \cdots) \Big|_{\epsilon=0} = 0 \qquad \forall\, w \in \mathcal{Q}(0) \tag{2.2}$$

This equation leaves a variational formulation that includes a trial function u, and a test function w. The equation must hold for any arbitrary function w that satisfies $u + w \in \mathcal{Q}(u_D)$, which means that w must be zero on the Dirichlet boundary. Galerkin's method then proposes to confine the test and trial function to finite dimensional subspaces of $\mathcal{Q}(u_D)$ and $\mathcal{Q}(0)$ respectively. This formulation may then be written as a matrix problem.

During the development of the VMS framework it was speculated that the loss of fine-scale information induced by confining u to some finite dimensional subspace of $\mathcal{Q}(u_D)$ was the source of the loss of stability. An alternative approach was proposed. Rather than reducing the dimensionality of the space $\mathcal{Q}(\cdot)$, it is *decomposed* into the finite dimensional 'coarse-scale' finite element approximation space $\bar{\mathcal{Q}}(\cdot)$, and an additional infinite dimensional 'fine-scale' space $\mathcal{Q}'(\cdot)$. The solution u may then be represented by a coarse-scale finite element solution $\bar{u}$ plus a fine-scale contribution u':

$$u = \bar{u} + u' \tag{2.3}$$

The following decomposition is then used in the Gâteaux derivative of Eq. (2.2):

$$u = \bar{u} + u' + \epsilon\,(\bar{w} + w') \tag{2.4}$$

The obtained weak formulation must hold for arbitrary $\bar{w}$ and w' in their respective function spaces. They can thus be split into two different weak formulations:

$$\begin{cases} B(\bar{u} + u', \bar{w}) \;= L(\bar{w}) & \forall\, \bar{w} \in \bar{\mathcal{Q}}(0) \\ B(\bar{u} + u', w') = L(w') & \forall\, w' \in \mathcal{Q}'(0) \end{cases} \tag{2.5}$$

In these equations, $B(\,\cdot\,,\,\cdot\,)$ is the bilinear form of the corresponding minimization problem, and $L(\cdot)$ is the linear form. The first line in Eq. (2.5) is the weak formulation corresponding to the finite element problem that will be solved. In the follow-up papers [2,3] it is shown that identical weak formulations may be derived by using a weighted residual approach.

For linear problems, the equations may often be rewritten to the form:

$$B(\bar{u}, \bar{w}) + \int_\Omega \mathcal{L}^* \bar{w}\, u' = \int_\Omega \bar{w}\, f \tag{2.6}$$

In this equation $\mathcal{L}^*$ is the adjoint of the partial differential equation (PDE) that corresponds to the minimization problem of Eq. (2.1). In the manipulation from Eq. (2.5) to Eq. (2.6) it is assumed that the coarse-scale solution satisfied the Dirichlet boundary

conditions strongly. Additionally, sufficient continuity of the coarse-scale and fine-scale bases is required. Else, element boundary contributions would occur. In most of the work on VMS for $\mathcal{C}^0$ finite element implementation, it is assumed that the fine-scale solution vanishes on element boundaries.

In Eq. (2.6), the complete scale interaction is governed by the volumetric fine-scale term. Substitution of a suitable fine-scale model may be beneficial for the stability, and predictive capability, of the finite element scheme.

Initially, researchers looked at the physical nature of the problem to develop the fine-scale models. A typical example is the modeling of a high-Reynolds number Navier-Stokes equation. Taking into account the scale interaction is hugely important for capturing the turbulent behavior of the flow. Turbulence theory tells us that the scale interaction that occurs is mostly of a dissipative nature. Typical practice for other modeling techniques, i.e. large eddy-simulation and Reynolds average Navier-Stokes modeling, is to add a so-called 'eddy viscosity'. Similarly, in the VMS framework, the fine-scale occurrences were first modeled as appropriately scaled diffusion terms [29–31].

The problem with eddy-viscosity models (and thus also the equivalent diffusion models in the VMS framework) is that they purely act as an energy sink for the coarse-scale solution. They do not account for backscatter, which is the feeding of energy from the fine-scale solution back into the coarse-scale solution. More complete fine-scale models can analytically be derived from the fine-scale problem in Eq. (2.5). Due to linearity of this equation, it may be rewritten into the following form.

$$B(u', w') = L(w') - B(\bar{u}, w') \equiv \mathrm{Res}(w', \bar{u}) \tag{2.7}$$

In this new form, it becomes clear that the fine-scale problem is analogous to the coarse-scale problem, but with a new source term. This source term involves the residual of the coarse-scale solution. This realization lead to the development of the so-called 'residual-based fine-scale models' [4, 32, 33].

Fine-scale problem Eq. (2.7) may formally be inverted by means of a Green's function (or fundamental solution). The Green's function is the function $g(x, y)$ for which:

$$u'(x) = \int_{\Omega} g(x, y) \mathcal{R}_{\bar{u}}(y) \, \mathrm{d}y \tag{2.8}$$

where $\mathcal{R}_{\bar{u}}(y)$ is the residual of the coarse-scale solution. Most often, this inversion is a global problem. However, by carrying over the earlier approximation that fine-scale

solutions vanish on element boundaries, Eq. (2.8) may be split in per-element contributions:

$$u'(x) \approx \int_K g(x,y)\mathcal{R}_{\bar{u}}(y)\,\mathrm{d}y \tag{2.9}$$

where K denotes an element domain.

Then, it is realized that the weighted occurrence of the fine-scale solution in Eq. (2.6) suggests further approximations:

$$\int_\Omega \mathcal{L}^*\bar{w}(x)\,u'(x)\,\mathrm{d}x \approx \sum_K \int_K \mathcal{L}^*\bar{w}(x) \int_K g(x,y)\mathcal{R}_{\bar{u}}(y)\,\mathrm{d}y\;\mathrm{d}x \tag{2.10}$$

$$\approx \sum_K \int_K \mathcal{L}^*\bar{w}(x) \int_K g(x,y)\,\mathrm{d}y\;\mathcal{R}_{\bar{u}}(x)\,\mathrm{d}x \tag{2.11}$$

$$\approx \sum_K \int_K \mathcal{L}^*\bar{w}(x)\,\frac{1}{|K|}\int_K\int_K g(\hat{x},y)\,\mathrm{d}\hat{x}\,\mathrm{d}y\;\mathcal{R}_{\bar{u}}(x)\,\mathrm{d}x \tag{2.12}$$

$$\equiv \sum_K \int_K \mathcal{L}^*\bar{w}(x)\,\tau\mathcal{R}_{\bar{u}}(x)\,\mathrm{d}x \tag{2.13}$$

From Eq. (2.10) to Eq. (2.11), the residual is pulled from the inner integral. From Eq. (2.11) to Eq. (2.12), the Green's function is averaged on the element domain. This averaged Green's function is denoted τ in Eq. (2.13). All these approximation steps are identities in the case of a one-dimensional advection-diffusion equation with constant coefficients, discretized with piecewise linear basis functions. This fact has inspired researchers to explore the effectiveness of the same model for applications beyond those restrictions.

At this stage, a reference back to the SUPG stabilization method introduced at the beginning of this section can be made. It has been known for a long time that many stabilization techniques, such as the SUPG, PSPG and GLS methods, may be interpreted as the addition of the following term to the weak formulation [1, 10, 27].

$$\sum_{K\in\mathcal{T}} \int_K \mathcal{L}_{\mathrm{s}}w(x)\;\tau\,\mathcal{R}_{u_h}(x)\;\mathrm{d}x \tag{2.14}$$

Different stabilization methods are obtained for different choices of the differential operator $\mathcal{L}_{\mathrm{s}}$. The parameter τ is the stabilization parameter, and $\mathcal{R}_{u_h}$ is the residual of the finite element solution u_h. Equivalence of Eq. (2.14) and Eq. (2.13) holds when $\mathcal{L}_{\mathrm{s}}$ is chosen as the adjoint differential operator, and τ as the averaged Green's function [34,35].

Even though the stabilization techniques were initially introduced with an 'upwinding' and diffusion-balancing interpretation in mind, in retrospect, it can be shown that the formulation actually incorporates the multiscale nature of the solution.

Throughout the development of the VMS method, the level of continuity of the coarse-scale basis has always been a precarious issue. The use of discontinuous basis functions in this thesis warrants a careful reflection on the importance of continuity for the VMS methodology. Initially the issue of continuity was dismissed with the suggestion that the fine-scale solution would vanish on element boundaries, which was already called a "rather strong assumption" in the original 1995 paper [1]. The simplest approach for mitigating the problem is to use a finite element basis that is sufficiently smooth. Hence the use of non-uniform rational B-splines (NURBS) in the introductory work on the residual-based model of Eq. (2.13) [4]. However, in practice the same model is also implemented in standard nodal finite element frameworks [8, 9, 36, 37]. The effect of the lack of continuity on the residual-based model was experimentally evaluated for simulations of turbulent flow in [38], where higher order continuous basis functions indeed outperformed the nodal finite element equivalent.

An attempt to develop the same VMS formalism in a $\mathcal{C}^0$ continuous finite element framework was made in [10]. There, it was argued that Eq. (2.6) is still valid, as long as higher order derivatives on the test function on element interfaces are taken into account as so-called 'Dirac-layers'. These are multidimensional Dirac-delta distributions on element surfaces. Similarly, the inversion of the fine-scale problem per Eq. (2.8) is still valid, as long as the Dirac-layers in the residual are included. These Dirac-layer contributions are written out explicitly as:

$$\begin{aligned}\int_\Omega \mathcal{L}^*\bar{w}(x)\, u'(x)\,\mathrm{d}x = \sum_K \sum_K \Big[&\int_K \int_K \mathcal{L}^*\bar{w}(x)\, g(x,y) \mathcal{R}_{\bar{u}}(y)\,\mathrm{d}y\ \mathrm{d}x \\ &+ \int_K \int_{\partial K} \mathcal{L}^*\bar{w}(x)\, g(x,y) \mathbb{D}(\mathcal{R}_{\bar{u}}(y)\,)\,\mathrm{d}y\ \mathrm{d}x \\ &+ \int_{\partial K} \int_K \mathbb{D}(\mathcal{L}^*\bar{w}(x)\,)\, g(x,y) \mathcal{R}_{\bar{u}}(y)\,\mathrm{d}y\ \mathrm{d}x \\ &+ \int_{\partial K} \int_{\partial K} \mathbb{D}(\mathcal{L}^*\bar{w}(x)\,)\, g(x,y)\, \mathbb{D}(\mathcal{R}_{\bar{u}}(y)\,)\,\mathrm{d}y\ \mathrm{d}x \Big]\end{aligned} \tag{2.15}$$

where $\mathbb{D}(\,\cdot\,)$ denotes a generic operator that captures the magnitude of the Dirac-layer of the argument. The first term on the right hand side is identical to that discussed earlier. In the second term, the Green's function distributes the Dirac-layers in the residual

throughout the domain. The third and fourth terms incorporate the Dirac-layers originating from the test function which were missing in the first and second term. While the complete scale interaction is captured in this equation, the terms are difficult to interpret. Indeed, no additional modeling strategies have been developed based on this expression.

Tracking the effect of the Dirac-layers in Eq. (2.15) becomes significantly more cumbersome when the PDE is several orders higher than the order of continuity of the finite element approximation basis. Then, the equation would involve differential operators acting on Dirac-layers. As an alternative, the domain decomposition variant of the variational multiscale method may be used. It offers a systematic approach for deriving the weak formulations, regardless of the order of continuity of the coarse-scale basis functions. This approach also serves as the basis for the development of the formulations for mixed PDEs in this work. The strategy is outlined in the following section.

2.2 The domain decomposition variational multiscale method

In this section, the domain decomposition variational multiscale method is outlined, and the necessary mathematical preliminaries are provided. The approach described here is developed by the author in earlier work [11–13]. The principal idea is based on the realization that the shortcomings of the standard VMS methodology all originate from the element interfaces. The lack of continuity presents problems for the inversion of the differential operator. If, instead, the differential equation is expressed on a single element, and transmission conditions are imposed to couple these elements, then clean multiscale formulations can be derived irrespective of the level of continuity of the underlying basis.

Constraining the PDE to a subdomain and enforcing appropriate coupling conditions, or transmission conditions, is the principle behind the domain decomposition method. When suitable transmission conditions are chosen, then the solution of the PDE remains well defined. Consider, for instance, the following classical boundary value problem:

$$\begin{cases} -\Delta u = f & \text{in } \Omega \subset \mathbb{R}^d \\ u = u_D & \text{on } \partial\Omega \end{cases} \tag{2.16}$$

with domain Ω of dimension d, domain boundary $\partial\Omega$, source term f, and Dirichlet boundary data u_D.

This PDE remains well defined under the following domain decomposition [23]:

$$\begin{cases} -\Delta u = f & \text{in } K \subset \Omega, \forall K \in \mathcal{T} \\ u^+ = u^- & \text{on } \bigcup_{K\in\mathcal{T}} \partial K \backslash \partial\Omega \\ \nabla u^+ \cdot n^+ = \nabla u^- \cdot n^- & \text{on } \bigcup_{K\in\mathcal{T}} \partial K \backslash \partial\Omega \\ u = u_D & \text{on } \partial\Omega \end{cases} \tag{2.17}$$

where $\mathcal{T} = \{K\}$ is some partitioning of the original domain Ω. The signs $+$ and $-$ arbitrarily refer to either side of the boundary of subdomain K, and n is the outward unit normal of this domain on its boundary.

The format of Eq. (2.17) will serve as the basis of the weak formulation. Transitioning to a finite element framework, the subdomains may be chosen to be the elements of the computational mesh. To facilitate the use of arbitrarily chosen basis functions later on, the following, quite non-restrictive, function space will be used for the weak formulation:

$$\mathcal{V}(g) = \{v \in L^2(\Omega) : v\big|_K \in H^s(K)\ \forall\, K \in \mathcal{T},\ v = g \text{ on } \partial\Omega\} \tag{2.18}$$

The order s of the Sobolev space on K is such that the weak formulation is well defined.

The following weak formulation is obtained from Eq. (2.17) by using the method of weighted residuals. The Dirichlet boundary conditions are incorporated into the function space definition. Refer to Table 2.1 for clarification of the notation used in the formulation.

Find $u \in \mathcal{V}(u_D)$ s.t. $\forall\, w \in \mathcal{V}(0)$:

$$\begin{cases} -(\Delta u, w)_{\Omega_K} = (f, w)_{\Omega_K} \\ [\![u]\!] \quad = 0 \qquad \text{on } \Gamma \\ [\![\nabla u]\!] = 0 \qquad \text{on } \Gamma \end{cases} \tag{2.19}$$

The transmission conditions are included as separate constraints, denoted as zero jumps.

Next, the solution u is split into a coarse-scale solution $\bar{u}$ and a fine-scale solution u'. The coarse-scale solution is the solution that can be found in the finite element space. For now, consider the following function space for the finite element approximation. No inter-element continuity is enforced yet, so such a space would typically be used for discontinuous

Table 2.1: *Collection of frequently used definitions.*

Jump operator	$[\![w]\!]$	$= w^+ n^+ + w^- n^-$
Average operator	$\{\!\{w\}\!\}$	$= \frac{1}{2}\left(w^+ + w^-\right)$
Volume L^2-inner product	$(u,w)_K$	$= \int\limits_K u\, w$
Surface L^2-inner product	$\langle u, w\, n\rangle_{\partial K}$	$= \int\limits_{\partial K} u\, w\, n$
Numerical interior domain	Ω_K	$= \bigcup\limits_{K\in\mathcal{T}} K$
		$(w,u)_{\Omega_K} = \sum\limits_{K\in\mathcal{T}} (w,u)_K$
Interior facets (Excludes domain boundary)	Γ	$= \left[\bigcup\limits_{K\in\mathcal{T}} \partial K\right] \backslash \partial\Omega$
		$\langle [\![w]\!], 1\rangle_\Gamma = \sum\limits_{K\in\mathcal{T}} \langle w\, n, 1\rangle_{\partial K\backslash\partial\Omega}$
		$\langle \{\!\{w\}\!\}, 1\rangle_\Gamma = \sum\limits_{K\in\mathcal{T}} \langle \frac{1}{2} w, 1\rangle_{\partial K\backslash\partial\Omega}$

Galerkin methods. Additional continuity may be enforced in the space later on.

$$\overline{\mathcal{V}}(g) = \{v \in L^2(\Omega) : v\big|_K \in P^p(K)\ \forall\, K \in \mathcal{T},\ v = \mathcal{I}_h g \text{ on } \partial\Omega\} \tag{2.20}$$

In this definition, $P^p(K)$ denotes the space of polynomial functions up to order p defined on element K. The operator $\mathcal{I}_h$ is some interpolator, or projector, that ensures that v is an accurate approximation of g while it may be represented as the trace of $P^p(K)$ on $\partial\Omega \cap \partial K$. The subscript h denotes a mesh dependency.

The function space $\overline{\mathcal{V}}(g)$ is constructed such that it is a subspace of $V(\cdot)$:

$$\overline{\mathcal{V}}(g) \subset \mathcal{V}(g) \tag{2.21}$$

The solution $\bar{u} \in \overline{\mathcal{V}}(u_D)$ is not immediately defined. Many different functions in $\overline{\mathcal{V}}(u_D)$ would count as approximations to u. To define the split of u into $\bar{u}$ and u' precisely, a projector is required that does just that. This projector is denoted $\mathcal{P}$, so that $\mathcal{P} : \mathcal{V}(\cdot) \to \overline{\mathcal{V}}(\cdot)$. The projector is assumed to be a linear mapping. Thereby, the projection $\mathcal{P}$ is also

idempotent, meaning: $\mathcal{P}(\mathcal{P}u) = \mathcal{P}u$. Then, the following definitions arise:

$$\bar{u} \equiv \mathcal{P}u \in \overline{\mathcal{V}}(\cdot) \tag{2.22}$$

$$u' \equiv u - \bar{u} \;\Rightarrow\; u = \bar{u} + u' \tag{2.23}$$

$$\mathcal{P}u' = \mathcal{P}(u - \bar{u}) = \mathcal{P}u - \mathcal{P}(\mathcal{P}u) = 0 \;\Rightarrow\; u' \in \ker(\mathcal{P}) \subset \mathcal{V}(\cdot) \tag{2.24}$$

The fine-scale solution u' is thus an element of the space $\ker(\mathcal{P})$. This space naturally emerges as the fine-scale space:

$$\mathcal{V}'(g) = \{v \in V(g) : \mathcal{P}v = 0\} \tag{2.25}$$

Finally, $\mathcal{P}$ must be a surjective mapping, meaning that:

$$\forall\, \bar{v} \in \overline{\mathcal{V}}(\cdot)\; \exists\; v \in \mathcal{V}(\cdot)\; :\; \mathcal{P}v = \bar{v} \tag{2.26}$$

With the earlier assumption of idempotency, and since $\overline{\mathcal{V}} \subset \mathcal{V}$, this means that $\mathcal{P}\bar{v} = \bar{v}$ for every $\bar{v} \in \overline{\mathcal{V}}(\cdot)$. By the definition of $\mathcal{V}'$ in Eq. (2.25), it follows that $\overline{\mathcal{V}} \cap \mathcal{V}' = \{0\}$. In turn, this means that a direct sum decomposition of $\mathcal{V}$ into the spaces $\overline{\mathcal{V}}$ and $\mathcal{V}'$ is possible:

$$\mathcal{V} = \overline{\mathcal{V}} \oplus \mathcal{V}' \tag{2.27}$$

By definition of a direct sum decomposition, every function $u \in \mathcal{V}$ maps *uniquely* into a coarse-scale component $\bar{u} \in \overline{\mathcal{V}}$ and a fine-scale component $u' \in \mathcal{V}'$. This property will ensure the well-posedness of the scale decomposition of the variational formulation.

The transmission conditions may also be written in a multiscale format. Due to linearity of the jump operator, one may write:

$$[\![u]\!] = 0 = [\![\bar{u} + u']\!] = [\![\bar{u}]\!] + [\![u']\!] \quad\Rightarrow\quad [\![\bar{u}]\!] = -[\![u']\!] \quad \text{on } \Gamma \tag{2.28}$$

$$[\![\nabla u]\!] = 0 = [\![\nabla\bar{u} + \nabla u']\!] = [\![\nabla\bar{u}]\!] + [\![\nabla u']\!] \quad\Rightarrow\quad [\![\nabla\bar{u}]\!] = -[\![\nabla u']\!] \quad \text{on } \Gamma \tag{2.29}$$

These conditions thus offer relationships between the coarse-scale and fine-scale solutions on the interior facets.

With all these definitions at hand, the multiscale equivalent of Eq. (2.19) may be constructed. The definitions of Eqs. (2.22) to (2.24) and relations Eqs. (2.28) and (2.29) are substituted into the weak form Eq. (2.19). It is assumed that the Dirichlet boundary conditions can be perfectly represented in the coarse-scale function space. Therefore, the

fine-scale solution equals zero on the domain boundary. Then:

$$\text{Find } \bar{u}, u' \in \overline{\mathcal{V}}(u_D) \times \mathcal{V}'(0) \text{ s.t. } \forall\, \bar{w} \in \overline{\mathcal{V}}(0) \text{ and } \forall\, w' \in \mathcal{V}(0):$$
$$\begin{cases} -(\Delta(\bar{u}+u'),\bar{w}\,)_{\Omega_K} = (f,\bar{w})_{\Omega_K} \\ -(\Delta(\bar{u}+u'),w')_{\Omega_K} = (f,w')_{\Omega_K} \\ [\![\bar{u}]\!] = -[\![u']\!] \qquad \text{on } \Gamma \\ [\![\nabla\bar{u}]\!] = -[\![\nabla u']\!] \qquad \text{on } \Gamma \end{cases} \tag{2.30}$$

The two variational formulations in Eq. (2.30) are the coarse-scale and fine-scale formulations respectively. The coarse-scale weak formulation serves as the basis for a multiscale finite element formulation that precisely incorporates the effects of the fine scales onto the finite element solution. In turn, the fine-scale formulation may be manipulated to inspire fine-scale models that help close the multiscale finite element formulation.

Due to linearity of the differential operator, the coarse-scale and fine-scale terms in the first line of Eq. (2.30) may be treated separately. The following equation is obtained by subsequent use of integration by parts. Each integration by parts is performed on separate elements. This yields the surface integrals on the element boundaries.

$$\text{Find } \bar{u} \in \overline{\mathcal{V}}(u_D) \text{ s.t. } \forall\, \bar{w} \in \overline{\mathcal{V}}(0):$$
$$\begin{cases} (\nabla\bar{u},\nabla\bar{w})_{\Omega_K} - (u',\Delta\bar{w})_{\Omega_K} + \sum\limits_{K\in\mathcal{T}} \Big[-\langle \nabla\bar{u}\cdot n,\bar{w}\rangle_{\partial K\setminus\partial\Omega} \\ \qquad -\langle \nabla u'\cdot n,\bar{w}\rangle_{\partial K\setminus\partial\Omega} + \langle u'\,n,\nabla\bar{w}\rangle_{\partial K\setminus\partial\Omega}\Big] = (f,\bar{w})_{\Omega_K} \\ [\![\bar{u}]\!] = -[\![u']\!] \qquad \text{on } \Gamma \\ [\![\nabla\bar{u}]\!] = -[\![\nabla u']\!] \qquad \text{on } \Gamma \end{cases} \tag{2.31}$$

As can be observed from the first line, integration by parts has been performed once on the coarse-scale term. This is in line with typical finite element formulations of Poisson's equation. Staying closely in line with standard formulations will help with comparing the formulations in the end. On the other hand, integration by parts has been performed twice on the fine-scale term. Thereby, the fine-scale field is free of any differential operators in the volumetric integral, which will help in the incorporation of fine-scale models.

In the weak formulation of Eq. (2.31), the elements are completely uncoupled. There is no communication between the solutions on neighboring elements. This element coupling is enforced by the multiscale transmission conditions in Eq. (2.31). However, having these conditions separate from the weak formulations makes them difficult to deal with. The

following strategy is proposed to incorporate the transmission conditions directly into the weak formulation. First, write the solution u' on either side of the element boundary as:

$$\begin{aligned} u'^{\pm}\, n^{\pm} &= \frac{1}{2}(u'^{+} + u'^{-})\, n^{\pm} + \frac{1}{2}(u'^{+} n^{+} + u'^{-} n^{-}) \\ &= \{\!\{u'\}\!\}\, n^{\pm} + \frac{1}{2}[\![u']\!] \end{aligned} \tag{2.32}$$

$$\begin{aligned} \nabla u'^{\pm} \cdot n^{\pm} &= \frac{1}{2}(\nabla u'^{+} + \nabla u'^{-}) \cdot n^{\pm} + \frac{1}{2}(\nabla u'^{+} \cdot n^{+} + \nabla u'^{-} \cdot n^{-}) \\ &= \{\!\{\nabla u'\}\!\} \cdot n^{\pm} + \frac{1}{2}[\![\nabla u']\!] \end{aligned} \tag{2.33}$$

Next, the transmission conditions are substituted into these identities.

$$u'^{\pm}\, n^{\pm} = \{\!\{u'\}\!\}\, n^{\pm} - \frac{1}{2}[\![\bar{u}]\!] \tag{2.34}$$

$$\nabla u'^{\pm} \cdot n^{\pm} = \{\!\{\nabla u'\}\!\} \cdot n^{\pm} - \frac{1}{2}[\![\nabla \bar{u}]\!] \tag{2.35}$$

When these relations are then substituted in the weak form of Eq. (2.31), and after some manipulation, one obtains:

$$\begin{aligned} &\text{Find } \bar{u} \in \overline{\mathcal{V}}(u_D) \text{ s.t. } \forall\, \bar{w} \in \overline{\mathcal{V}}(0): \\ &\quad (\nabla \bar{u}, \nabla \bar{w})_{\Omega_K} - \langle \{\!\{\nabla \bar{u}\}\!\}, [\![\bar{w}]\!] \rangle_{\Gamma} - \langle [\![\bar{u}]\!], \{\!\{\nabla \bar{w}\}\!\} \rangle_{\Gamma} \\ &\qquad - (u', \Delta \bar{w})_{\Omega_K} - \langle \{\!\{\nabla u'\}\!\}, [\![\bar{w}]\!] \rangle_{\Gamma} + \langle \{\!\{u'\}\!\}, [\![\nabla \bar{w}]\!] \rangle_{\Gamma} = (f, \bar{w})_{\Omega_K} \end{aligned} \tag{2.36}$$

Until now, no assumptions, approximations or simplifications have been introduced. Equation (2.36) represents the true weak formulation of the problem, including all coarse-scale/fine-scale interaction. Closure of the weak formulation is a matter of 'choosing' the right expressions for the fine-scale terms. These are, in turn, defined by the projector $\mathcal{P}$ introduced earlier.

Two types of fine-scale contributions occur in Eq. (2.36). The first is a volumetric term, which is often the only scale interaction considered when variational multiscale models are proposed. The second are two element boundary integrals that involve the fine-scale solution. They correspond to the additional integrals in Eq. (2.15), although now presented more explicitly. The occurrence of these terms depends on the finite element framework that is being used, or more specifically, the level of continuity of the finite element basis functions. Different orders of continuity are considered separately in the following.

2.2.1 $\mathcal{C}^1$ - $\mathcal{C}^\infty$ continuous basis functions

Many types of finite elements that exhibit $\mathcal{C}^1$ - $\mathcal{C}^\infty$ level of continuity were constructed in the 60s. Notable examples include the Argyris triangle [39], the Bell reduced triangle [40], and the Hsieh-Clough-Tocher triangle [41]. Refer to [42] for a comprehensive overview. All these examples involve basis functions on two-dimensional triangular elements. More recently, isogeometric analysis has sparked much interest in the computational mechanics research community [43, 44]. In isogeometric analysis, the approximation space is constructed as the span of a set of NURBS. Even though the use of B-splines originates from computer graphics, where they are primarily used to describe surfaces, this framework is not limited to two-dimensional applications. The order of continuity of each B-spline basis functions may be arbitrarily controlled. When, for instance, second order splines are used, then each NURBS is an element of the Sobolev space:

$$B_i \in H^2(\Omega) \tag{2.37}$$

And, without being very specific, the approximation space may be constructed as:

$$\mathcal{V}_h(g) = \{v \in \text{span}\{B_i\}_{i=0}^n : v = g \text{ on } \partial\Omega\} \tag{2.38}$$

Since each spline is essentially a number of patched polynomial functions, also:

$$\mathcal{V}_h \subset \overline{\mathcal{V}} \tag{2.39}$$

with $\overline{\mathcal{V}}$ defined in Eq. (2.20). The derivation presented earlier is therefore also applicable when $\bar{u} \in \mathcal{V}_h$.

While the weak formulation of Eq. (2.36) is valid, many of the terms are identically zero. The continuity of the function space directly implies that $[\![v]\!] = [\![\nabla v]\!] = 0$ along any interface and for all $v \in \mathcal{V}_h(\cdot)$. This means that all surface terms vanish. The remaining formulation is:

$$\begin{aligned} &\text{Find } \bar{u} \in \mathcal{V}_h(u_D) \text{ s.t. } \forall\, \bar{w} \in \mathcal{V}_h(0): \\ &\quad (\nabla\bar{u}, \nabla\bar{w})_{\Omega_K} - (u', \Delta\bar{w})_{\Omega_K} = (f, \bar{w})_{\Omega_K} \end{aligned} \tag{2.40}$$

The volumetric fine-scale term is the only fine-scale contribution. This term thus captures the complete scale interaction. If one would want to introduce a fine-scale model, then one would only need to concern themselves with this weighted volumetric term. This explains why the residual-based fine-scale model, discussed in Section 2.1, was introduced in an isogeometric framework [4].

2.2.2 $\mathcal{C}^0$ continuous basis functions

Most 'standard' finite element frameworks make use of $\mathcal{C}^0$ continuous basis functions. These are typically polynomial functions, such as Lagrange polynomials, Legendre polynomials or Chebyshev polynomials, confined to a single element. The approximation space may then be written as:

$$\mathcal{V}_h(g) = \{v \in H^1(\Omega) : v|_K \in P^p(K) \; \forall \, K \in \mathcal{T}, \; v = g \text{ on } \partial\Omega\} \tag{2.41}$$

with $P^p(K)$ the span of polynomial functions up to order p on element K. Again, this space satisfies:

$$\mathcal{V}_h \subset \overline{\mathcal{V}} \tag{2.42}$$

confirming the validity of Eq. (2.36). For this space, however, the continuity implies $[\![v]\!] = 0$ on any interface and for all $v \in \mathcal{V}_h(\cdot)$, such that Eq. (2.36) simplifies to:

$$\begin{aligned} &\text{Find } \bar{u} \in \mathcal{V}_h(u_D) \text{ s.t. } \forall \, \bar{w} \in \mathcal{V}_h(0): \\ &\quad (\nabla \bar{u}, \nabla \bar{w})_{\Omega_K} - (u', \Delta \bar{w})_{\Omega_K} + \langle \{\!\{u'\}\!\}, [\![\nabla \bar{w}]\!] \rangle_\Gamma = (f, \bar{w})_{\Omega_K} \end{aligned} \tag{2.43}$$

Compared to Eq. (2.40), the scale interaction now also involves contributions on element surfaces. A closure measure for this set of equations thus requires a model for the volumetric term, as well as a model for the surface term. In practice, however, the same residual-based model is used [8, 9, 36, 37]. The derivation of this model assumes vanishing fine scales on element interfaces. This, in itself, may be considered a fine-scale closure model. Employed in Eq. (2.43), this would remove the interface term altogether.

The standard $\mathcal{C}^0$ finite element formulation for Poisson's equation is:

$$\begin{aligned} &\text{Find } \bar{u} \in \mathcal{V}_h(u_D) \text{ s.t. } \forall \, \bar{w} \in \mathcal{V}_h(0): \\ &\quad (\nabla \bar{u}, \nabla \bar{w})_{\Omega_K} = (f, \bar{w})_{\Omega_K} \end{aligned} \tag{2.44}$$

The right-hand sides of Eq. (2.43) and Eq. (2.44) may be equated. Then, it becomes clear that by solving Eq. (2.44) ones implicitly makes use of the following closure model:

$$-(u', \Delta \bar{w})_{\Omega_K} + \langle \{\!\{u'\}\!\}, [\![\nabla \bar{w}]\!] \rangle_\Gamma = (\nabla u', \nabla \bar{w})_{\Omega_K} = 0 \quad \forall \, \bar{w} \in \mathcal{V}_h(0) \tag{2.45}$$

From now on, this type of closure model is referred to as a fine-scale constraint, and

Eq. (2.45) as a fine-scale constraint equation. This terminology is preferred since 'closure model' implies an approximation, while equations such as Eq. (2.45) are identically satisfied. The fine-scale constraint dictates much of the behavior of the numerical scheme, as will be illustrated in upcoming sections.

The equivalence between the method's fine-scale constraint equation and its 'error equation' should also be highlighted at this point. Since the fine-scale solution is in effect the error of the computational solution, Eq. (2.45) could be interpreted as the error equation. Yet, referring to Eq. (2.45) as the error equation does not appropriately reflect its significance. The error, by nature, is an a posteriori measure; it follows from the obtained approximation. The fine-scale solution is an a priori quantity; the scale decomposition lies at the heart of the finite element approximation. Equation (2.45) plays a central role in characterizing the scale decomposition, and thereby the finite element method. As such, the equation is more fundamental than what is implied by the term 'error equation'.

2.2.3 Discontinuous basis functions

For discontinuous Galerkin methods, the continuity constraints are completely released on the element interfaces. The approximation space becomes:

$$\mathcal{V}_h(g) = \{v \in L^2(\Omega) : v\big|_K \in P^p(K)\ \forall\, K \in \mathcal{T},\ v = g \text{ on } \partial\Omega\} \tag{2.46}$$

Then, indeed:

$$\mathcal{V}_h(g) = \overline{\mathcal{V}}(g) \tag{2.47}$$

and the weak form of Eq. (2.36) is directly applicable without further simplification:

$$\begin{aligned}&\text{Find } \bar{u} \in \mathcal{V}_h(u_D) \text{ s.t. } \forall\, \bar{w}\ \in \mathcal{V}_h(0):\\ &\left(\nabla\bar{u}, \nabla\bar{w}\right)_{\Omega_K} - \left\langle \{\!\{\nabla\bar{u}\}\!\}, [\![\bar{w}]\!]\right\rangle_\Gamma - \left\langle [\![\bar{u}]\!], \{\!\{\nabla\bar{w}\}\!\}\right\rangle_\Gamma \\ &\qquad - \left(u', \Delta\bar{w}\right)_{\Omega_K} - \left\langle \{\!\{\nabla u'\}\!\}, [\![\bar{w}]\!]\right\rangle_\Gamma + \left\langle \{\!\{u'\}\!\}, [\![\nabla\bar{w}]\!]\right\rangle_\Gamma = \left(f, \bar{w}\right)_{\Omega_K}\end{aligned} \tag{2.48}$$

Despite the discontinuous basis functions, Eq. (2.48) offers a formulation where the finite element solution communicates between elements. This was due to the incorporation of the transmission conditions in the derivation. After substitution of a suitable closure model for the remaining fine-scale terms, Eq. (2.48) can thus be solved to obtain a finite element approximation.

Typically, discontinuous Galerkin formulations are also derived on a per-element basis. Then, element coupling is achieved by substituting 'numerical fluxes' in place of the surface terms obtained from the integration by parts. These numerical fluxes are "approximations to the exact solution on the boundary of the element", as paraphrased from [45]. However, with Eq. (2.48) at hand, a different interpretation becomes apparent. Consider, for example, the interior penalty formulation:

$$\begin{aligned} &\text{Find } \bar{u} \in \mathcal{V}_h(u_D) \text{ s.t. } \forall\, \bar{w} \in \mathcal{V}_h(0): \\ &\quad (\nabla \bar{u}, \nabla \bar{w})_{\Omega_K} - \langle \{\!\{\nabla \bar{u}\}\!\}, [\![\bar{w}]\!] \rangle_\Gamma - \langle [\![\bar{u}]\!], \{\!\{\nabla \bar{w}\}\!\} \rangle_\Gamma + \langle \eta h^{-1} [\![\bar{u}]\!], [\![\bar{w}]\!] \rangle_\Gamma = (f, \bar{w})_{\Omega_K} \end{aligned} \tag{2.49}$$

By equating the right-hand sides of Eq. (2.49) and Eq. (2.48) one can conclude that the interior penalty method actually employs the following closure model, or fine-scale constraint:

$$-(u', \Delta \bar{w})_{\Omega_K} + \langle \eta h^{-1} [\![u']\!] - \{\!\{\nabla u'\}\!\}, [\![\bar{w}]\!] \rangle_\Gamma + \langle \{\!\{u'\}\!\}, [\![\nabla \bar{w}]\!] \rangle_\Gamma = 0 \quad \forall\, \bar{w} \in \mathcal{V}_h(0) \tag{2.50}$$

This idea was introduced by the author in [13]. Much of that article dealt with the interpretation of the fine-scale constraint equation. In particular, in a one-dimensional setting, Eq. (2.50) gives rise to certain pointwise identities that dictate the nature of the finite element solution.

While the interior penalty method may be written as a single-line weak formulation, most of the discontinuous Galerkin methods for Poisson's equation cannot naturally be expressed as such. Instead, they originate from a mixed formulation of the PDE. Hence, it was hypothesized already in [13] that an adaptation of the VMS framework described in this section to mixed forms of PDEs may prove fruitful.

Chapter 3

Extension towards mixed and hybrid formulations

With the domain decomposition version of the variational multiscale framework firmly developed, the mixed formulation variant can now be introduced. This chapter begins with a brief introduction of finite element formulations for mixed partial differential equations. Their basic development and advantages are discussed. In particular, the saddle point problem that they represent is highlighted. Subsequently, the domain decomposition variational multiscale method is adapted to suit the use of mixed formulations of partial differential equations. Three example formulations are considered. First, the mixed multiscale formulations for Poisson's equation are derived in Section 3.2. Then, in Section 3.3, the mixed advection-diffusion problem is investigated. Finally, a hybrid formulation of Poisson's equation is examined in Section 3.4. The mixed multiscale formulation is derived for each of these problems. The scale decomposition is ensured to be suitable for the use of discontinuous coarse-scales. The obtained formulations are used and analyzed in upcoming chapters.

3.1 Introduction to mixed formulations

Typically, the partial differential equations that govern physical systems are expressed in their primal formulation. This is a single PDE that involves only the primal variable. A classical example is once again an (anisotropic) Poisson equation:

$$\begin{cases} -\nabla \cdot (D\nabla P) = 0 & \text{in } \Omega \subset \mathbb{R}^d \\ P = P_D & \text{on } \partial\Omega_D \\ -D\nabla P \cdot n = \varphi_N \cdot n & \text{on } \partial\Omega_N \end{cases} \tag{3.1}$$

For the current example this will describe the flow field in a porous medium. Then, P is the piezometric head, which is a measure of the pressure in the body, and D is the permeability tensor which describes the material porosity. The second and third line represent the essential and natural boundary conditions respectively.

An alternative way to represent the same partial differential equation is by writing it as a system of lower order PDEs. This is referred to as the mixed formulation of the problem. It requires the introduction of the auxiliary variable φ:

$$\begin{cases} \varphi = -D\nabla P & \text{in } \Omega \subset \mathbb{R}^d \\ \nabla \cdot \varphi = 0 & \text{in } \Omega \\ P = P_D & \text{on } \partial\Omega_D \\ \varphi \cdot n = \varphi_N \cdot n & \text{on } \partial\Omega_N \end{cases} \tag{3.2}$$

The format of Eq. (3.2) more closely resembles the underlying physics. The auxiliary variable φ represents the velocity field. It relates to the piezometric head via the first line, which is Darcy's law, a reformulation of Newton's second law for porous media flow [46]. The second line may then be identified as the incompressibility constraint. The boundary condition in the third line becomes a natural boundary condition, whereas the condition in the final line, which is an inflow/outflow boundary condition, becomes the essential boundary condition.

The idea to use mixed formulations as a basis for finite element schemes was proposed in the 60s [14–16], and currently forms a thoroughly studied branch of finite element

methods [23]. There are a number of reasons to favor Eq. (3.2) over Eq. (3.1) as the basis of a finite element formulation. Firstly, in many applications the auxiliary variable is the variable of interest rather than the primal variable. Also in the case of porous media flow considered in this example, the velocity field is likely to be of more interest to the researcher than the piezometric head. Other examples are heat flux in the heat equation to understand necessity of installing insulatory devices, or stress/strain in structural mechanics applications. In all these examples, the variable of interest is not represented in the primal formulation. Instead, post-processing in the form of numerical differentiation would required to obtain the quantity of interest from the primal variable. This typically introduces error, or at least reduces the order of accuracy of the scheme. Additionally, the derived quantity would remain ill-defined on element boundaries when the order of continuity of the finite element approximation space is insufficiently high. By developing finite element schemes based on Eq. (3.2), the quantity of interest may directly be obtained from the approximation.

Another reason lies in the physical nature of the PDE. A finite element scheme based on Eq. (3.1) is not inherently mass conservative [47]. This would require specially constructed 'divergence free' finite element spaces [48], or specialized post-processing [49]. The explicit occurrence of the incompressibility constraint equation in Eq. (3.2) may serve as a handle for crafting finite element formulations that adhere to such constraints more naturally [50].

Finally, the nature of the problem is changed such that finite element methods can make use of approximation spaces that might otherwise fail. For example, PDEs that involve high orders of derivatives, such as the fourth order biharmonic operator used to describe the deflection of thin shells, cannot directly be solved by using off-the-shelf H^1 finite element function spaces. By writing the partial differential equation in a reduced order mixed form, the existing technology is once again suitable. Additionally, since both the primal and auxiliary variable are represented by their respective solution field, both natural and essential type boundary conditions can be incorporated directly in the function space definition.

Mixed finite element schemes are based on mixed weak formulations. Such mixed variational formulations may be obtained in a variety of ways. Classically, variational formulations often correspond to some minimization problem. In that case, mixed variational formulations immerse when a constraint is added. Consider the minimization case of some

functional of the form:

$$\inf_{\substack{v\in V\\ Bv=0}} \frac{1}{2}a(v,v) - b(v) \tag{3.3}$$

where V is some suitable function space, $a(\cdot,\cdot)$ is some bilinear form, $b(\cdot)$ some linear form, and $Bv = 0$ is the constraint that is imposed. The constraint may be incorporated more naturally as follows:

$$\inf_{v\in V} \Big[\frac{1}{2}a(v,v) - b(v) + \sup_{q\in L^2(\Omega)} \int_\Omega q\, Bv \Big] \tag{3.4}$$

or, written as a saddle point problem:

$$\inf_{v\in V} \sup_{q\in L^2(\Omega)} \Big[\frac{1}{2}a(v,v) - b(v) + \int_\Omega q\, Bv \Big] \tag{3.5}$$

The added term is infinite when $Bv \neq 0$ anywhere on the domain, so the infimum corresponds to solutions v that do satisfy the constraint. The infimum and supremum are reached when the functional derivatives equal zero, resulting in the variational formulation:

$$\begin{aligned} &\text{Find } \varphi, P \in V(\varphi_N) \times L^2(\Omega) \text{ s.t. } \forall\, v \in V(0) \text{ and } \forall\, q \in L^2(\Omega): \\ &\begin{cases} a(\varphi, v) + \displaystyle\int_\Omega P\, Bv = b(v) \\ \displaystyle\int_\Omega q\, B\varphi = 0 \end{cases} \end{aligned} \tag{3.6}$$

To propose a tangible example, consider again the case of porous media flow. This is characterized by the functionals:

$$a(v,v) = \int_\Omega D^{-1}v \cdot v \tag{3.7}$$

$$b(v) = -\int_{\partial\Omega_D} P_D n \cdot v \tag{3.8}$$

and the incompressibility constraint:

$$Bv = -\nabla \cdot v \tag{3.9}$$

With those definitions, Eq. (3.6) becomes the variational formulation of the Darcy

equations:

$$\begin{aligned}&\text{Find } \varphi, P \in V(\varphi_N) \times L^2(\Omega) \text{ s.t. } \forall\, v \in V(0) \text{ and } \forall\, q \in L^2(\Omega):\\ &\begin{cases} \int\limits_{\Omega} D^{-1}\varphi \cdot v = \int\limits_{\Omega} P\, \nabla \cdot v - \int\limits_{\partial\Omega_D} P_D\, n \cdot v \\ \int\limits_{\Omega} \nabla \cdot \varphi\, q = 0 \end{cases}\end{aligned} \tag{3.10}$$

The pressure P can then be identified as the Lagrange multiplier associated to the incompressibility constraint.

If, instead, a variational formulation is sought based on a system of PDEs, rather than from functional minimization, then the method of weighted residuals may be employed. For example, to obtain the weak formulation of Eq. (3.2), both PDEs are multiplied by a (vector valued or scalar valued) test function. Depending on the problem at hand, integration by parts is required to reduce the maximum order of differentiation, or to yields access to natural boundary conditions. This could potentially result in:

$$\begin{aligned}&\text{Find } \varphi, P \in V(\varphi_N) \times L^2(\Omega) \text{ s.t. } \forall\, v \in V(0) \text{ and } \forall\, q \in L^2(\Omega):\\ &\begin{cases} \int\limits_{\Omega} D^{-1}\varphi \cdot v = \int\limits_{\Omega} P\, \nabla \cdot v - \int\limits_{\partial\Omega_D} P_D\, n \cdot v \\ \int\limits_{\Omega} \nabla \cdot \varphi\, q = 0 \end{cases}\end{aligned} \tag{3.11}$$

which is exactly the same weak form as Eq. (3.10).

The function spaces involved in this weak formulation require some careful thought. Typically in finite element formulations of Poisson's equation, the solution variable is sought in the $H^1(\Omega)$ Sobolev space. Interestingly, in Eq. (3.11), the restriction on the primal variable is loosened such that it is now sought in the $L^2(\Omega)$ space. For the auxiliary variable φ, on the other hand, some subtleties are involved. The weak forms in Eq. (3.11) require that the divergence is well defined in the domain, which is slightly less restrictive than $H^1(\Omega)$. This space is denoted $H(\mathrm{div};\Omega)$:

$$H(\mathrm{div};\Omega) = \{v \in [L^2(\Omega)]^d : \nabla \cdot v \in L^2(\Omega)\} \tag{3.12}$$

where d is the (spatial) dimension of the problem. Then, for completion, the space $V(\cdot)$ as used in Eq. (3.11) may be defined as:

$$V(g) = \{v \in H(\mathrm{div};\Omega) : v\big|_{\partial\Omega_N} = g\} \tag{3.13}$$

Some years after mixed formulations were suggested as a basis for finite element methods by Fraeijs de Veubeke in the 60s [14–16], it was realized that the subtleties present in the required function space $V(\cdot)$ are important in the construction of appropriate finite element schemes. Early focus of research was thus on constructing finite dimensional subspaces of $H(\mathrm{div};\Omega)$ suitable for finite element implementations. Examples include the Hellan-Herrmann-Johnson finite element for plate bending [51–53], the famous Raviart-Thomas finite element [54], and shortly after also the Brezzi-Douglas-Marini family of finite elements [55, 56]. Early error and stability analysis of finite element schemes that adopt these function spaces was performed in [57].

Discontinuous Galerkin methods also often make use of mixed formulations of the PDE, but the required finite element spaces are less restrictive than what is described above. This is achieved by confining the PDE to a single element. Element surface terms are introduced via integration by parts. Then, the approximation spaces are introduced, and the element surface contributions are approximated by so-called 'numerical traces':

$$\begin{aligned}&\text{Find } \varphi_h, P_h \in V_h(K) \times Q_h(K) \text{ s.t. } \forall\, v \in V_h(K) \text{ and } \forall\, q \in Q_h(K) : \\ &\begin{cases} \int\limits_K D^{-1}\varphi_h \cdot v = \int\limits_K P_h \nabla \cdot v - \int\limits_{\partial K} \widehat{Pn} \cdot v \\ -\int\limits_K \varphi_h \cdot \nabla q + \int\limits_{\partial K} \widehat{\varphi \cdot n}\, q = 0 \end{cases}\end{aligned} \tag{3.14}$$

Choice of the numerical traces (the quantities denoted with the hats) will determine the behavior of the finite element scheme. At the same time, they must ensure element coupling, such that the global system can be solved. The choice of the approximation spaces V_h and Q_h may now be quite nonrestrictive. Typically, one would make use of:

$$V_h = \{v \in [L^2(\Omega)]^d : v\big|_K \in [P^p]^d(K)\ \forall\, K \in \mathcal{T}\} \tag{3.15}$$

$$Q_h = \{\xi \in L^2(\Omega) : \xi\big|_K \in P^q(K)\ \forall\, K \in \mathcal{T}\} \tag{3.16}$$

where p and q are the polynomial orders of the respective basis functions, and $\mathcal{T} = \{K\}$ denotes the collection of elements that forms the computational mesh. No inter-element continuity is required, hence the name 'discontinuous Galerkin'.

Clearly, mixed formulations arise in many different ways, and they come accompanied with a wide variety of finite element methods. This leaves the question how to proceed with the variational multiscale framework. The aim is to remain as general as possible. With that in mind, a strategy similar to the derivation of discontinuous Galerkin methods will be adopted. The method of weighted residuals will be used in combination with

nonrestrictive coarse-scale function spaces similar to those in Eqs. (3.15) and (3.16). At the end of the derivation, further restrictions can potentially be imposed on the coarse-scale function spaces to reduce them to the $H(\mathrm{div}, \Omega)$ subspaces (similar to the approach in Sections 2.2.1 to 2.2.3). Thereby, the same methodology results in multiscale formulations corresponding to those classes of finite element methods.

3.2 Mixed multiscale weak formulation for the second order elliptic problem

In this section, the VMS function space decomposition is used for both the primal and the auxiliary variable, while the PDE is represented in a domain decomposition form. Thereby, a mixed weak formulations is retrieved that capture the complete scale interaction irrespective of the continuity of the coarse-scale basis functions. Starting with the mixed form of Poisson's equation:

$$\begin{cases} \sigma = \nabla u & \text{in } \Omega \subset \mathbb{R}^d \\ -\nabla \cdot \sigma = f & \text{in } \Omega \\ u = u_D & \text{on } \partial\Omega_D \\ \sigma \cdot n = \sigma_N \cdot n & \text{on } \partial\Omega_N \end{cases} \tag{3.17}$$

where d is the spatial dimension, u is the scalar primal variable, and σ is the auxiliary flux variable. Note the equivalence with Eq. (3.2), although the notation of variables has changed.

A domain decomposition description of the same problem would read:

$$\begin{cases} \sigma = \nabla u & \text{in } K \subset \Omega \\ -\nabla \cdot \sigma = f & \text{in } K \\ u^+ n^+ = -u^- n^- & \text{on } \partial K \setminus \partial\Omega \\ \sigma^+ \cdot n^+ = -\sigma^- \cdot n^- & \text{on } \partial K \setminus \partial\Omega \\ u = u_D & \text{on } \partial\Omega_D \\ \sigma \cdot n = \sigma_N \cdot n & \text{on } \partial\Omega_N \end{cases} \tag{3.18}$$

which should hold for all potential subdomains $K \subset \Omega$. This formulation is equivalent to Eq. (3.17) and the same unique solution exists [23,58]. In the following, these subdomains

will be the individual elements in the mesh that covers the complete domain Ω. This partition of Ω is denoted $\mathcal{T}$. Through the method of weighted residuals, Eq. (3.18) may be rewritten in a weak form:

Find $\sigma, u \in \Sigma \times U$ s.t. $\forall\, \tau \in \Sigma$ and $\forall\, v \in U$:

$$\begin{cases} (\sigma, \tau)_{\Omega_K} = (\nabla u, \tau)_{\Omega_K} \\ -(\nabla \cdot \sigma, v)_{\Omega_K} = (f, v)_{\Omega_K} \\ [\![u]\!] = 0 \qquad \text{on } \Gamma \\ [\![\sigma]\!] = 0 \qquad \text{on } \Gamma \\ u = u_D \qquad \text{on } \partial\Omega_D \\ \sigma = \sigma_N \qquad \text{on } \partial\Omega_N \end{cases} \tag{3.19}$$

Refer to Table 2.1 for details regarding the notation. Suitable function spaces Σ and U need to be chosen. Since the differential operators only act in the (open) element domains, continuity requirements of Σ and U may be quite loose. Specifically:

$$U = \{u \in L^2(\Omega) : u\big|_K \in H^1(K)\ \forall\, K \in \mathcal{T}\} \tag{3.20}$$

$$\Sigma = \{\sigma \in [L^2(\Omega)]^d : \sigma\big|_K \in H(\mathrm{div}, K)\ \forall\, K \in \mathcal{T}\} \tag{3.21}$$

where d again denotes the spatial dimension of the problem. Neither of these spaces incorporates the respective boundary conditions strongly. Instead, they are stated explicitly in Eq. (3.19). This will facilitate the use of weak boundary conditions later on.

Next, finite dimensional subspaces of Σ and U are proposed. These will be the finite element approximation spaces for the eventual finite element methods. The following spaces correspond to discontinuous Galerkin methods.

$$\overline{U} = \{u \in L^2(\Omega) : u\big|_K \in P^p(K)\ \forall\, K \in \mathcal{T}\} \tag{3.22}$$

$$\overline{\Sigma} = \{\sigma \in [L^2(\Omega)]^d : \sigma\big|_K \in [P^q(K)]^d\ \forall\, K \in \mathcal{T}\} \tag{3.23}$$

where p and q are the order of the polynomial basis functions. These spaces are relatively nonrestrictive, and thereby lead to very general multiscale formulations. As was shown in Sections 2.2.1 to 2.2.3, these formulations may later be simplified in the case of higher order continuous finite element approximation spaces, or potentially $H(\mathrm{div}, \Omega)$ conforming spaces.

A projector must once again be defined in order to establish the split of the exact solutions into coarse-scale and fine-scale components. In this case, two projectors are required; one to define $\bar{u}$ and one to define $\bar{\sigma}$:

$$\mathcal{P}_u : U \to \overline{U} \tag{3.24}$$
$$\mathcal{P}_\sigma : \Sigma \to \overline{\Sigma} \tag{3.25}$$

Thereby, the coarse-scale and fine-scale components are defined as:

$$\bar{u} \equiv \mathcal{P}_u u \in \overline{U} \tag{3.26}$$
$$u' \equiv u - \bar{u} \tag{3.27}$$
$$\bar{\sigma} \equiv \mathcal{P}_\sigma \sigma \in \overline{\Sigma} \tag{3.28}$$
$$\sigma' \equiv \sigma - \bar{\sigma} \tag{3.29}$$

Under the assumption that the projectors $\mathcal{P}_u$ and $\mathcal{P}_\sigma$ are linear, idempotent, surjective mappings, the fine-scale solutions lie in the kernel of the respective projector (refer to Section 2.2 for the argumentation). This space is thereby denoted the fine-scale space. The fine-scale space and the coarse-scale space form a direct sum decomposition of Σ and U. This is summarized with:

$$u' \in \ker \mathcal{P}_u \equiv U' \tag{3.30}$$
$$\overline{U} \cap U' = \{0\} \quad \Rightarrow \quad U = \overline{U} \oplus U' \tag{3.31}$$
$$\sigma' \in \ker \mathcal{P}_\sigma \equiv \Sigma' \tag{3.32}$$
$$\overline{\Sigma} \cap \Sigma' = \{0\} \quad \Rightarrow \quad \Sigma = \overline{\Sigma} \oplus \Sigma' \tag{3.33}$$

Due to the direct sum decomposition of Σ and U into their respective coarse-scale and fine-scale spaces, any function σ or u in Σ and U maps *uniquely* to components in the coarse-scale and fine-scale spaces:

$$u \in U \quad \Leftrightarrow \quad \bar{u}, u' \in \overline{U} \times U' \tag{3.34}$$
$$\sigma \in \Sigma \quad \Leftrightarrow \quad \bar{\sigma}, \sigma' \in \overline{\Sigma} \times \Sigma' \tag{3.35}$$

Thereby, the weak form of Eq. (3.19) may equivalently be written as:

$$\text{Find } \bar{\sigma}, \bar{u}, \sigma', u' \in \overline{\Sigma} \times \overline{U} \times \Sigma' \times U' \text{ s.t.:}$$

$$\begin{cases} (\bar{\sigma} + \sigma', \bar{\tau})_{\Omega_K} = (\nabla \bar{u} + \nabla u', \bar{\tau})_{\Omega_K} & \forall\, \bar{\tau} \in \overline{\Sigma} \\ -(\nabla \cdot \bar{\sigma} + \nabla \cdot \sigma', \bar{v})_{\Omega_K} = (f, \bar{v})_{\Omega_K} & \forall\, \bar{v} \in \overline{U} \\ (\bar{\sigma} + \sigma', \tau')_{\Omega_K} = (\nabla \bar{u} + \nabla u', \tau')_{\Omega_K} & \forall\, \tau' \in \Sigma' \\ -(\nabla \cdot \bar{\sigma} + \nabla \cdot \sigma', v')_{\Omega_K} = (f, v')_{\Omega_K} & \forall\, v' \in U' \\ [\![\bar{u}]\!] = -[\![u']\!] & \text{on } \Gamma \\ [\![\bar{\sigma}]\!] = -[\![\sigma']\!] & \text{on } \Gamma \\ \bar{u} + u' = u_D & \text{on } \partial\Omega_D \\ \bar{\sigma} + \sigma' = \sigma_N & \text{on } \partial\Omega_N \end{cases} \tag{3.36}$$

where the transmission conditions from Eq. (3.19) have been written in their multiscale form.

The first two lines are closely related to finite element formulations. Focusing on those terms, and integrating by parts, results in:

$$\text{Find } \bar{\sigma}, \bar{u} \in \overline{\Sigma} \times \overline{U} \text{ s.t. } \forall\, \bar{\tau} \in \overline{\Sigma} \text{ and } \forall\, \bar{v} \in \overline{U} :$$

$$\begin{cases} (\bar{\sigma} + \sigma', \bar{\tau})_{\Omega_K} = -(\bar{u} + u', \nabla \cdot \bar{\tau})_{\Omega_K} + \sum\limits_{K \in \mathcal{T}} \langle \bar{u} + u', \bar{\tau} \cdot n \rangle_{\partial K} \\ (\bar{\sigma} + \sigma', \nabla \bar{v})_{\Omega_K} - \sum\limits_{K \in \mathcal{T}} \langle \bar{\sigma} + \sigma', \bar{v}\, n \rangle_{\partial K} = (f, \bar{v})_{\Omega_K} \end{cases} \tag{3.37}$$

where, for brevity, the transmission conditions and boundary conditions are omitted. The boundary conditions may directly be substituted into the weak form, and are thereby weakly enforced. The transmission conditions may be built into the weak form analogously to what was discussed in Section 2.2. This means that the following two relations are substituted in place of the fine-scale solution on internal element interfaces:

$$u'^{\pm}\, n^{\pm} = \{\!\{u'\}\!\} n^{\pm} - \frac{1}{2}[\![\bar{u}]\!] \tag{3.38}$$

$$\sigma'^{\pm} \cdot n^{\pm} = \{\!\{\sigma'\}\!\} \cdot n^{\pm} - \frac{1}{2}[\![\bar{\sigma}]\!] \tag{3.39}$$

The transmission conditions have already been incorporated into these identities. By also incorporating the Dirichlet and Neumann boundary conditions in a weak sense, the mixed

multiscale weak form becomes:

Find $\bar{\sigma}, \bar{u} \in \overline{\Sigma} \times \overline{U}$ s.t. $\forall\, \bar{\tau} \in \overline{\Sigma}$ and $\forall\, \bar{v} \in \times \overline{U}$:

$$\begin{cases} (\bar{\sigma}, \bar{\tau})_{\Omega_K} + (\sigma', \bar{\tau})_{\Omega_K} = -(\bar{u}, \nabla \cdot \bar{\tau})_{\Omega_K} - (u', \nabla \cdot \bar{\tau})_{\Omega_K} + \langle \{\!\{ \bar{u} \}\!\}, [\![\bar{\tau}]\!] \rangle_{\Gamma} \\ \qquad + \langle \{\!\{ u' \}\!\}, [\![\bar{\tau}]\!] \rangle_{\Gamma} + \langle u_D, \bar{\tau} \cdot n \rangle_{\partial\Omega_D} + \langle \bar{u} + u', \bar{\tau} \cdot n \rangle_{\partial\Omega_N} \\ (\bar{\sigma}, \nabla \bar{v})_{\Omega_K} + (\sigma', \nabla \bar{v})_{\Omega_K} - \langle \{\!\{ \bar{\sigma} \}\!\}, [\![\bar{v}]\!] \rangle_{\Gamma} - \langle \{\!\{ \sigma' \}\!\}, [\![\bar{v}]\!] \rangle_{\Gamma} \\ \qquad - \langle \sigma_N, \bar{v}\, n \rangle_{\partial\Omega_N} - \langle \bar{\sigma} + \sigma', \bar{v}\, n \rangle_{\partial\Omega_D} = (f, \bar{v})_{\Omega_K} \end{cases} \tag{3.40}$$

3.3 Mixed multiscale weak formulation for the advection-diffusion problem

In a similar fashion, the mixed multiscale formulation for the steady advection-diffusion equation can be derived. For reasons discussed in Section 2.1, it is challenging to develop finite element formulations that are well suited for advection based PDEs. These challenges are closely related to capturing the scale interaction in the finite element scheme. Hence, the advection-diffusion model problem is a valuable study subject. The strong form of the advection-diffusion equation that is considered herein reads:

$$\begin{cases} \nabla \cdot (a\, u) - \nabla \cdot (\nu \nabla u) = f & \text{in } \Omega \subset \mathbb{R}^d \\ u = u_D & \text{on } \partial\Omega_D \\ \nabla u \cdot n = \sigma_N \cdot n & \text{on } \partial\Omega_N \end{cases} \tag{3.41}$$

where a is the advection field, ν is the diffusion coefficient and f a source function. First, a mixed formulation of the PDE has to be chosen. The following three formulations are used throughout literature:

$$\begin{cases} \sigma = \nabla u & \text{in } \Omega \subset \mathbb{R}^d \\ a \cdot \sigma - \nabla \cdot (\nu \sigma) = f & \text{in } \Omega \\ \text{Boundary conditions} & \text{on } \partial\Omega \end{cases} \tag{3.42}$$

which is used, for instance, in [59]. A solonoidal advection field is assumed to obtain Eq. (3.42) from Eq. (3.41) (i.e. $\nabla \cdot a = 0$).

Secondly:

$$\begin{cases} \sigma = a\,u - \nu \nabla u & \text{in } \Omega \subset \mathbb{R}^d \\ \nabla \cdot \sigma = f & \text{in } \Omega \\ \text{Boundary conditions} & \text{on } \partial\Omega \end{cases} \tag{3.43}$$

As used in [22,60]. In this case, σ represents the 'total flux', meaning that in the transient equivalent problem the increase of u in a control volume will be the inflow of σ through the surface of the control volume, plus the contribution of the source function inside the control volume. Since the steady problem is considered here, these two contributions always balance on any arbitrary volume.

And thirdly:

$$\begin{cases} \nu^{-1}\sigma = \nabla u & \text{in } \Omega \subset \mathbb{R}^d \\ \nabla \cdot (a\,u - \sigma) = f & \text{in } \Omega \\ \text{Boundary conditions} & \text{on } \partial\Omega \end{cases} \tag{3.44}$$

Used in [61, 62]. The mixed format is exclusively used for the diffusive term, and the advective term is left untouched. This means that integration by parts can still be performed on the advective term. Typically, discontinuous Galerkin methods make use of specially constructed numerical fluxes to treat the resulting surface terms. A classical example is the use of upwind-type flux formulations.

Upwind numerical fluxes have played an important role throughout the development of discontinuous Galerkin formulations. They were already used in the introductory work by Reed and Hill [63]. A multiscale interpretation of these flux formulations might prove insightful. With this in mind, Eq. (3.44) is used in the following. A suitable set of transmission conditions for this problem statement reads:

$$\begin{cases} [\![u]\!] = 0 & \text{on } \Gamma \\ [\![a\,u - \sigma]\!] = 0 & \text{on } \Gamma \end{cases} \tag{3.45}$$

The derivation of the mixed multiscale weak formulation is analogous to the derivation in Section 3.2 for Poisson's equation. The same same function spaces are suitable for the current problem, and discontinuous Galerkin approximation spaces may be used to obtain the coarse-scale weak formulation. All these steps will therefore not be repeated. Instead,

the resulting mixed multiscale weak formulation is presented here directly:

Find $\bar{\sigma}, \bar{u} \in \overline{\Sigma} \times \overline{U}$ s.t. $\forall\, \bar{\tau} \in \overline{\Sigma}$ and $\forall\, \bar{v} \in \overline{U}$:

$$\begin{cases} (\nu^{-1}\bar{\sigma}, \bar{\tau})_{\Omega_K} + (\nu^{-1}\sigma', \bar{\tau})_{\Omega_K} = -(\bar{u}, \nabla\bar{\tau})_{\Omega_K} - (u', \nabla\bar{\tau})_{\Omega_K} \\ \qquad +\langle \{\!\{\bar{u}\}\!\}, [\![\bar{\tau}]\!] \rangle_\Gamma + \langle \{\!\{u'\}\!\}, [\![\bar{\tau}]\!] \rangle_\Gamma + \langle u_D, \bar{\tau}\, n \rangle_{\partial\Omega_D} + \langle \bar{u} + u', \bar{\tau} \cdot n \rangle_{\partial\Omega_N} \\ -(a\,\bar{u}, \nabla\bar{v})_{\Omega_K} - (a\,u', \nabla\bar{v})_{\Omega_K} + \langle \{\!\{a\,\bar{u}\}\!\}, [\![\bar{v}]\!] \rangle_\Gamma + \langle \{\!\{a\,u'\}\!\}, [\![\bar{v}]\!] \rangle_\Gamma \\ \qquad +\langle a\,u_D, \bar{v}\, n \rangle_{\partial\Omega_D} + \langle a\,\bar{u} + a\,u', \bar{v}\, n \rangle_{\partial\Omega_N} + (\bar{\sigma}, \nabla\bar{v})_{\Omega_K} \\ \qquad +(\sigma', \nabla\bar{v})_{\Omega_K} - \langle \{\!\{\bar{\sigma}\}\!\}, [\![\bar{v}]\!] \rangle_\Gamma - \langle \{\!\{\sigma'\}\!\}, [\![\bar{v}]\!] \rangle_\Gamma \\ \qquad -\langle \sigma_N, \bar{v}\, n \rangle_{\partial\Omega_N} - \langle \bar{\sigma} + \sigma', \bar{v}\, n \rangle_{\partial\Omega_D} = (f, \bar{v})_{\Omega_K} \end{cases} \tag{3.46}$$

3.4 Hybrid mixed multiscale weak formulation for the second order elliptic problem

As a final effort to establish the DDVMS method as a general strategy for developing multiscale weak formulations, also the class of hybrid formulations is incorporated into the framework. Quoting from Ciarlet's 1978 book *The Finite Element Method for Elliptic Problems*, a hybrid formulation is classified as a formulation where (one of) "the unknown(s) is a function together with some derivatives of this function along the boundaries of appropriate subdomains of the set Ω" [64]. Considering again Poisson's equation as a model problem. A new hybrid mixed strong form reads:

$$\begin{cases} \sigma = \nabla u & \text{in } K \subset \Omega \\ -\nabla \cdot \sigma = f & \text{in } K \\ u^+ = \hat{u} = u^- & \text{on } \partial K \setminus \partial\Omega \\ [\![\sigma]\!] = 0 & \text{on } \partial K \setminus \partial\Omega \\ u = u_D & \text{on } \partial\Omega_D \\ \sigma \cdot n = \sigma_N \cdot n & \text{on } \partial\Omega_N \end{cases} \tag{3.47}$$

A subtle difference is introduced in this formulation compared to that of Eq. (3.18) which was used in Section 3.2. In Eq. (3.18) the transmission conditions dictates that the jump of u equals zero. This condition is stated in Eq. (3.47) as $u^+ = \hat{u} = u^-$, which says that the solution u on either side of the interface equals the (single valued) variable $\hat{u}$. Hence,

the required transmission condition is implicitly satisfied. The newly introduced variable $\hat{u}$ is the unknown referred to by Ciarlet in the earlier quote.

This new variable, which is only defined on element interfaces and on the domain boundary, requires a new function space:

$$\mathcal{M}(g) = \{\mu \in L^2(\Gamma \cup \partial\Omega) : \mu = g \text{ on } \partial\Omega_D\} \tag{3.48}$$

The weak formulation of Eq. (3.47) may be obtained with the method of weighted residuals. Integration by parts is performed on the first line of Eq. (3.47) on each element, and the hybrid variable $\hat{u}$ is substituted in place of the boundary value u. This incorporates the transmission condition that involves u. The transmission condition that involves σ is weakly enforced by weighting against a test function from $\mathcal{M}(0)$. The resulting weak formulation reads:

$$\begin{aligned}
&\text{Find } \sigma, u, \hat{u} \in \Sigma \times U \times \mathcal{M}(u_D) \text{ s.t. } \forall\, \tau \in \Sigma \text{ and } \forall\, v \in U \text{ and } \forall\, \mu \in \mathcal{M}(0) : \\
&\begin{cases}
(\sigma, \tau)_{\Omega_K} = -(u, \nabla \cdot \tau)_{\Omega_K} + \langle \hat{u}, [\![\tau]\!] \rangle_{\Gamma} + \langle \hat{u}, \tau \cdot n \rangle_{\partial\Omega} \\
-(\nabla \cdot \sigma, v)_{\Omega_K} = (f, v)_{\Omega_K} \\
\langle [\![\sigma]\!], \mu \rangle_{\Gamma} + \langle \sigma \cdot n, \mu \rangle_{\partial\Omega} = \langle \sigma_N \cdot n, \mu \rangle_{\partial\Omega_N}
\end{cases}
\end{aligned} \tag{3.49}$$

where the spaces U and Σ are still those used in Section 3.2 defined in Eqs. (3.20) and (3.21).

The associated multiscale formulation requires the additional projector $\mathcal{P}_{\hat{u}} : \mathcal{M}(g) \to \overline{\mathcal{M}}(g)$. Here, $\overline{\mathcal{M}}(g)$ denotes the coarse-scale space, typically defined as:

$$\overline{\mathcal{M}}(g) = \{\mu \in L^2(\Gamma \cup \partial\Omega) : \mu\big|_e \in P^p(e)\ \forall\, e \in \Gamma \cup \partial\Omega,\ \mu = g \text{ on } \partial\Omega\} \tag{3.50}$$

where e denotes a facet or an edge of the computational mesh.

Under assumptions similar to those discussed earlier for $\mathcal{P}_u$ and $\mathcal{P}_\sigma$, the fine-scale space $\mathcal{M}'$ is then defined as:

$$\mathcal{M}' = \{\mu \in \mathcal{M}(0) : \mathcal{P}_{\hat{u}}\mu = 0\} \tag{3.51}$$

such that any $\hat{u} \in \mathcal{M}(u_D)$ uniquely splits into a coarse-scale component $\bar{\hat{u}} \in \overline{\mathcal{M}}(u_D)$ and a fine-scale component $\hat{u}' \in \mathcal{M}'$.

The decomposition of u, σ and $\hat{u}$, as well as the decomposition of the corresponding test functions, may now be substituted into Eq. (3.49). The coarse-scale weak formulation reads:

$$\begin{aligned}
&\text{Find } \bar{\sigma}, \bar{u}, \bar{\hat{u}} \in \overline{\Sigma} \times \overline{U} \times \overline{\mathcal{M}}(u_D) \text{ s.t. } \forall\, \bar{\tau} \in \overline{\Sigma} \text{ and } \forall\, \bar{v} \in \overline{U} \text{ and } \forall\, \bar{\mu} \in \overline{\mathcal{M}}(0) : \\
&\begin{cases}
(\bar{\sigma} + \sigma', \bar{\tau})_{\Omega_K} = -(\bar{u} + u', \nabla \cdot \bar{\tau})_{\Omega_K} + \langle \bar{\hat{u}} + \hat{u}', [\![\bar{\tau}]\!] \rangle_{\Gamma} + \langle \bar{\hat{u}} + \hat{u}', \bar{\tau} \cdot n \rangle_{\partial\Omega} \\
-(\nabla \cdot \bar{\sigma}, \bar{v})_{\Omega_K} + (\sigma', \nabla \bar{v})_{\Omega_K} - \langle \{\!\{\sigma'\}\!\}, [\![\bar{v}]\!] \rangle_{\Gamma} - \langle [\![\sigma']\!], \{\!\{\bar{v}\}\!\} \rangle_{\Gamma} - \langle \sigma', \bar{v}\, n \rangle_{\partial\Omega} = (f, \bar{v})_{\Omega_K} \\
\langle [\![\bar{\sigma}]\!] + [\![\sigma']\!], \bar{\mu} \rangle_{\Gamma} + \langle \bar{\sigma} \cdot n + \sigma' \cdot n, \bar{\mu} \rangle_{\partial\Omega} = \langle \sigma_N \cdot n, \bar{\mu} \rangle_{\partial\Omega_N}
\end{cases}
\end{aligned} \tag{3.52}$$

where integration by parts has been performed on the fine-scale term in the second line.

A few comments have to be made at this point. The DDVMS framework used in the previous two sections offers a novel derivation of discontinuous Galerkin methods in the sense that the transmission conditions are naturally incorporated into the weak formulation, instead of being hidden in the choice of numerical fluxes. This is no longer applicable for the weak form of Eq. (3.52), since the transmission conditions are explicitly included as additional weak forms. Then, the contribution of the DDVMS framework is limited to the substitution of the scale decomposition. This might appear trivial. Yet, it still shows that a closure model in terms of a fine-scale constraint is required to obtain a closed finite-element formulation. This closure model goes hand in hand with the projector that governs the scale decomposition. The projectors that are implicitly employed by existing finite element formulations (the Hybridizable DG method in particular) may then be revealed by comparing the finite element formulation to the multiscale weak formulation. Such endeavors are the general focus of Chapter 4.

Chapter 4

Analysis of existing methods for second order problems

The mixed multiscale formulations derived in the previous chapter can not immediately be used as finite element formulations. A closure model must first be substituted in place of the fine-scale terms. It turns out that many discontinuous Galerkin methods can be interpreted as particular choices of closure models. This concept is explored in this chapter.

In Sections 4.1 to 4.4, Poisson's equation is investigated. First, the closure models implicitly incorporated in standard discontinuous Galerkin formulations are expressed as fine-scale constraint equations. Next, in Section 4.2, the effect of the fine-scale constraint equations for the different methods is evaluated. In the one-dimensional case, a variety of strong, pointwise, identities may be derived for each of the methods. The mixed multiscale formulations are altered slightly in Section 4.3 such that the fine-scale constraints corresponding to the Raviart-Thomas and Brezzi-Douglas-Marini methods can be derived. Then, in Section 4.4, the hybridized multiscale formulation for Poisson's equation is used to obtain the fine-scale constraints associated to Hybridizable discontinuous Galerkin formulation. Sections 4.5 and 4.6 address similar points for the advection-diffusion model problem. The fine-scale constraint equations are derived in Section 4.5, where the use of upwind numerical fluxes is central. In Section 4.6, the obtained equations are analyzed. For brevity, only the one-dimensional case is considered. Throughout this chapter it is shown for a number of finite element methods that the fine-scale constraints directly correspond to minimization or saddle-point problems which characterize the projector that captures the scale decomposition.

4.1 Fine-scale constraints of classical discontinuous Galerkin formulations for second order elliptic problems

In order to place the classical discontinuous Galerkin method in this new context, an overview of the methods is first provided. To shorten the equations, the weak forms are collapsed into single-line expressions of the following form:

$$B\big((u_h,\sigma_h),(\bar{v},\bar{\tau})\big) = L\big((\bar{v},\bar{\tau})\big) \qquad \forall\, \bar{v},\bar{\tau} \in \overline{U}\times\overline{\Sigma} \tag{4.1}$$

where u_h and σ_h are the finite element approximations, $B(\cdot,\cdot)$ is the bilinear form that involves both test functions and both trial functions simultaneously and $L(\cdot)$ is the linear form. The bilinear forms of different classical methods are collected in Table 4.1. Boundary terms are omitted for brevity.

Table 4.1: *Overview of discontinuous Galerkin formulations for second order elliptic problems. Based on flux formulations from [45].*

Method name	**Bilinear form** $B\big((u_h,\sigma_h),(\bar{v},\bar{\tau})\big)$
Bassi-Rebay [65]	$(\sigma_h,\bar{\tau})_{\Omega_K} + (u_h,\nabla\cdot\bar{\tau})_{\Omega_K} - \langle\{\!\{u_h\}\!\},[\![\bar{\tau}]\!]\rangle_\Gamma + (\sigma_h,\nabla\bar{v})_{\Omega_K} - \langle\{\!\{\sigma_h\}\!\},[\![\bar{v}]\!]\rangle_\Gamma$
IP [66]	$(\sigma_h,\bar{\tau})_{\Omega_K} + (u_h,\nabla\cdot\bar{\tau})_{\Omega_K} - \langle\{\!\{u_h\}\!\},[\![\bar{\tau}]\!]\rangle_\Gamma + (\sigma_h,\nabla\bar{v})_{\Omega_K}$ $- \langle\{\!\{\nabla u_h\}\!\},[\![\bar{v}]\!]\rangle_\Gamma + \langle\eta h^{-1}[\![u_h]\!],[\![\bar{v}]\!]\rangle_\Gamma$
Local DG [67]	$(\sigma_h,\bar{\tau})_{\Omega_K} + (u_h,\nabla\cdot\bar{\tau})_{\Omega_K} - \langle\{\!\{u_h\}\!\},[\![\bar{\tau}]\!]\rangle_\Gamma + (\sigma_h,\nabla\bar{v})_{\Omega_K} - \langle\{\!\{\sigma_h\}\!\},[\![\bar{v}]\!]\rangle_\Gamma$ $- \langle\beta[\![\sigma_h]\!],[\![\bar{v}]\!]\rangle_\Gamma + \langle\eta h^{-1}[\![u_h]\!],[\![\bar{v}]\!]\rangle_\Gamma$
Baumann-Oden [68]	$(\sigma_h,\bar{\tau})_{\Omega_K} - \langle\{\!\{u_h\}\!\},[\![\bar{\tau}]\!]\rangle_\Gamma - \langle 2[\![u_h]\!],\{\!\{\bar{\tau}\}\!\}\rangle_\Gamma + (\sigma_h,\nabla\bar{v})_{\Omega_K}$ $+ (u_h,\nabla\cdot\bar{\tau})_{\Omega_K} - \langle\{\!\{\nabla u_h\}\!\},[\![\bar{v}]\!]\rangle_\Gamma$
NIPG [69]	$(\sigma_h,\bar{\tau})_{\Omega_K} - \langle\{\!\{u_h\}\!\},[\![\bar{\tau}]\!]\rangle_\Gamma - \langle 2[\![u_h]\!],\{\!\{\bar{\tau}\}\!\}\rangle_\Gamma + (\sigma_h,\nabla\bar{v})_{\Omega_K}$ $+ (u_h,\nabla\cdot\bar{\tau})_{\Omega_K} - \langle\{\!\{\nabla u_h\}\!\},[\![\bar{v}]\!]\rangle_\Gamma + \langle\eta h^{-1}[\![u_h]\!],[\![\bar{v}]\!]\rangle_\Gamma$

The linear form for this problem is the same for all methods:

$$L\big((\bar{v},\bar{\tau})\big) = \big(f,\bar{v}\big)_{\Omega_K} + \big\langle u_D, \bar{\tau}\cdot n\big\rangle_{\partial\Omega_D} + \big\langle \sigma_N, \bar{v}\, n\big\rangle_{\partial\Omega_N} \tag{4.2}$$

The finite element solutions u_h and σ_h that occur in the formulations in Table 4.1 are members of $\overline{U}$ and $\overline{\Sigma}$. They may thus be *defined* as the solutions $\bar{u}$ and $\bar{\sigma}$ obtained as the projections of u and σ onto $\overline{U}$ and $\overline{\Sigma}$ by the projectors $\mathcal{P}_u$ and $\mathcal{P}_\sigma$. When these formulations are then compared to the exact multiscale formulation of Eq. (3.40), one can conclude that different closure models have been incorporated into the multiscale formulation in order to obtain each of the formulations in Table 4.1.

To explore this concept more rigorously, the mixed multiscale formulations of Eq. (3.40) must first be written in a form similar to Eq. (4.1). For the case of Eq. (3.40) this would lead to:

$$B^*\big((\bar{u},u',\bar{\sigma},\sigma'),(\bar{v},\bar{\tau})\big) = L\big((\bar{v},\bar{\tau})\big) \qquad \forall\, \bar{v},\bar{\tau} \in \overline{U}\times\overline{\Sigma} \tag{4.3}$$

Since the linear form in Eq. (4.3) equals the linear form in Eq. (4.1), the left-hand sides of these equations may be equated. The fine-scale constraint equations that are implicitly satisfied by the methods in Table 4.1 may then be obtained by canceling the coarse-scale terms that occur on either side. Consider, for example, the Bassi-Rebay method (but now including the domain boundary terms):

$$\begin{aligned}
&\big(\bar{\sigma},\bar{\tau}\big)_{\Omega_K} + \big(\bar{u},\nabla\cdot\bar{\tau}\big)_{\Omega_K} - \big\langle\{\!\{\bar{u}\}\!\},[\![\bar{\tau}]\!]\big\rangle_\Gamma + \big(\bar{\sigma},\nabla\bar{v}\big)_{\Omega_K} - \big\langle\{\!\{\bar{\sigma}\}\!\},[\![\bar{v}]\!]\big\rangle_\Gamma \\
&\qquad - \big\langle\bar{u},\bar{\tau}\cdot n\big\rangle_{\partial\Omega_N} - \big\langle\bar{\sigma},\bar{v}\,n\big\rangle_{\partial\Omega_D} \\
&\qquad\qquad = \\
&\big(\bar{\sigma},\bar{\tau}\big)_{\Omega_K} + \big(\sigma',\bar{\tau}\big)_{\Omega_K} + \big(\bar{u},\nabla\cdot\bar{\tau}\big)_{\Omega_K} + \big(u',\nabla\cdot\bar{\tau}\big)_{\Omega_K} - \big\langle\{\!\{\bar{u}\}\!\},[\![\bar{\tau}]\!]\big\rangle_\Gamma - \big\langle\{\!\{u'\}\!\},[\![\bar{\tau}]\!]\big\rangle_\Gamma \\
&\qquad + \big(\bar{\sigma},\nabla\bar{v}\big)_{\Omega_K} + \big(\sigma',\nabla\bar{v}\big)_{\Omega_K} - \big\langle\{\!\{\bar{\sigma}\}\!\},[\![\bar{v}]\!]\big\rangle_\Gamma - \big\langle\{\!\{\sigma'\}\!\},[\![\bar{v}]\!]\big\rangle_\Gamma \\
&\qquad - \big\langle\bar{u}+u',\bar{\tau}\cdot n\big\rangle_{\partial\Omega_N} - \big\langle\bar{\sigma}+\sigma',\bar{v}\,n\big\rangle_{\partial\Omega_D}
\end{aligned} \tag{4.4}$$

And after canceling identical terms:

Bassi-Rebay:

$$\begin{aligned}
&\big(\sigma',\bar{\tau}\big)_{\Omega_K} + \big(u',\nabla\cdot\bar{\tau}\big)_{\Omega_K} - \big\langle\{\!\{u'\}\!\},[\![\bar{\tau}]\!]\big\rangle_\Gamma - \big\langle u',\bar{\tau}\cdot n\big\rangle_{\partial\Omega_N} = 0 \\
&\big(\sigma',\nabla\bar{v}\big)_{\Omega_K} - \big\langle\{\!\{\sigma'\}\!\},[\![\bar{v}]\!]\big\rangle_\Gamma - \big\langle\sigma',\bar{v}\,n\big\rangle_{\partial\Omega_D} = 0
\end{aligned} \tag{4.5}$$

which holds for all $\bar{v}\in\overline{U}$ and all $\bar{\tau}\in\overline{\Sigma}$.

These fine-scale constraint equations close the finite element formulation from a multiscale perspective. They are the fundamental difference between the Bassi-Rebay method and the other methods in Table 4.1, which make use of different fine-scale constraints. In this sense, these equations define the Bassi-Rebay method. More specifically, they define the projectors $\mathcal{P}_u : U \to \overline{U}$ and $\mathcal{P}_\sigma : \Sigma \to \overline{\Sigma}$ that are implicitly employed by the Bassi-Rebay method. In this particular case, the projectors may even be interpreted as saddle point problems. Notice that Eq. (4.5) is the variational formulation of:

$$\inf_{\bar{u}\in\overline{U}} \sup_{\bar{\sigma}\in\overline{\Sigma}} \int_{\Omega_K} \frac{1}{2}(\nabla u - \nabla\bar{u})^2 - \frac{1}{2}(\bar{\sigma} - \nabla\bar{u})^2 + \int_{\Gamma} [\![\bar{u}]\!] \cdot \{\!\{\sigma - \bar{\sigma}\}\!\} - \int_{\partial\Omega_D} (u - \bar{u}) n \cdot (\sigma - \bar{\sigma}) \tag{4.6}$$

where the true solutions u and σ are treated as data. By solving the Bassi-Rebay finite element formulation, one thus obtains the coarse-scale solution that best approximates the true solution according to the saddle point problem of Eq. (4.6).

In a similar fashion, the fine-scale constraints corresponding to all the other methods in Table 4.1 may be derived. Below follows an overview of the obtained expressions.

The fine-scale constraint employed by the symmetric interior penalty (IP) method reads:

Symmetric interior penalty:

$$\begin{aligned} &(\sigma', \bar{\tau})_{\Omega_K} + (u', \nabla\cdot\bar{\tau})_{\Omega_K} - \langle \{\!\{u'\}\!\}, [\![\bar{\tau}]\!] \rangle_{\Gamma} - \langle u', \bar{\tau}\cdot n\rangle_{\partial\Omega_N} = 0 \\ &(\sigma', \nabla\bar{v})_{\Omega_K} - \langle \{\!\{\nabla u'\}\!\}, [\![\bar{v}]\!] \rangle_{\Gamma} + \langle \tfrac{\eta}{h}[\![u']\!], [\![\bar{v}]\!] \rangle_{\Gamma} - \langle \nabla u', \bar{v}\, n\rangle_{\partial\Omega_D} + \langle \tfrac{\eta}{h} u'\, n, \bar{v}\, n\rangle_{\partial\Omega_D} = 0 \end{aligned} \tag{4.7}$$

for which the associated projectors $\mathcal{P}_u$ and $\mathcal{P}_\sigma$ do not immediately correspond to a saddle point problem. However, if $\nabla\bar{v} \in \overline{\Sigma}\ \forall\, \bar{v} \in \overline{U}$, then by choosing $\bar{\tau} = \nabla\bar{v}$ in Eq. (4.7) this equation may be collapsed into a single expression referring to the primal form [45]. The associated projector $\mathcal{P}_u$ is the minimizer of:

$$\begin{aligned} J_{\bar{u}}(\bar{u}, \nabla\bar{u}; u, \nabla u) = &\int_{\Omega_K} \frac{1}{2}(\nabla u - \nabla\bar{u})^2 + \int_{\Gamma} [\![\bar{u}]\!] \{\!\{\nabla u - \nabla\bar{u}\}\!\} + \frac{1}{2}\eta h^{-1} [\![\bar{u}]\!]^2 \\ &+ \int_{\partial\Omega_D} -(u - \bar{u}) n \cdot (\nabla u - \nabla\bar{u}) + \frac{1}{2}\eta h^{-1}(u - \bar{u})^2 \end{aligned} \tag{4.8}$$

where, again, u and σ are treated as data. Subsequently, $\bar{\sigma}$ is obtained with $\mathcal{P}_\sigma$, which is the minimizer of:

$$J_{\bar{\sigma}}(\bar{\sigma}; \bar{u}, \nabla\bar{u}, u, \nabla u) = \int_{\Omega_K} \frac{1}{2}(\bar{\sigma} - \nabla\bar{u})^2 - \int_{\Gamma} [\![\bar{u}]\!] \cdot \{\!\{\sigma - \bar{\sigma}\}\!\} + \int_{\partial\Omega_D} (u - \bar{u}) n \cdot (\sigma - \bar{\sigma}) \tag{4.9}$$

where now also $\bar{u}$ is treated as data, since it has been obtained earlier with $\mathcal{P}_u$.

The fine-scale constraint equation for the Local DG method reads:

Local DG:

$$\begin{aligned}
&(\sigma', \bar{\tau})_{\Omega_K} + (u', \nabla \cdot \bar{\tau})_{\Omega_K} - \langle \{\!\{ u' \}\!\}, [\![\bar{\tau}]\!] \rangle_{\Gamma} + \langle \beta \cdot [\![u']\!], [\![\bar{\tau}]\!] \rangle_{\Gamma} - \langle u', \bar{\tau} \cdot n \rangle_{\partial\Omega_N} = 0 \\
&(\sigma', \nabla \bar{v})_{\Omega_K} - \langle \{\!\{ \sigma' \}\!\}, [\![\bar{v}]\!] \rangle_{\Gamma} - \langle \sigma', \bar{v}\, n \rangle_{\partial\Omega_D} \\
&\qquad - \langle \beta [\![\sigma']\!], [\![\bar{v}]\!] \rangle_{\Gamma} + \langle \tfrac{\eta}{h} [\![u']\!], [\![\bar{v}]\!] \rangle_{\Gamma} + \langle \tfrac{\eta}{h} u'\, n, \bar{v}\, n \rangle_{\partial\Omega_D} = 0
\end{aligned} \tag{4.10}$$

which is the variational form of the following saddle point problem:

$$\begin{aligned}
\inf_{\bar{u} \in \overline{U}} \sup_{\bar{\sigma} \in \overline{\Sigma}} & \int_{\Omega_K} \frac{1}{2} (\nabla u - \nabla \bar{u})^2 - \frac{1}{2} (\bar{\sigma} - \nabla \bar{u})^2 + \int_{\Gamma} [\![\bar{u}]\!] \{\!\{ \sigma - \bar{\sigma} \}\!\} + \frac{1}{2} \eta h^{-1} [\![\bar{u}]\!]^2 - \beta \cdot [\![\bar{u}]\!] [\![\bar{\sigma}]\!] \\
& + \int_{\partial\Omega_D} -(u - \bar{u}) n \cdot (\sigma - \bar{\sigma}) + \frac{1}{2} \eta h^{-1} (u - \bar{u})^2
\end{aligned} \tag{4.11}$$

which again offers an explicit interpretation of the nature of the projectors $\mathcal{P}_u : U \to \overline{U}$ and $\mathcal{P}_\sigma : \Sigma \to \overline{\Sigma}$ for the Local DG method.

The Baumann-Oden method corresponds to the following fine-scale constraint equation:

Baumann-Oden:

$$\begin{aligned}
&(\sigma', \bar{\tau})_{\Omega_K} + (u', \nabla \cdot \bar{\tau})_{\Omega_K} - \langle \{\!\{ u' \}\!\}, [\![\bar{\tau}]\!] \rangle_{\Gamma} - \langle 2 [\![u']\!], \{\!\{ \bar{\tau} \}\!\} \rangle_{\Gamma} - \langle u', \bar{\tau} \cdot n \rangle_{\partial\Omega_N} = 0 \\
&(\sigma', \nabla \bar{v})_{\Omega_K} - \langle \{\!\{ \nabla u' \}\!\}, [\![\bar{v}]\!] \rangle_{\Gamma} - \langle \nabla u', \bar{v}\, n \rangle_{\partial\Omega_D} = 0
\end{aligned} \tag{4.12}$$

For which the author has not been able to find an associated saddle point problem. Nor has this been found for the fine-scale constraint of the nonsymmetric interior penalty Galerkin (NIPG) method:

Nonsymmetric interior penalty Galerkin:

$$\begin{aligned}
&(\sigma', \bar{\tau})_{\Omega_K} + (u', \nabla \cdot \bar{\tau})_{\Omega_K} - \langle \{\!\{ u' \}\!\}, [\![\bar{\tau}]\!] \rangle_{\Gamma} - \langle 2 [\![u']\!], \{\!\{ \bar{\tau} \}\!\} \rangle_{\Gamma} - \langle u', \bar{\tau} \cdot n \rangle_{\partial\Omega_N} = 0 \\
&(\sigma', \nabla \bar{v})_{\Omega_K} - \langle \{\!\{ \nabla u' \}\!\}, [\![\bar{v}]\!] \rangle_{\Gamma} + \langle \tfrac{\eta}{h} [\![u']\!], [\![\bar{v}]\!] \rangle_{\Gamma} - \langle \nabla u', \bar{v}\, n \rangle_{\partial\Omega_D} + \langle \tfrac{\eta}{h} u'\, n, \bar{v}\, n \rangle_{\partial\Omega_D} = 0
\end{aligned} \tag{4.13}$$

4.2 Analysis of discontinuous Galerkin formulations for second order elliptic problems

In this section, the fine-scale constraints of Eqs. (4.5), (4.7), (4.10), (4.12) and (4.13) are analyzed. Since the fine-scale solution may equivalently be interpreted as the approximation error, these fine-scale constraints provide information on how the error behaves. The fine-scale constraints hold for all test functions $\bar{\tau} \in \overline{\Sigma}$ and all $\bar{v} \in \overline{U}$. Useful error expressions can be obtained by choosing specific functions for $\bar{\tau}$ and $\bar{v}$, and substituting these into the fine-scale constraint equations. This is the general approach adopted throughout this section.

A subdivision into different problem statements and different classes of methods is required to provide a clean overview of the resulting error expressions. In particular are the one-dimensional case and the multidimensional case considered separately. Additionally, it proves beneficial to subdivided the methods in those that are 'conservative' and those that are 'non-conservative'. A discontinuous Galerkin formulation is conservative if the following properties hold:

$$\begin{cases} \int\limits_D \sigma_h \cdot \tau_c + \int\limits_{\partial D} g(u_h, \sigma_h)\tau_c \cdot n = 0 \\ \int\limits_D f + \int\limits_{\partial D} h(u_h, \sigma_h) \cdot n = 0 \end{cases} \tag{4.14}$$

where D is a subdomain of Ω comprised of any collection of finite elements, and $g(u_h, \sigma_h)$ and $h(u_h, \sigma_h)$ are fluxes that depend on the method at hand. For the conservative methods, this identity may be obtained by choosing the constant test functions $\bar{v} = 1$ and $\bar{\tau} = \tau_c$ inside D, and with zero values outside of D (which is possible because of the discontinuous nature of the coarse-scale approximation spaces). Equation (4.14) is retrieved if the flux formulations employed for the discontinuous Galerkin method are single valued on element interfaces. These are the Bassi-Rebay method, the IP method and the Local DG method. If the surface integrals from the element boundaries interior to D would not cancel, then the flux formulations are non-conservative. This is the case for the Baumann-Oden method and the NIPG method.

The fine-scale constraints of each of the conservative methods, i.e. Eqs. (4.5), (4.7)

and (4.10), may be written in the following general form:

$$\text{Find } \bar{\sigma}, \bar{u} \in \overline{\Sigma} \times \overline{U} \text{ s.t.:}$$
$$\begin{cases} (\sigma', \bar{\tau})_{\Omega_K} + (u', \nabla \cdot \bar{\tau})_{\Omega_K} - \langle \mathcal{A}', [\![\bar{\tau}]\!] \rangle_{\Gamma} - \langle \mathcal{N}', \bar{\tau} \cdot n \rangle_{\partial\Omega_N} = 0 \\ (\sigma', \nabla \bar{v})_{\Omega_K} - \langle \mathcal{B}', [\![\bar{v}]\!] \rangle_{\Gamma} - \langle \mathcal{D}', \bar{v} \rangle_{\partial\Omega_D} = 0 \end{cases} \tag{4.15}$$

where $\mathcal{A}'$ and $\mathcal{B}'$ are functions of u' and σ' on Γ, and $\mathcal{N}'$ and $\mathcal{D}'$ are functions of u' and σ' on $\partial\Omega_N$ and $\partial\Omega_D$ respectively. Table 4.2 provides an overview of their expressions for the different methods.

The Baumann-Oden and the NIPG method are non-conservative in their $\widehat{un}$ description. This leads to an additional terms in the corresponding fine-scale constraint equations, Eqs. (4.12) and (4.13). The general formulation of these fine-scale constraints reads:

$$\text{Find } \bar{\sigma}, \bar{u} \in \overline{\Sigma} \times \overline{U} \text{ s.t.:}$$
$$\begin{cases} (\sigma', \bar{\tau})_{\Omega_K} + (u', \nabla \cdot \bar{\tau})_{\Omega_K} - \langle \mathcal{A}', [\![\bar{\tau}]\!] \rangle_{\Gamma} - \langle \mathcal{H}', \{\!\{\bar{\tau}\}\!\} \rangle_{\Gamma} - \langle \mathcal{N}', \bar{\tau} \cdot n \rangle_{\partial\Omega_N} = 0 \\ (\sigma', \nabla \bar{v})_{\Omega_K} - \langle \mathcal{B}', [\![\bar{v}]\!] \rangle_{\Gamma} - \langle \mathcal{D}', \bar{v} \rangle_{\partial\Omega_D} = 0 \end{cases} \tag{4.16}$$

where $\mathcal{H}'$ is newly introduced as some function of u' and σ' on Γ. The expressions for $\mathcal{A}'$, $\mathcal{H}'$, $\mathcal{N}'$, $\mathcal{B}'$ and $\mathcal{D}'$ for the Baumann-Oden and the NIPG method are provided in Table 4.3.

The analysis of the fine-scale constraint equations is performed on the general formulations of Eqs. (4.15) and (4.16) rather than for all the methods separately. The expressions for $\mathcal{A}'$, $\mathcal{H}'$, $\mathcal{N}'$, $\mathcal{B}'$ and $\mathcal{D}'$ are substituted in the end.

Table 4.2: *Collection of $\mathcal{A}'$, $\mathcal{N}'$, $\mathcal{B}'$ and $\mathcal{D}'$ expressions for the conservative methods.*

	Bassi-Rebay	**IP**	**Local DG**
$\mathcal{A}'$	$\{\!\{u'\}\!\}$	$\{\!\{u'\}\!\}$	$\{\!\{u'\}\!\}$
$\mathcal{N}'$	u'	u'	u'
$\mathcal{B}'$	$\{\!\{\sigma'\}\!\}$	$\{\!\{\nabla u'\}\!\} - \eta h^{-1} [\![u']\!]$	$\{\!\{\sigma'\}\!\} + \beta [\![\sigma']\!] - \eta h^{-1} [\![u']\!]$
$\mathcal{D}'$	$\sigma' \cdot n$	$\nabla u' \cdot n - \eta h^{-1} u'$	$\sigma' \cdot n - \eta h^{-1} u'$

Table 4.3: *Collection of $\mathcal{A}'$, $\mathcal{H}'$, $\mathcal{N}'$, $\mathcal{B}'$ and $\mathcal{D}'$ expressions for the non-conservative methods.*

	Baumann-Oden	**NIPG**
$\mathcal{A}'$	$\{\!\{u'\}\!\}$	$\{\!\{u'\}\!\}$
$\mathcal{H}'$	$2\,[\![u']\!]$	$2\,[\![u']\!]$
$\mathcal{N}'$	u'	u'
$\mathcal{B}'$	$\{\!\{\nabla u'\}\!\}$	$\{\!\{\nabla u'\}\!\} - \eta h^{-1}[\![u']\!]$
$\mathcal{D}'$	$\nabla u' \cdot n$	$\nabla u' \cdot n - \eta h^{-1} u'$

4.2.1 One-dimensional case

The simplicity of the one-dimensional case makes it a valuable study subject for developing an intuitive understanding of Equations (4.15) and (4.16). First, the conservative methods captured by Eq. (4.15) are evaluated, and then the same approach is used for the non-conservative methods corresponding to Eq. (4.16). The obtained results are tabulated at the end of the analysis for either of the classes of methods.

Analysis of the conservative methods

Equation (4.15) can be split into a system of equations by considering each of the potential test functions separately. Meaningful expressions may be obtained by using carefully constructed test functions.

Consider, for example, a constant test function $\bar{v}$ as shown in Figure 4.1. Substitution of $\bar{v}$ into the second line of Eq. (4.15) only leaves the integral on the Dirichlet boundary. If both the left side of the domain and the right side of the domain are Dirichlet boundaries, then the integrals on those boundaries must add up to zero. If only one of the two domain boundaries is a Dirichlet boundary, then the integral on that boundary alone must equal zero. Since surface integrals on one-dimension are simply pointwise values, the following expressions remain:

For two Dirichlet boundaries:	**For one Dirichlet boundary:**	
$\mathcal{D}'\big\vert_{\partial\Omega_\mathrm{l}} + \mathcal{D}'\big\vert_{\partial\Omega_\mathrm{r}} = 0$	$\mathcal{D}' = 0 \qquad \text{at } \partial\Omega_D$	(4.17)

where $\partial\Omega_\mathrm{l}$ and $\partial\Omega_\mathrm{r}$ denote the left and right domain boundary respectively.

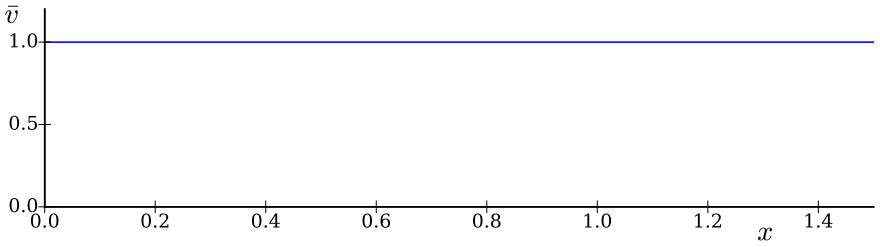

Fig. 4.1: *Test function one, constant value.*

Since the left and right boundary are the only boundaries of Ω, two Dirichlet boundaries automatically means that there is no Neumann boundary. If, for that case, the same constant value as shown in Figure 4.1 is substituted in place of $\bar{\tau}$ into the first line of Eq. (4.15), then one obtains:

For two Dirichlet boundaries:

$$\int_{\Omega} \sigma' = 0 \tag{4.18}$$

Then, by choosing a test function $\bar{v}$ according to Figure 4.2, and by substituting this into the second line of Eq. (4.15):

For two Dirichlet boundaries:

$$\mathcal{D}'\big|_{\partial\Omega_\mathrm{l}} = -\frac{1}{|\Omega|}\int_{\Omega} \sigma' = 0 = \mathcal{D}'\big|_{\partial\Omega_\mathrm{r}} \tag{4.19}$$

where $|\Omega|$ denotes the width of the domain, which is introduced due to the differentiation of $\bar{v}$. So in both the case of one Dirichlet boundary, and the case of two Dirichlet boundaries, $\mathcal{D}' = 0$ on both domain boundaries.

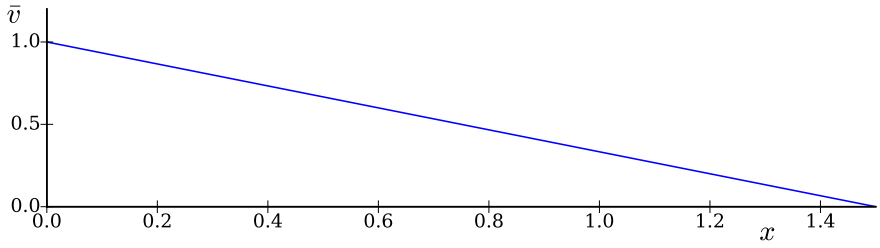

Fig. 4.2: *Test function two, constant slope.*

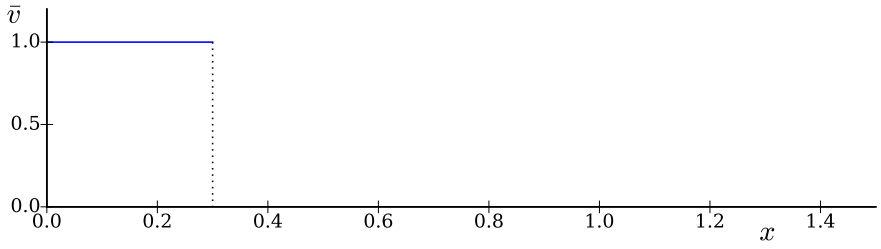

Fig. 4.3: *Test function three, step function.*

Next, take $\bar{v}$ as a step function that equals 1 to the left of some element interface point $\hat{x}$, and 0 to its right. Such a function is illustrated in Figure 4.3.

Substitution thereof into the second line of Eq. (4.15) only leaves a single jumps term, and potentially a Dirichlet term. Since it was just shown that this Dirichlet term is identically zero, it follows that:

For one or two Dirichlet boundaries:

$$\mathcal{B}'\big|_{\hat{x}} = 0 \qquad \forall\, \hat{x} \in \Gamma \tag{4.20}$$

In summary, for either one or two Dirichlet boundaries:

$$\begin{cases} \mathcal{D}' = 0 & \text{on } \partial\Omega_D \\ \mathcal{B}' = 0 & \text{on } \Gamma \end{cases} \tag{4.21}$$

Substituting this back into the fine-scale constraint also results in:

$$\left(\sigma', \nabla\bar{v}\right)_{\Omega_K} = 0 \quad \forall\, \bar{v} \in \overline{U} \tag{4.22}$$

This relation may be written more explicitly as:

$$\int_K \sigma' x^{\hat{p}-1} = 0 \qquad \forall\, \hat{p} \in \mathbb{Z} : 1 \leq \hat{p} \leq p\,, \quad \forall\, K \in \mathcal{T} \tag{4.23}$$

where p is the polynomial order associated to $\overline{U}$.

Under the assumption that $p \geq 1$, which is already implicitly assumed in Figure 4.2, the $\left(\sigma', \bar{\tau}\right)_{\Omega_K}$ term in the first line of Eq. (4.15) cancels for piecewise constant $\bar{\tau}$. An analogous

analysis as before, but now for the $\bar{\tau}$ test function rather than for $\bar{v}$, yields:

$$\begin{cases} \mathcal{N}' = 0 & \text{on } \partial\Omega_N \\ \mathcal{A}' = 0 & \text{on } \Gamma \end{cases} \tag{4.24}$$

Therefore, the remaining volumetric relation is:

$$(\sigma', \bar{\tau})_{\Omega_K} + (u', \nabla \cdot \bar{\tau})_{\Omega_K} = 0 \quad \forall\, \bar{\tau} \in \overline{\Sigma} \tag{4.25}$$

which can be written more explicitly as:

$$\int_K \sigma' x^{\hat{q}} + \hat{q}\, u' x^{\hat{q}-1} = 0 \qquad \forall\, \hat{q} \in \mathbb{Z} : 1 \leq \hat{q} \leq q\,, \quad \forall\, K \in \mathcal{T} \tag{4.26}$$

where q is the polynomial order associated to $\overline{\Sigma}$. Combined with Eq. (4.23) this would also result in zero integrals of $u' x^{\hat{q}-1}$ for polynomial orders up to $\hat{q} = \hat{p} - 1$.

Summary and illustrations for the conservative methods

All the obtained expressions are summarized in Table 4.4. The expressions for $\mathcal{A}'$, $\mathcal{B}'$, $\mathcal{D}'$ and $\mathcal{N}'$ are filled in for the Bassi-Rebay, the IP and the Local DG methods.

Some of these identities are illustrated in Figs. 4.4 to 4.6. These concern numerical experiments on a domain $\Omega = [\,-1, 4\,]$ discretized with 3 elements. Linear basis functions are used to construct $\overline{U}$ and quadratics are used for the construction of $\overline{\Sigma}$. The boundary conditions are $\sigma = 1.8$ at the left boundary and $u = 6.5$ at the right boundary. The source function is described by:

$$f = -6x + 2.4x^2 \tag{4.27}$$

which leads to the exact solution:

$$u = 1.7 - 2x + x^3 - 0.2x^4 \tag{4.28}$$

$$\sigma = -2 + 3x^2 - 0.8x^3 \tag{4.29}$$

Figure 4.4 shows the resulting coarse-scale solution for the Bassi-Rebay method. The figure illustrates that the average fine-scale solutions are zero at element interfaces, and

Table 4.4: *Identities for the conservative methods for a one-dimensional Poisson equation. Assuming that the polynomial basis for the primal variable is at least of order one.*

	Bassi-Rebay	**IP**	**Local DG**
On Γ:	$\{\!\{u'\}\!\} = 0$	$\{\!\{u'\}\!\} = 0$	$\{\!\{u'\}\!\} - \beta \cdot [\![u']\!] = 0$
On Γ:	$\{\!\{\sigma'\}\!\} = 0$	$\{\!\{\nabla u'\}\!\} - \frac{\eta}{h}[\![u']\!] = 0$	$\{\!\{\sigma'\}\!\} + \beta[\![\sigma']\!] - \frac{\eta}{h}[\![u']\!] = 0$
On $\partial\Omega_N$:	$u' = 0$	$u' = 0$	$u' = 0$
On $\partial\Omega_D$:	$\sigma' \cdot n = 0$	$\nabla u' \cdot n - \frac{\eta}{h}u' = 0$	$\sigma' \cdot n - \frac{\eta}{h}u' = 0$
$\forall\, K \in \mathcal{T}$:	$\int_K \sigma' x^{\hat{p}-1} = 0 \qquad \forall\, \hat{p} \in \mathbb{Z} : 1 \leq \hat{p} \leq p$		
$\forall\, K \in \mathcal{T}$:	$\int_K \sigma' x^{\hat{q}} + \hat{q}\, u' x^{\hat{q}-1} = 0 \qquad \forall\, \hat{q} \in \mathbb{Z} : 1 \leq \hat{q} \leq q$		

thus that the average coarse-scale solutions equal the exact solution. It also shows that the coarse-scale primal variable equals the exact solution at the Neumann boundary, and that the coarse-scale auxiliary variable is exact at the Dirichlet boundary. Similarly, Figure 4.4 shows the pointwise identities corresponding to the symmetric interior penalty method. Those that involve $\nabla u'$ have been numerically verified, but are not illustrated. Finally, the identities obtained for the Local DG method are shown in Figure 4.6. The left figure shows that the magnitudes of $\{\!\{u'\}\!\}$ and $[\![u']\!]$ are equal (since for these experiments $\beta = 1$). The right figure shows that $\{\!\{\sigma'\}\!\}$ is a weighted sum of $[\![\sigma']\!]$ and $[\![u']\!]$.

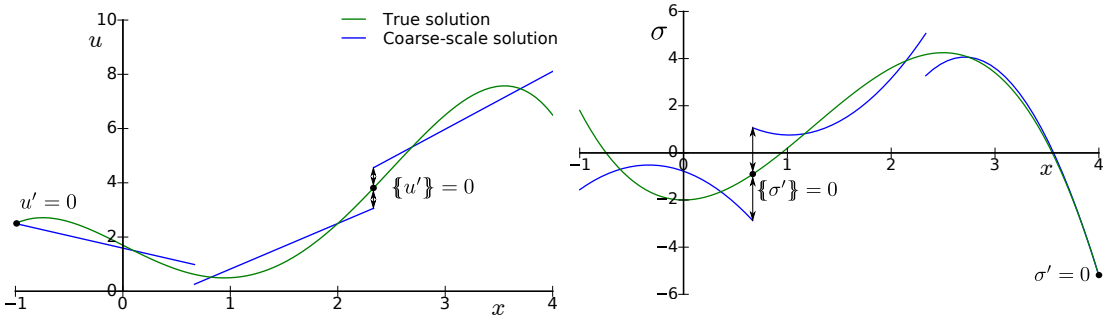

(a) Primal variable **(b)** Auxiliary variable

Fig. 4.4: *Illustration of the pointwise fine-scale identities for the Bassi-Rebay method.*

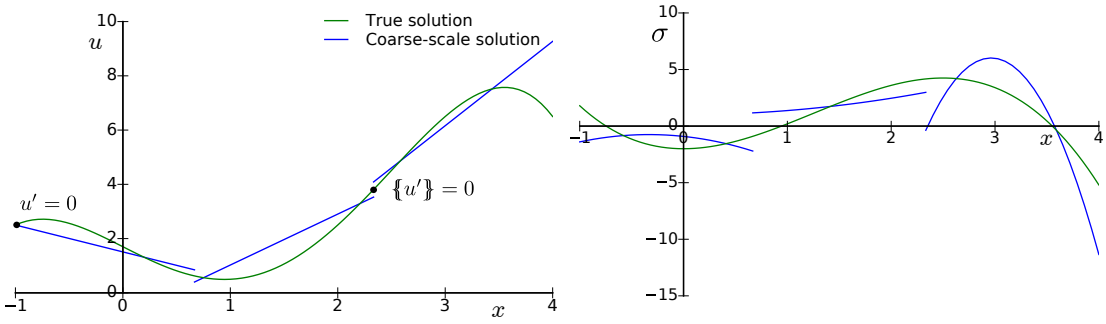

(a) Primal variable **(b)** Auxiliary variable

Fig. 4.5: *Illustration of the pointwise fine-scale identities for the IP method. Using* $\eta h^{-1} = 3$.

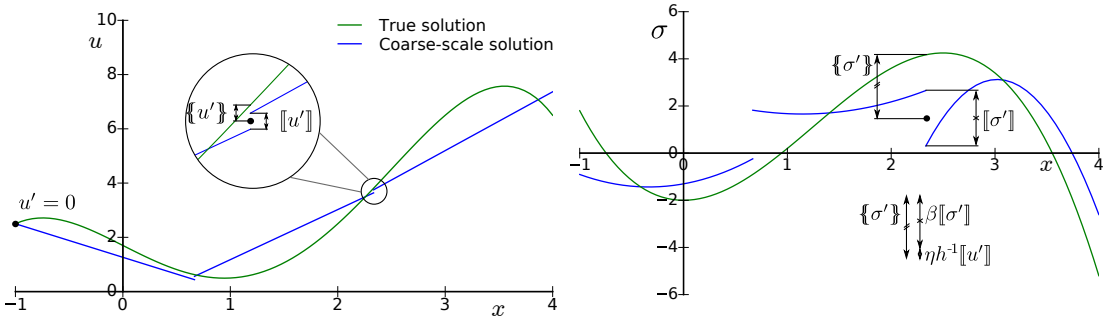

(a) Primal variable **(b)** Auxiliary variable

Fig. 4.6: *Illustration of the pointwise fine-scale identities for the Local DG method. Using* $\eta h^{-1} = 3$ *and* $\beta = 1$.

Analysis of the non-conservative methods

The clean pointwise identities that were just proven to hold for conservative methods do not hold for non-conservative methods. This may already be observed in the first part of the analysis. In the case of a single Dirichlet boundary, the conclusions drawn from Figures 4.1 and 4.2 are still valid. Then indeed:

For one Dirichlet boundary:

$$\begin{cases} \mathcal{D}' = 0 & \text{on } \partial\Omega_D \\ \mathcal{B}' = 0 & \text{on } \Gamma \\ (\sigma', \nabla\bar{v})_{\Omega_K} = 0 & \forall\, \bar{v} \in \overline{U} \end{cases} \tag{4.30}$$

However, the alternative proof provided for two Dirichlet boundaries is no longer applicable. If the test function $\bar{\tau}$ from Figure 4.1 is substituted into the first line of the non-conservative fine-scale constraint equation, then one does no longer obtain that the integral of σ' over the complete domain vanishes, which impedes the follow up analysis. Indeed, numerical experiments verify that the pointwise identities in Eq. (4.30) do not hold when two Dirichlet boundaries are used.

Still, useful identities can be obtained by a systematic choice of test functions. By using a step function for $\bar{v}$ as shown in Figure 4.3, and subsequently a constant value for $\bar{v}$ as shown in Figure 4.1, then one obtains:

$$\mathcal{D}\big|_{\partial\Omega_\mathrm{l}} = -\mathcal{D}\big|_{\partial\Omega_\mathrm{r}} = \mathcal{B}'\big|_{\hat{x}} \qquad \forall\, \hat{x} \in \Gamma \tag{4.31}$$

Additionally, by choosing $\bar{v}$ as a single saw tooth function as illustrated in Figure 4.7, then:

$$\frac{1}{|K_i|}\int_{K_i} \sigma' = \mathcal{B}'\big|_{x_i} \tag{4.32}$$

where x_i is the right node of the element K_i. Since all values of $\mathcal{B}'$ are the same, also all element averages of σ' are the same.

Finally, if higher order basis functions are used for the construction of $\overline{U}$, then substitution of bubble functions into $\bar{v}$, as illustrated in Figure 4.8, leads to:

$$\int_{K_i} \sigma' \frac{\mathrm{d}}{\mathrm{d}x}\big((x_{i-1} - x)(x_i - x)\big) = \int_{K_i} \sigma'(2x - x_{i-1} - x_i) = 0 \tag{4.33}$$

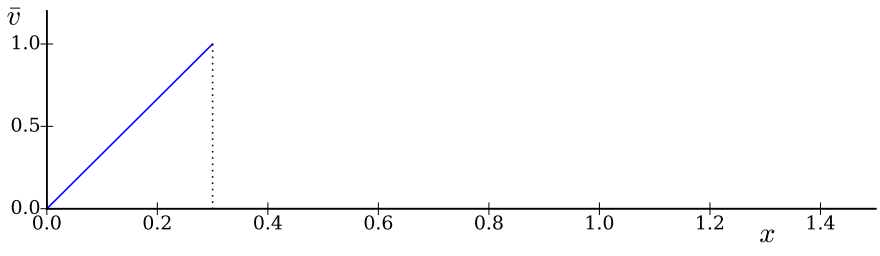

Fig. 4.7: *Test function four, saw tooth function.*

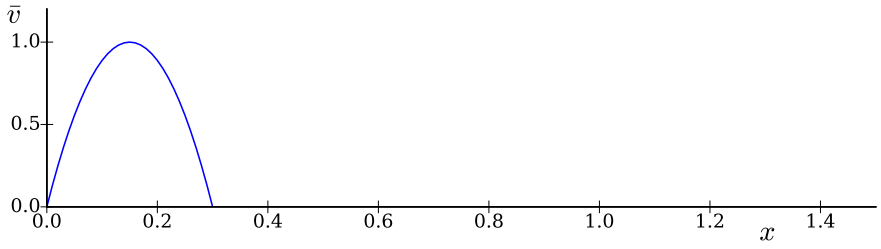

Fig. 4.8: *Test function five, bubble function.*

Or, more general:

$$\int_K \sigma' \frac{\mathrm{d}}{\mathrm{d}x} f(x) = 0 \tag{4.34}$$

where $f(x)$ is some polynomial function contained in element K, with zero values on the boundary of K.

Moving on to the first line in Eq. (4.16), and by substituting a test function $\bar{\tau}$ as illustrated in Figure 4.9, the remaining identity states:

$$H'|_{\hat{x}_i} = \frac{1}{|K_i|} \int_{K_i} (u' + (x - \hat{x}_{i-1})\sigma') - \frac{1}{|K_{i+1}|} \int_{K_{i+1}} (u' + (x - \hat{x}_{i+1})\sigma') \tag{4.35}$$

Similarly, an expression for $\mathcal{A}'$ may be derived by choosing $\bar{\tau}$ according to Figure 4.10:

$$2\mathcal{A}'|_{\hat{x}_i} = \frac{1}{|K_i|} \int_{K_i} (u' + (x - \hat{x}_{i-1})\sigma') + \frac{1}{|K_{i+1}|} \int_{K_{i+1}} (u' + (x - \hat{x}_{i+1})\sigma') \tag{4.36}$$

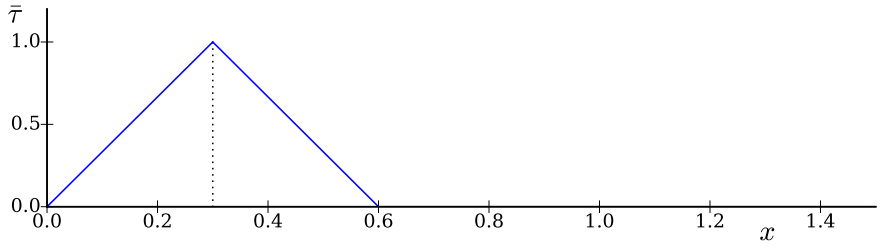

Fig. 4.9: *Test function six, unit average, zero jump.*

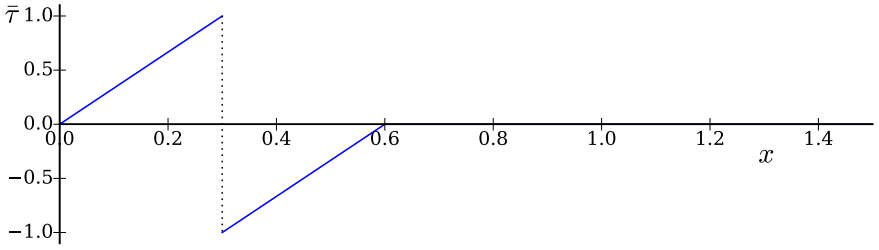

Fig. 4.10: *Test function seven, zero average, jump of 2.*

To also consider the boundary information, $\bar{\tau}$ may be chosen according to Figure 4.11. Depending on whether the boundary is a Neumann or a Dirichlet boundary one obtains:

$$\mathcal{N}' = \frac{1}{|K|}\int_K (u' + (x - \hat{x}^*)\sigma') \qquad \text{when } K \text{ neighbors } \partial\Omega_N \tag{4.37}$$

$$0 \quad = \frac{1}{|K|}\int_K (u' + (x - \hat{x}^*)\sigma') \qquad \text{when } K \text{ neighbors } \partial\Omega_D \tag{4.38}$$

Finally, consider a bubble function for $\bar{\tau}$ similar to that shown for $\bar{v}$ in Figure 4.8. Then:

$$\int_K \sigma' f(x) + u' \frac{\mathrm{d}}{\mathrm{d}x} f(x) = 0 \qquad \forall\, K \in \mathcal{T} \tag{4.39}$$

where $f(x)$ is the polynomial function contained in the element K.

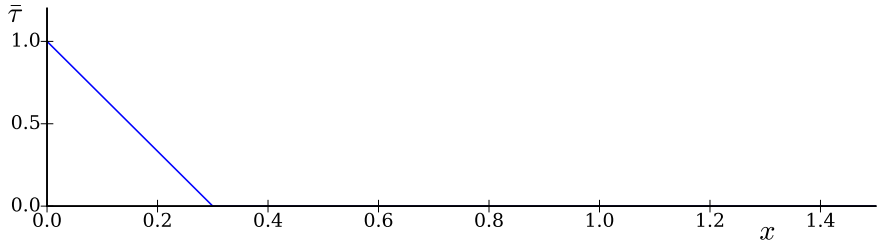

Fig. 4.11: *Test function eight, boundary triangle.*

Summary of the non-conservative methods

The expressions obtained for these non-conservative methods are collected in Table 4.5. A subdivision into expressions for one or two Dirichlet boundaries is made.

Table 4.5: *Identities for the non-conservative methods for a one-dimensional Poisson equation. Assuming that the polynomial basis for the auxiliary variable is at least of order one.*

	Baumann-Oden	**NIPG**
	One Dirichlet boundary	
On Γ:	$\{\!\{\nabla u'\}\!\} = 0$	$\{\!\{\nabla u'\}\!\} - \frac{\eta}{h}[\![u']\!] = 0$
On $\partial\Omega_D$:	$\nabla u' \cdot n = 0$	$\nabla u' \cdot n - \frac{\eta}{h} u' = 0$
	Two Dirichlet boundaries	
	$\nabla u' \cdot n\big\vert_{\partial\Omega_\mathrm{l}} = -\nabla u' \cdot n\big\vert_{\partial\Omega_\mathrm{r}}$	$\left[\nabla u' \cdot n - \frac{\eta}{h} u'\right]_{\partial\Omega_\mathrm{l}} = -\left[\nabla u' \cdot n - \frac{\eta}{h} u' n\right]_{\partial\Omega_\mathrm{r}}$
x_i on Γ:	$\{\!\{\nabla u'\}\!\}\big\vert_{x_i} = \nabla u' \cdot n\big\vert_{\partial\Omega_\mathrm{l}}$	$\{\!\{\nabla u'\}\!\}\big\vert_{x_i} - \frac{\eta}{h}[\![u']\!]\big\vert_{x_i} = \left[\nabla u' \cdot n - \frac{\eta}{h} u'\right]_{\partial\Omega_\mathrm{l}}$
	One or two Dirichlet boundaries	
x_i on Γ:	$\frac{1}{\lvert K_i\rvert}\int_{K_i} \sigma' = \{\!\{\nabla u'\}\!\}\big\vert_{x_i}$	$\frac{1}{\lvert K_i\rvert}\int_{K_i} \sigma' = \{\!\{\nabla u'\}\!\}\big\vert_{x_i} - \frac{\eta}{h}[\![u']\!]\big\vert_{x_i}$
x_i on Γ:	$2\{\!\{u'\}\!\}\big\vert_{\hat{x}_i} = \frac{1}{\lvert K_i\rvert}\int_{K_i}(u' + (x - \hat{x}_{i-1})\sigma') + \frac{1}{\lvert K_{i+1}\rvert}\int_{K_{i+1}}(u' + (x - \hat{x}_{i+1})\sigma')$	
x_i on Γ:	$2[\![u']\!]\big\vert_{\hat{x}_i} = \frac{1}{\lvert K_i\rvert}\int_{K_i}(u' + (x - \hat{x}_{i-1})\sigma') - \frac{1}{\lvert K_{i+1}\rvert}\int_{K_{i+1}}(u' + (x - \hat{x}_{i+1})\sigma'))$	
	$u'\big\vert_{\partial\Omega_N} = \frac{1}{\lvert K\rvert}\int_K (u' + (x - \hat{x}^*)\sigma')$ when K neighbors $\partial\Omega_N$	
	$0 = \frac{1}{\lvert K\rvert}\int_K (u' + (x - \hat{x}^*)\sigma')$ when K neighbors $\partial\Omega_D$	
$\forall\, K \in \mathcal{T}$:	$\int_K \sigma' \frac{\mathrm{d}}{\mathrm{d}x} f(x) = 0$ with $f(x)$ a bubble function.	
$\forall\, K \in \mathcal{T}$:	$\int_K \sigma' f(x) + u' \frac{\mathrm{d}}{\mathrm{d}x} f(x) = 0$ with $f(x)$ a bubble function.	

4.2.2 Multidimensional case

The pointwise identities for the one-dimensional case do not translate directly to the multi-dimensional case. However, some meaningful expressions may still be derived. Consider, for example, a test function $\bar{v}$ that is 1 inside an element K and 0 outside of this element. Then, for both the conservative and the non-conservative methods:

$$\int_{\partial K \setminus \partial\Omega} \mathcal{B}' \cdot n + \int_{\partial K \cap \partial\Omega_D} \mathcal{D}' \cdot n = 0 \tag{4.40}$$

Similarly, by choosing some constant (potentially normalized) $\bar{\tau} = \tau_c$ inside element K, and the zero vector outside of element K, then for conservative methods:

$$\int_{K} \sigma' \cdot \tau_c - \int_{\partial K \setminus \partial\Omega} \mathcal{A}'\tau_c \cdot n - \int_{\partial K \cap \partial\Omega_N} \mathcal{N}'\tau_c \cdot n = 0 \tag{4.41}$$

and an additional term is added for non-conservative methods:

$$\int_{K} \sigma' \cdot \tau_c - \int_{\partial K \setminus \partial\Omega} \left[\mathcal{A}'\tau_c \cdot n + \frac{1}{2}\mathcal{H}' \cdot \tau_c\right] - \int_{\partial K \cap \partial\Omega_N} \mathcal{N}'\tau_c \cdot n = 0 \tag{4.42}$$

For the Local DG method, Eqs. (4.40) and (4.41) result in:

$$\int_{\partial K \setminus \partial\Omega} \left[\{\!\{\sigma'\}\!\} + \beta[\![\sigma']\!] - \eta h^{-1}[\![u']\!]\right] \cdot n + \int_{\partial K \cap \partial\Omega_D} \left[\sigma' - \eta h^{-1} u' n\right] \cdot n = 0 \tag{4.43}$$

$$\int_{K} \sigma' \cdot \tau_c - \int_{\partial K \setminus \partial\Omega} [\{\!\{u'\}\!\} n - \beta[\![u']\!]] \cdot \tau_c - \int_{\partial K \cap \partial\Omega_N} u'\tau_c \cdot n = 0 \tag{4.44}$$

And to also include a non-conservative method, the NIPG method results in:

$$\int_{\partial K \setminus \partial\Omega} \left[\{\!\{\sigma'\}\!\} - \eta h^{-1}[\![u']\!]\right] \cdot n + \int_{\partial K \cap \partial\Omega_D} \left[\sigma' - \eta h^{-1} u' n\right] \cdot n = 0 \tag{4.45}$$

$$\int_{K} \sigma' \cdot \tau_c - \int_{\partial K \setminus \partial\Omega} [\{\!\{u'\}\!\} n + [\![u']\!]] \cdot \tau_c - \int_{\partial K \cap \partial\Omega_N} u'\tau_c \cdot n = 0 \tag{4.46}$$

While such relations are by no means a complete description of the behavior of the fine-scale constraint equations, they do provide insights into the behavior of the methods. The fine-scale solution is in effect the error of the finite element solutions. Equations (4.43)

to (4.46) are thus relations that describe how the error of the finite-element solution will behave. The first lines of these equations show that the average quantity of some error measure on the element boundary equals zero, while the second lines relate the total error of $\bar{\sigma}$ to error expressions on the element boundary.

4.3 Fine-scale constraints of the Raviart-Thomas method and the Brezzi-Douglas-Marini method

As introduced in Section 3.1, the Raviart-Thomas (RT) and Brezzi-Douglas-Marini (BDM) finite element spaces are finite dimensional subspaces of $H(\mathrm{div}, \Omega)$. Thereby, they permit finite element formulations of the form:

$$\begin{aligned} &\text{Find } \sigma_h, u_h \in \mathcal{K}(\sigma_N) \times \overline{U} \text{ s.t. } \forall\, \bar{\tau} \in \mathcal{K}(0) \text{ and } \forall\, \bar{v} \in \overline{U} : \\ &\begin{cases} (\sigma_h, \bar{\tau})_{\Omega_K} + (u_h, \nabla \cdot \bar{\tau})_{\Omega_K} = \langle u_D, \bar{\tau} \cdot n \rangle_{\partial\Omega_D} \\ -(\nabla \cdot \sigma_h, \bar{v})_{\Omega_K} = (f, \bar{v})_{\Omega_K} \end{cases} \end{aligned} \tag{4.47}$$

where $\mathcal{K}(\cdot)$ is either the RT or the BDM space. In these spaces, the Neumann conditions can be enforced strongly. Within each element, functions in these spaces are simple polynomials, similar to typical $H^1(\Omega)$-conforming finite elements. Specifically, the BDM space is defined as:

$$\begin{aligned} BDM_k(g) &= H(\mathrm{div}, \Omega) \cap \left\{ \sigma \in [L^2(\Omega)]^d \,:\, \sigma|_K \in [P^k(K)]^d \;\forall\, K \in \mathcal{T},\, \sigma = \mathcal{I}_h g \text{ on } \partial\Omega \right\} \\ &= H(\mathrm{div}, \Omega) \cap \overline{\Sigma}(g) \end{aligned} \tag{4.48}$$

Indicating that the BDM space is a subspace of the discontinuous vector function space $\overline{\Sigma}(\cdot)$ introduced in Eq. (3.23), although now including boundary data. In turn, this means that the mixed multiscale weak formulation derived in Section 3.2 is applicable.

To construct an RT space on an element K, a polynomial vector function of the form $x\,\tilde{P}^k(K)$ is added, where x denotes the position vector and $\tilde{P}^k(K)$ is a homogeneous polynomial of order k. So, on element K:

$$RT_k = [P^k(K)]^d + x\,\tilde{P}^k(K) \tag{4.49}$$

It follows that on the complete domain:

$$RT_k \subset BDM_{k+1} \tag{4.50}$$

Since this is again a subspace of $\overline{\Sigma}(\cdot)$ (with increased polynomial order) the mixed multiscale weak formulation derived in Section 3.2 is also applicable for the RT method.

The specialty of the RT and BDM approximation spaces is that they retain a continuous normal component across element interfaces, while the tangential components may be discontinuous. Indeed, any vector function $\sigma \in H(\mathrm{div}, \Omega)$ by definition of the space must satisfy:

$$\begin{aligned}
&\int_K \nabla\cdot\sigma\,\varphi + \int_K \sigma\cdot\nabla\varphi = \int_{K_1} \nabla\cdot\sigma\,\varphi + \int_{K_2} \nabla\cdot\sigma\,\varphi + \int_{K_1} \sigma\cdot\nabla\varphi + \int_{K_2} \sigma\cdot\nabla\varphi \\
&\qquad = \int_{\partial K} \sigma\cdot n\,\varphi = \int_{\partial K_1} \sigma\cdot n\,\varphi + \int_{\partial K_2} \sigma\cdot n\,\varphi \qquad \forall\,\varphi \in H^\infty(K) \\
&\Rightarrow \int_{\partial K_2\cap\partial K_1} \sigma^+\cdot n^+\varphi + \int_{\partial K_2\cap\partial K_1} \sigma^-\cdot n^-\varphi = \int_{\partial K_2\cap\partial K_1} (\sigma^+\cdot n^+ + \sigma^-\cdot n^-)\varphi = 0 \quad \forall\,\varphi \in H^\infty(K) \\
&\Rightarrow \quad \sigma^+\cdot n^+ + \sigma^-\cdot n^- = 0 \qquad \text{on } \partial K_2 \cap \partial K_1
\end{aligned} \tag{4.51}$$

with K any simply connected subdomain of Ω and with K_1 and K_2 any simply connected subdomains of K such that $K = K_1 \cap K_2$.

Due to the strong satisfaction of the condition $[\![\tau]\!] = 0$ on Γ, and since $\tau = 0$ on $\partial\Omega_N$ by construction, the mixed multiscale weak formulation for Poisson's equation simplifies to the following:

Find $\bar\sigma, \bar u \in \overline{\Sigma} \times \overline{U}$ s.t. $\forall\,\bar\tau \in \overline{\Sigma}$ and $\forall\,\bar v \in \times\overline{U}$:

$$\begin{cases}
(\bar\sigma, \bar\tau)_{\Omega_K} + (\sigma', \bar\tau)_{\Omega_K} + (\bar u, \nabla\cdot\bar\tau)_{\Omega_K} + (u', \nabla\cdot\bar\tau)_{\Omega_K} = \langle u_D, \bar\tau\cdot n\rangle_{\partial\Omega_D} \\
-(\nabla\cdot\bar\sigma, \bar v)_{\Omega_K} + (\sigma', \nabla\bar v)_{\Omega_K} - \langle \{\!\{\sigma'\}\!\}, [\![\bar v]\!]\rangle_\Gamma - \langle \sigma', \bar v\, n\rangle_{\partial\Omega} = (f, \bar v)_{\Omega_K}
\end{cases} \tag{4.52}$$

Next, the finite element solutions in Eq. (4.47) are defined as the coarse-scale solutions in Eq. (4.52). The fine scale constraints employed by the RT and BDM methods can then be derived by equating the left-hand sides of Eq. (4.52) and Eq. (4.47), which is valid because

the right-hand sides are equal. After canceling identical terms one obtains:

RT or BDM method:

$$\begin{aligned}&(\sigma', \bar{\tau})_{\Omega_K} + (u', \nabla \cdot \bar{\tau})_{\Omega_K} = 0 \\ &(\sigma', \nabla \bar{v})_{\Omega_K} - \langle \{\!\{\sigma'\}\!\}, [\![\bar{v}]\!] \rangle_{\Gamma} - \langle \sigma', \bar{v}\, n \rangle_{\partial\Omega} = 0\end{aligned} \tag{4.53}$$

which captures the projector that defines the coarse-scale finite element solutions in Eq. (4.47). In particular, this fine-scale constraint equation corresponds to the variational form of the following saddle point problem:

$$\inf_{\bar{u}\in\overline{U}} \sup_{\bar{\sigma}\in\mathcal{K}(\sigma_N)} \int_{\Omega_K} \frac{1}{2}(\nabla u - \nabla \bar{u})^2 - \frac{1}{2}(\bar{\sigma} - \nabla \bar{u})^2 + \int_{\Gamma} [\![\bar{u}]\!] \cdot \{\!\{\sigma - \bar{\sigma}\}\!\} - \int_{\partial\Omega} (u - \bar{u}) n \cdot (\sigma - \bar{\sigma}) \tag{4.54}$$

This saddle point problem provides an explicit interpretation of the projectors $\mathcal{P}_u$ and $\mathcal{P}_\sigma$ employed by the RT and BDM methods. Interestingly, this is the same saddle point problem as that of the Bassi-Rebay method, shown in Eq. (4.6). The only difference is that the supremum is sought for $\bar{\sigma}$ in the RT or BDM space $\mathcal{K}(\sigma_N)$ instead of the discontinuous Galerkin space $\overline{\Sigma}$.

4.4 Fine-scale constraint of the Hybridizable discontinuous Galerkin method

Depending on the precise finite element formulation and the choices of finite element approximation spaces that are used to discretize the hybrid mixed formulation, one could obtain hybridized versions of the Raviart-Thomas method, the Brezzi-Douglas-Marini method, or indeed of a special class of discontinuous Galerkin method. The latter being introduced in [70]. The resulting finite element solutions would be identical to those obtained by directly solving the corresponding RT, BDM or discontinuous Galerkin formulation, plus an additional finite element approximation of the hybrid variable. The advantage of the hybridized scheme is that static condensation techniques may be employed to exclusively solve for the hybrid variable. In a second step, the other two solution fields may be obtained by solving element local problems where the hybrid variable is used as boundary data. Overall, this greatly reduces the required computational cost.

Since the hybridized versions of the RT and BDM methods yield solutions identical to those

obtained with the RT or BDM method itself, the same multiscale analysis is applicable. The results from Section 4.3 thus hold. Similarly, the Hybridizable discontinuous Galerkin method could already have been included in Section 4.1. However, since the finite element formulation only reduces to a discontinuous Galerkin method for particular choices of parameters, a more general multiscale analysis is possible. Additionally, a multiscale analysis of the behavior of the finite element approximation to the hybrid variable may prove fruitful.

The general form of the Hybridizable discontinuous Galerkin method for Poisson's equation reads:

$$\begin{aligned}
&\text{Find } \sigma_h, u_h, \hat{u}_h \in \overline{\Sigma} \times \overline{U} \times \overline{\mathcal{M}}(u_D) \text{ s.t. } \forall\, \bar{\tau} \in \overline{\Sigma} \text{ and } \forall\, \bar{v} \in \overline{U} \text{ and } \forall\, \bar{\mu} \in \overline{\mathcal{M}}(0) : \\
&\begin{cases}
(\sigma_h, \bar{\tau})_{\Omega_K} = -(u_h, \nabla \cdot \bar{\tau})_{\Omega_K} + \langle \hat{u}_h, [\![\bar{\tau}]\!] \rangle_{\Gamma} + \langle \hat{u}_h, \bar{\tau} \cdot n \rangle_{\partial\Omega} \\
-(\nabla \cdot \sigma_h, \bar{v})_{\Omega_K} + \sum\limits_{K \in \mathcal{T}} \langle t\,(u_h - \hat{u}_h), \bar{v} \rangle_{\partial K} = (f, \bar{v})_{\Omega_K} \\
\langle [\![\sigma_h]\!], \bar{\mu} \rangle_{\Gamma} + \langle \sigma_h \cdot n, \bar{\mu} \rangle_{\partial\Omega} + \sum\limits_{K \in \mathcal{T}} \langle t\,(u_h - \hat{u}_h), \bar{\mu} \rangle_{\partial K} = \langle \sigma_N \cdot n, \bar{\mu} \rangle_{\partial\Omega_N}
\end{cases}
\end{aligned} \tag{4.55}$$

where t is a double valued scalar function on the faces of the computational mesh. The terms that involve t are introduced to stabilize the formulation. Existence and uniqueness of the solution is based on the choice of t as well as the choice of finite element spaces. For particular choices of t and $\overline{\mathcal{M}}$ it can be shown that a discontinuous Galerkin solution is retrieved.

To determine the fine-scale constraint employed by this formulation, the finite element solutions σ_h, u_h and $\hat{u}_h$ are defined as the coarse-scale solutions $\bar{\sigma}$, $\bar{u}$ and $\bar{\hat{u}}$ obtained with the projectors $\mathcal{P}_\sigma$, $\mathcal{P}_u$ and $\mathcal{P}_{\hat{u}}$. Then Eq. (4.55) is subtracted from the multiscale formulation of Eq. (3.52) derived earlier. Integration by parts is used on one of the fine-scale terms. This leaves:

Hybridizable DG:

$$\begin{aligned}
&(\sigma', \bar{\tau})_{\Omega_K} = (\nabla u', \bar{\tau})_{\Omega_K} + \sum_{K \in \mathcal{T}} \langle (\hat{u}' - u'), \bar{\tau} \cdot n \rangle_{\partial K} \\
&(\sigma', \nabla \bar{v})_{\Omega_K} - \sum_{K \in \mathcal{T}} \langle t\,(\hat{u}' - u') + \sigma' \cdot n, \bar{v} \rangle_{\partial K} = 0 \\
&\sum_{K \in \mathcal{T}} \langle t\,(\hat{u}' - u') + \sigma' \cdot n, \bar{\mu} \rangle_{\partial K} = 0
\end{aligned} \tag{4.56}$$

The following identity is also used in Eq. (4.56) to switch between coarse-scale and fine-

scale solutions on element boundaries:

$$\bar{u}^{\pm} + u'^{\pm} = \bar{\hat{u}} + \hat{u}' \quad \Rightarrow \quad \bar{u}^{\pm} - \bar{\hat{u}} = \hat{u}' - u'^{\pm} \tag{4.57}$$

Inspired by the static condensation techniques that are frequently adopted for Hybridizable DG formulations, the fine-scale constraint equation may be interpreted as a set of element local equations, plus an additional global equation. The local equations are the first two lines in Eq. (4.56), where the hybrid variable is treated as data. The third line in Eq. (4.56) is the global equation, which ties the elements together. Based on this concept, the fine-scale constraint equation may be interpreted as the variational formulation of the following saddle point and minimization problems:

$$\inf_{\bar{u}\in\overline{U}} \sup_{\bar{\sigma}\in\overline{\Sigma}} \sum_{K\in\mathcal{T}} \int_K \frac{1}{2}(\nabla u - \nabla\bar{u})^2 - \frac{1}{2}(\bar{\sigma} - \nabla\bar{u})^2 - \int_{\partial K} (\bar{\hat{u}} - \bar{u})(\sigma - \bar{\sigma})\cdot n + \frac{1}{2}(\bar{\hat{u}} - \bar{u})^2 t \tag{4.58}$$

$$\inf_{\bar{\hat{u}}\in\overline{\mathcal{M}}(u_D)} \int_\Gamma \left(\sqrt{\{\!\{t\}\!\}}\,\bar{\hat{u}} - \frac{1}{\sqrt{\{\!\{t\}\!\}}}\{\!\{\bar{u}\,t\}\!\} - \frac{1}{2\sqrt{\{\!\{t\}\!\}}}[\![\sigma']\!]\right)^2 + \int_{\partial\Omega_N} \left(\sqrt{t}\,\bar{\hat{u}} - \sqrt{t}\,\bar{u} + \frac{1}{2\sqrt{t}}\sigma'\cdot n\right)^2 \tag{4.59}$$

Following the static condensation procedure, $\bar{u}$ and σ' in Eq. (4.59) may be replaced by $\mathcal{P}_u u$ and $\sigma - \mathcal{P}_\sigma\sigma$ respectively. These projectors are captured by the saddle point problem of Eq. (4.58), which again depends on $\bar{\hat{u}}$. Thereby, the second line of Eq. (4.59) becomes a closed formulation for $\bar{\hat{u}}$.

4.5 Fine-scale constraints of upwind discontinuous Galerkin formulations of the advection-diffusion problem

The mixed multiscale weak formulation for the steady advection-diffusion problem, Equation (3.46), suggests the use of average values on element boundaries, also for the advection term. This does not correspond directly to the use of upwind flux formulations, where the element boundary integrals make use of the values from the upwind side of the interface:

$$u_h^{\mathrm{upw}}(x) = u_h(\lim_{\epsilon\to 0} x - \epsilon a) \tag{4.60}$$

Consider, for example, a finite element formulation where the Bassi-Rebay method is used to treat the diffusion term, and upwind numerical fluxes are used for the advection term:

$$\begin{aligned}&\text{Find } \sigma_h, u_h \in \overline{\Sigma} \times \overline{U} \text{ s.t. } \forall\, \bar{\tau} \in \overline{\Sigma} \text{ and } \forall\, \bar{v} \in \overline{U} : \\ &\begin{cases} \left(\nu^{-1}\sigma_h, \bar{\tau}\right)_{\Omega_K} + \left(u_h, \nabla\bar{\tau}\right)_{\Omega_K} - \left\langle \{\!\{u_h\}\!\}, [\![\bar{\tau}]\!] \right\rangle_\Gamma - \left\langle u_h, \bar{\tau}\, n \right\rangle_{\partial\Omega_N} = \left\langle u_D, \bar{\tau}\, n \right\rangle_{\partial\Omega_D} \\ -\left(a\, u_h, \nabla\bar{v}\right)_{\Omega_K} + \left\langle a\, u_h^{\text{upw}}, [\![\bar{v}]\!] \right\rangle_\Gamma + \left\langle a\, u_h, \bar{v}\, n \right\rangle_{\partial\Omega\setminus\partial\Omega_D^{\text{in}}} + \left(\sigma_h, \nabla\bar{v}\right)_{\Omega_K} \\ \qquad -\left\langle \{\!\{\sigma_h\}\!\}, [\![\bar{v}]\!] \right\rangle_\Gamma - \left\langle \sigma_h, \bar{v}\, n \right\rangle_{\partial\Omega_D} = \left(f, \bar{v}\right)_{\Omega_K} - \left\langle a\, u_D, \bar{v}\, n \right\rangle_{\partial\Omega_D^{\text{in}}} + \left\langle \sigma_N, \bar{v}\, n \right\rangle_{\partial\Omega_N} \end{cases}\end{aligned} \tag{4.61}$$

where it is assumed that the advection field is continuous at element interfaces. This is assumed throughout the remainder of this text.

To interpret the multiscale nature of the upwind formulation, the finite element solutions u_h and σ_h may once again be *defined* as the coarse-scale solutions $\bar{u}$ and $\bar{\sigma}$ obtained through the use of the projects $\mathcal{P}_u$ and $\mathcal{P}_\sigma$. Since the right-hand sides of Eq. (4.61) and Eq. (3.46) are equal, the left-hand sides of these formulations may be equated. When one attempts to cancel equal terms, the following expression needs to be dealt with:

$$\left\langle a\{\!\{\bar{u}\}\!\} - a\bar{u}^{\text{upw}}, [\![\bar{v}]\!] \right\rangle_\Gamma \tag{4.62}$$

For ease of notation $\bar{u}^{\text{upw}}$ is denoted $\bar{u}^+$, and the downwind value is denoted $\bar{u}^-$. By definition of the upwind flux it follows that $a \cdot n^+ > 0$. The term then simplifies according to:

$$\begin{aligned}\cdots &= \left\langle a\frac{1}{2}(\bar{u}^+ + \bar{u}^-) - a\bar{u}^+, v^+n^+ + v^-n^- \right\rangle_\Gamma \\ &= \left\langle (\frac{1}{2}u^- - \frac{1}{2}\bar{u}^+)\, a\cdot n^+, v^+ - v^- \right\rangle_\Gamma \\ &= \left\langle (\frac{1}{2}\bar{u}^- - \frac{1}{2}\bar{u}^+)\, |a\cdot n|\, n^+\cdot n^+, v^+ - v^- \right\rangle_\Gamma \\ &= \left\langle \frac{1}{2}|a\cdot n|\, (\bar{u}^- n^+ - \bar{u}^+ n^+), v^+n^+ - v^-n^+ \right\rangle_\Gamma \\ &= \left\langle -\frac{1}{2}|a\cdot n|\, (\bar{u}^- n^- + \bar{u}^+ n^+), v^+n^+ + v^-n^- \right\rangle_\Gamma \\ &= \left\langle -\frac{1}{2}|a\cdot n|\, [\![\bar{u}]\!], [\![\bar{v}]\!] \right\rangle_\Gamma \\ &= \left\langle \frac{1}{2}|a\cdot n|\, [\![u']\!], [\![\bar{v}]\!] \right\rangle_\Gamma\end{aligned} \tag{4.63}$$

which is an expression that does not explicitly depend on upwind/downwind values.

The fine-scale constraint employed by Eq. (4.61) is subsequently obtained as:

Upwind fluxes & Bassi-Rebay:

$$\begin{aligned}
&(\nu^{-1}\sigma', \bar{\tau})_{\Omega_K} + (u', \nabla\cdot\bar{\tau})_{\Omega_K} - \langle \{\!\{u'\}\!\}, [\![\bar{\tau}]\!]\rangle_{\Gamma} - \langle u', n\cdot\bar{\tau}\rangle_{\partial\Omega_N} = 0 \\
&-(a\,u', \nabla\bar{v})_{\Omega_K} + \langle a\,\{\!\{u'\}\!\}, [\![\bar{v}]\!]\rangle_{\Gamma} + \langle \tfrac{1}{2}|a\cdot n|\,[\![u']\!], [\![\bar{v}]\!]\rangle_{\Gamma} + \langle a\,u', \bar{v}\,n\rangle_{\partial\Omega\setminus\partial\Omega_D^{\text{in}}} \\
&\qquad + (\sigma', \nabla\bar{v})_{\Omega_K} - \langle \{\!\{\sigma'\}\!\}, [\![\bar{v}]\!]\rangle_{\Gamma} - \langle \sigma', n\,\bar{v}\rangle_{\partial\Omega_D} = 0
\end{aligned} \tag{4.64}$$

Some new fine-scale terms are introduced compared to the fine-scale constraint derived for the pure diffusion problem in Section 4.1. A particularly interesting term is the one obtained from the upwind fluxes. This compares well with the penalty terms introduced in, for instance, the symmetric interior penalty formulation. The effect of these added terms is more closely investigated in Section 4.6.

Similarly, the following fine-scale constraint equations may be derived for the different treatments of the diffusion term:

Upwind fluxes & Symmetric interior penalty:

$$\begin{aligned}
&(\nu^{-1}\sigma', \bar{\tau})_{\Omega_K} + (u', \nabla\cdot\bar{\tau})_{\Omega_K} - \langle \{\!\{u'\}\!\}, [\![\bar{\tau}]\!]\rangle_{\Gamma} - \langle u', n\cdot\bar{\tau}\rangle_{\partial\Omega_N} = 0 \\
&-(a\,u', \nabla\bar{v})_{\Omega_K} + \langle a\,\{\!\{u'\}\!\}, [\![\bar{v}]\!]\rangle_{\Gamma} + \langle a\,u', \bar{v}\,n\rangle_{\partial\Omega\setminus\partial\Omega_D^{\text{in}}} \\
&\qquad + (\sigma', \nabla\bar{v})_{\Omega_K} - \langle \{\!\{\nu\nabla u'\}\!\}, [\![\bar{v}]\!]\rangle_{\Gamma} + \langle (\tfrac{\eta}{h} + \tfrac{1}{2}|a\cdot n|)\,[\![u']\!], [\![\bar{v}]\!]\rangle_{\Gamma} \\
&\qquad - \langle \nu\nabla u', \bar{v}\,n\rangle_{\partial\Omega_D} + \langle \tfrac{\eta}{h}\,u'\,n, \bar{v}\,n\rangle_{\partial\Omega_D} = 0
\end{aligned} \tag{4.65}$$

where, indeed, the existing penalty parameter and the added term due to the upwinding may be collected into a new, increased, penalty parameter. The same thing holds for a Local DG treatment of the diffusive term:

Upwind fluxes & Local DG:

$$\begin{aligned}
&(\nu^{-1}\sigma', \bar{\tau})_{\Omega_K} + (u', \nabla\cdot\bar{\tau})_{\Omega_K} - \langle \{\!\{u'\}\!\}, [\![\bar{\tau}]\!]\rangle_{\Gamma} - \langle u', n\cdot\bar{\tau}\rangle_{\partial\Omega_N} + \langle \beta\cdot[\![u']\!], [\![\bar{\tau}]\!]\rangle_{\Gamma} = 0 \\
&-(a\,u', \nabla\bar{v})_{\Omega_K} + \langle a\,\{\!\{u'\}\!\}, [\![\bar{v}]\!]\rangle_{\Gamma} + \langle a\,u', \bar{v}\,n\rangle_{\partial\Omega\setminus\partial\Omega_D^{\text{in}}} \\
&\qquad + (\sigma', \nabla\bar{v})_{\Omega_K} - \langle \{\!\{\sigma'\}\!\}, [\![\bar{v}]\!]\rangle_{\Gamma} - \langle \sigma', n\,\bar{v}\rangle_{\partial\Omega_D} - \langle \beta[\![\sigma']\!], [\![\bar{v}]\!]\rangle_{\Gamma} \\
&\qquad + \langle (\tfrac{\eta}{h} + \tfrac{1}{2}|a\cdot n|)\,[\![u']\!], [\![\bar{v}]\!]\rangle_{\Gamma} + \langle \tfrac{\eta}{h}\,u'\,n, \bar{v}\,n\rangle_{\partial\Omega_D} = 0
\end{aligned} \tag{4.66}$$

For the Baumann-Oden method, the added penalty does not combine with an existing penalty term, but it stands alone:

Upwind fluxes & Baumann-Oden:

$$\begin{aligned}
&(\nu^{-1}\sigma', \bar{\tau})_{\Omega_K} + (u', \nabla \cdot \bar{\tau})_{\Omega_K} - \langle \{\!\{u'\}\!\}, [\![\bar{\tau}]\!] \rangle_\Gamma - \langle u', n \cdot \bar{\tau} \rangle_{\partial\Omega_N} - \langle 2[\![u']\!], \{\!\{\bar{\tau}\}\!\} \rangle_\Gamma = 0 \\
&-(a\,u', \nabla \bar{v})_{\Omega_K} + \langle a\,\{\!\{u'\}\!\}, [\![\bar{v}]\!] \rangle_\Gamma + \langle \tfrac{1}{2}|a \cdot n|\,[\![u']\!], [\![\bar{v}]\!] \rangle_\Gamma + \langle a\,u', \bar{v}\,n \rangle_{\partial\Omega \setminus \partial\Omega_D^{\text{in}}} \\
&\qquad + (\sigma', \nabla \bar{v})_{\Omega_K} - \langle \{\!\{\nu \nabla u'\}\!\}, [\![\bar{v}]\!] \rangle_\Gamma - \langle \nu \nabla u', \bar{v}\,n \rangle_{\partial\Omega_D} = 0
\end{aligned} \tag{4.67}$$

And finally, for the NIPG method, the existing penalty term is increased:

Upwind fluxes & Nonsymmetric interior penalty Galerkin:

$$\begin{aligned}
&(\nu^{-1}\sigma', \bar{\tau})_{\Omega_K} + (u', \nabla \cdot \bar{\tau})_{\Omega_K} - \langle \{\!\{u'\}\!\}, [\![\bar{\tau}]\!] \rangle_\Gamma - \langle u', n \cdot \bar{\tau} \rangle_{\partial\Omega_N} - \langle 2[\![u']\!], \{\!\{\bar{\tau}\}\!\} \rangle_\Gamma = 0 \\
&-(a\,u', \nabla \bar{v})_{\Omega_K} + \langle a\,\{\!\{u'\}\!\}, [\![\bar{v}]\!] \rangle_\Gamma + \langle a\,u', \bar{v}\,n \rangle_{\partial\Omega \setminus \partial\Omega_D^{\text{in}}} \\
&\qquad + (\sigma', \nabla \bar{v})_{\Omega_K} - \langle \{\!\{\nu \nabla u'\}\!\}, [\![\bar{v}]\!] \rangle_\Gamma + \langle (\tfrac{\eta}{h} + \tfrac{1}{2}|a \cdot n|)\,[\![u']\!], [\![\bar{v}]\!] \rangle_\Gamma \\
&\qquad - \langle \nu \nabla u', \bar{v}\,n \rangle_{\partial\Omega_D} + \langle \tfrac{\eta}{h}\,u'\,n, \bar{v}\,n \rangle_{\partial\Omega_D} = 0
\end{aligned} \tag{4.68}$$

4.6 Analysis of upwind discontinuous Galerkin formulations of the advection-diffusion problem

The goal of this section is not to derive pointwise identities for each of the formulations in Eqs. (4.64) to (4.68) as was the focus of Section 4.2. The use of such results would be too limited to a too specific model problem, and they would thereby loose their value. Instead, the aim of this section is twofold. First, the use upwind numerical fluxes is investigated by interpreting its effect on the fine-scale constraint equation. Secondly, compared to a pure diffusion problem, the fine-scale constraint equation for the advection-diffusion equation includes an additional volumetric term, the effect of which is evaluated.

It was already indicated in the derivation of Eqs. (4.64) to (4.68) that the use of upwind fluxes increases the effective penalty on the jump of the primary variable. To make this more explicit, consider a discontinuous Galerkin formulation where average fluxes are used rather than upwind fluxes, while a symmetric interior penalty method is used for the

diffusion term:

Find $\sigma_h, u_h \in \overline{\Sigma} \times \overline{U}$ s.t. $\forall\, \bar{\tau} \in \overline{\Sigma}$ and $\forall\, \bar{v} \in \overline{U}$:

$$\begin{cases} (\nu^{-1}\sigma_h, \bar{\tau})_{\Omega_K} + (u_h, \nabla\bar{\tau})_{\Omega_K} - \langle \{\!\{ u_h \}\!\}, [\![\bar{\tau}]\!] \rangle_\Gamma - \langle u_h, \bar{\tau}\, n \rangle_{\partial\Omega_N} = \langle u_D, \bar{\tau}\, n \rangle_{\partial\Omega_D} \\ -(a\, u_h, \nabla\bar{v})_{\Omega_K} + \langle a\, \{\!\{ u_h \}\!\}, [\![\bar{v}]\!] \rangle_\Gamma + \langle a\, u_D, \bar{v}\, n \rangle_{\partial\Omega_D} + \langle a\, u_h, \bar{v}\, n \rangle_{\partial\Omega_N} \\ \qquad +(\sigma_h, \nabla\bar{v})_{\Omega_K} - \langle \{\!\{ \nu\nabla u_h \}\!\}, [\![\bar{v}]\!] \rangle_\Gamma + \langle \tfrac{\eta^*}{h} [\![u_h]\!], [\![\bar{v}]\!] \rangle_\Gamma \\ \qquad -\langle \sigma_N, \bar{v}\, n \rangle_{\partial\Omega_N} - \langle \nu\nabla u_h, \bar{v}\, n \rangle_{\partial\Omega_D} + \langle \tfrac{\eta^*}{h} u_h, \bar{v}\, n \rangle_{\partial\Omega_D} = (f, \bar{v})_{\Omega_K} \end{cases} \tag{4.69}$$

where, for the sake of the upcoming argument, in the second line $\bar{u}$ is weakly enforced as u_D on the complete Dirichlet boundary, rather than only the inflow part. A new penalty parameter η^* is introduced to differentiate between the parameter η used for the analogous upwind & interior penalty formulation.

The fine-scale constraint associated with this finite element formulation may once again be obtained by defining $u_h := \bar{u}$ and $\sigma_h := \bar{\sigma}$, and equating the left-hand sides of Eq. (4.69) to the left-hand sides of the multiscale formulation Eq. (3.46). This results in the fine-scale constraint equations:

Average fluxes for advection term & Symmetric interior penalty:

$$\begin{aligned} &(\nu^{-1}\sigma', \bar{\tau})_{\Omega_K} + (u', \nabla\cdot\bar{\tau})_{\Omega_K} - \langle \{\!\{ u' \}\!\}, [\![\bar{\tau}]\!] \rangle_\Gamma - \langle u', n\cdot\bar{\tau} \rangle_{\partial\Omega_N} = 0 \\ &-(a\, u', \nabla\bar{v})_{\Omega_K} + \langle a\, \{\!\{ u' \}\!\}, [\![\bar{v}]\!] \rangle_\Gamma + \langle a\, u', \bar{v}\, n \rangle_{\partial\Omega_N} \\ &\qquad + (\sigma', \nabla\bar{v})_{\Omega_K} - \langle \{\!\{ \nu\nabla u' \}\!\}, [\![\bar{v}]\!] \rangle_\Gamma + \langle \tfrac{\eta^*}{h} [\![u']\!], [\![\bar{v}]\!] \rangle_\Gamma \\ &\qquad - \langle \nu\nabla u', \bar{v}\, n \rangle_{\partial\Omega_D} + \langle \tfrac{\eta^*}{h} u'\, n, \bar{v}\, n \rangle_{\partial\Omega_D} = 0 \end{aligned} \tag{4.70}$$

These fine-scale constraints can then be compared to those of the analogous upwind formulation in Eq. (4.65), repeated below for readability:

Upwind fluxes & Symmetric interior penalty:

$$\begin{aligned} &(\nu^{-1}\sigma', \bar{\tau})_{\Omega_K} + (u', \nabla\cdot\bar{\tau})_{\Omega_K} - \langle \{\!\{ u' \}\!\}, [\![\bar{\tau}]\!] \rangle_\Gamma - \langle u', n\cdot\bar{\tau} \rangle_{\partial\Omega_N} = 0 \\ &-(a\, u', \nabla\bar{v})_{\Omega_K} + \langle a\, \{\!\{ u' \}\!\}, [\![\bar{v}]\!] \rangle_\Gamma + \langle a\, u', \bar{v}\, n \rangle_{\partial\Omega\setminus\partial\Omega_D^{\text{in}}} \\ &\qquad + (\sigma', \nabla\bar{v})_{\Omega_K} - \langle \{\!\{ \nu\nabla u' \}\!\}, [\![\bar{v}]\!] \rangle_\Gamma + \langle (\tfrac{\eta}{h} + \tfrac{1}{2}|a\cdot n|)\, [\![u']\!], [\![\bar{v}]\!] \rangle_\Gamma \\ &\qquad - \langle \nu\nabla u', \bar{v}\, n \rangle_{\partial\Omega_D} + \langle \tfrac{\eta}{h} u'\, n, \bar{v}\, n \rangle_{\partial\Omega_D} = 0 \end{aligned} \tag{4.71}$$

The fine-scale constraint of Eq. (4.71) is completely identical to the fine-scale constraint

of Eq. (4.70) when:

$$\eta^* = \begin{cases} \eta & \text{on } \partial\Omega_D^{\text{in}} \cup \partial\Omega_N \\ \eta + \frac{1}{2}|a \cdot n| & \text{on } \Gamma \\ \eta + |a \cdot n| & \text{on } \partial\Omega_D^{\text{out}} \end{cases} \tag{4.72}$$

Since the fine-scale constraint closes the finite element formulation from a multiscale perspective, an identical fine-scale constraint must lead to an identical finite element solution. This is illustrated in Figure 4.12. Identical solutions are obtained for the scheme that uses upwind numerical fluxes and interior penalty versus average numerical fluxes and an increased penalty parameter according to Eq. (4.72). The numerical experiment in the figure concerned Dirichlet boundary on the left side, and a Neumann boundary on the right side. The parameters are kept constant at $a = 0.5$, $\nu = 0.15$ and $f = 6$. The corresponding exact solution is:

$$u = -\frac{10}{e^{10/3} - 1}\left(e^{x/0.3} - 1\right) + 12x \tag{4.73}$$

$$\sigma = -\frac{15}{3e^{10/3} - 3}\, e^{x/0.3} + 1.8 \tag{4.74}$$

Similarly, if either the Local DG method or the NIPG method are used to treat the diffusion term, then the use of upwind advective fluxes simply acts as an increased penalty parameter. If the Baumann-Oden method is used, then this added penalty term would result in a scheme that is equivalent to the use of NIPG, and if the Bassi-Rebay method is used, then a Local DG type scheme is retrieved for the special case of $\beta = 0$.

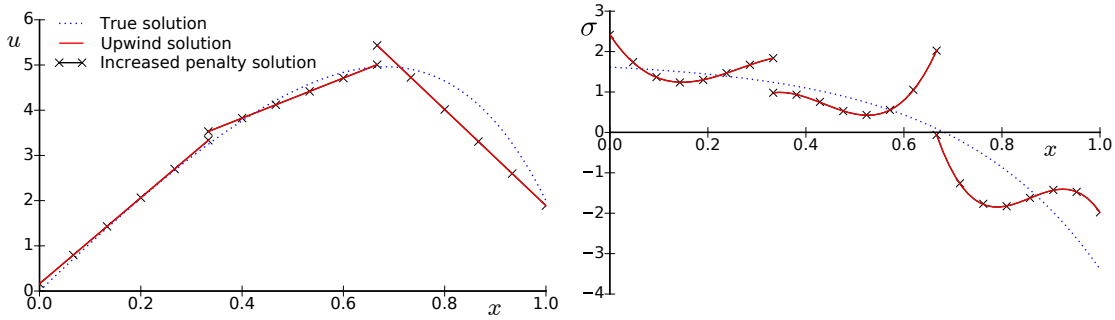

(a) Primal variable **(b)** Auxiliary variable

Fig. 4.12: *Identical solutions for the use of upwind numerical fluxes, and the use of average fluxes with an increased penalty parameter.*

Note that, even though Figure 4.12 is a one-dimensional example, no such assumption has been made in the previous argument. Also for higher-dimensional steady advection-diffusion problems should the use of upwind numerical fluxes be equivalent to increasing the penalty parameter in the flux treatment of the diffusion term.

Despite this equivalence, the fine-scale constraint equations for the advection-diffusion case, Eqs. (4.64) to (4.68), act differently from the fine-scale constraints of Eqs. (4.5), (4.7), (4.10), (4.12) and (4.13) for the case of pure diffusion. This is due to the following two additional terms in the second line of the constraint equations:

$$-(a\,u', \nabla\bar{v})_{\Omega_K} + \langle a\,\{\!\{u'\}\!\}, [\![\bar{v}]\!]\rangle_{\Gamma} \tag{4.75}$$

Note, however, that the structure of the fine-scale constraint equation is nearly unchanged. When the $\{\!\{u'\}\!\}$ term is absorbed into the $\mathcal{B}'$ that was defined in Section 4.2, then the second line of the fine-scale constraints may be written in the following general form:

$$(-a\,u' + \sigma', \nabla\bar{v})_{\Omega_K} - \langle \mathcal{B}', [\![\bar{v}]\!]\rangle_{\Gamma} - \langle \mathcal{D}', \bar{v}\,n\rangle_{\partial\Omega_D} = 0 \tag{4.76}$$

which is quite similar to Eq. (4.15) or Eq. (4.16). The analysis performed in Section 4.1 is thus applicable. In the one-dimensional case, for consistent flux formulations, or with only a single Dirichlet boundary, one obtains:

$$\begin{cases} \mathcal{D}' = 0 & \text{on } \partial\Omega_D \\ \mathcal{B}' = 0 & \text{on } \Gamma \\ \int\limits_K -a\,u' + \sigma' = 0 & \forall\, K \in \mathcal{T} \end{cases} \tag{4.77}$$

The third line now includes an advective contribution, which is the only difference compared to the pure diffusion case. However, this impedes the follow-up analysis. The pointwise identities obtained for the first lines in the fine-scale constraint equations hinge on a vanishing average σ' on each element. Since this is no longer the case, the more convoluted constraints derived for the non-consistent flux formulations become applicable.

Potentially, the finite element scheme behaves more favorable when it is altered slightly such that also the second set of pointwise identities holds. One would have to include a term that cancels the added advective effect in Eq. (4.77). This can be achieved by adding a residual-based model for u', which is investigated in Chapter 5.

Chapter 5

Residual-based modeling of fine scales for mixed finite element formulations

As emphasized a number of times throughout this report, a main feature of importance in variational multiscale formulations is the use of residual-based fine-scale models. An adaptation of the framework for mixed formulations would not be complete without incorporation of these techniques in this new setting. The objective of this chapter is therefore to incorporate the residual-based modeling of the volumetric fine-scale terms into the mixed multiscale formulations derived earlier. Since volumetric fine-scale effects are predominantly important for advection-based partial differential equations, these are the main focus.

As argued in Section 4.6, there is one particular volumetric fine-scale term that troubles the mixed weak formulation. A residual-based model of this term suitable for the use of discontinuous basis function has been introduced by this author in earlier work [12]. The derivation of this model is reviewed in Section 5.1. Afterwards, in Section 5.2, this model is used in the mixed finite element formulation of the advection-diffusion equation. A qualitative analysis of the performance of the model is provided based in a number of numerical experiments.

5.1 The residual-based modeling technique

According to the analysis presented in the previous section, the occurrence of the fine-scale component u' in the second line of equations Eqs. (4.64) to (4.68) constitutes a problem. With the intent of mitigating this problem, or reducing its effects, a model for u' may be incorporated in the finite element formulation as to remove it from the fine-scale constraint. This model will originate from the primal form of the PDE:

$$\mathcal{L}u = f \qquad \text{in } \Omega \subset \mathbb{R}^d \tag{5.1}$$

with, for the advection-diffusion problem:

$$\mathcal{L} = a \cdot \nabla - \nu\Delta \tag{5.2}$$

Similar to the derivation of the multiscale formulations, also the fine-scale model will be derived from a per-element perspective. The weak formulation of Eq. (5.3) may be obtained by multiplication with a test function and integration over the element domain K.

$$\left(\mathcal{L}u, w\right)_K = \left(f, w\right)_K \qquad \forall\, w \in L^2(K) \tag{5.3}$$

The multiscale split of u into $\bar{u}$ and u' is introduced. Due to linearity of the differential operator:

$$\left(\mathcal{L}\bar{u}, w\right)_K + \left(\mathcal{L}u', w\right)_K = \left(f, w\right)_K \qquad \forall\, w \in L^2(K) \tag{5.4}$$

The coarse-scale term is moved to the right-hand side, and together with the source function it becomes the residual of the coarse-scale solution. Additionally, Green's identities may be used to rewrite the fine-scale term, resulting in:

$$\left(u', \mathcal{L}^* w\right)_K + k(u', w; \partial K) = \left(\mathcal{R}_{\bar{u}}, w\right)_K \qquad \forall\, w \in L^2(K) \tag{5.5}$$

where $\mathcal{L}^*$ is the adjoint of the differential operator $\mathcal{L}$, and $k(\cdot, \cdot\,; \cdot)$ is a bilinear form that involves fine-scale quantities on the element boundary.

In Eq. (5.5), the restriction on w is quite loose. It is hypothesized that one can find a function in $L^2(K)$ that satisfies:

$$\begin{cases} \mathcal{L}^* g(x, y) = \delta_x & \text{for } y \in K \\ g(x, y) = 0 & \text{for } y \in \partial K \end{cases} \tag{5.6}$$

where δ_x is the Dirac-delta function at x, and the parameter of differentiation in the first line is y (for ease of notation further on). The function $g(x,y)$ is called the Green's function, or fundamental solution, of the PDE at hand. When this function is substituted as $w(y) = g(x,y)$ in Eq. (5.5), then:

$$\int_K \mathcal{L}^* g(x,y)\, u' \,\mathrm{d}y = \int_K \delta_x\, u' \,\mathrm{d}y = u'(x) = \int_K g(x,y)\, \mathcal{R}_{\bar{u}} \,\mathrm{d}y - k(g(x,y), u'; \partial K) \tag{5.7}$$

The term $k(g(x,y), u'; \partial K)$ effectively enforces the per-element fine-scale boundary conditions. Analysis is restricted to PDEs for which $k(\cdot,\cdot;\cdot)$ may be written as:

$$k(g(x,y), u'; \partial K) = \int_{\partial K} \mathbb{H} g(x,y)\, u'(y) \,\mathrm{d}y \tag{5.8}$$

with $\mathbb{H}$ some differential operator. This includes the advection-diffusion equation.

The original model, described in Section 2.1, assumes that the fine-scale solution vanishes on element boundaries. In combination with the vanishing Green's function as per Eq. (5.6) this means that the whole term equals zero. This assumption is particularly erroneous when discontinuous basis functions are used, since the discontinuity is a direct indication of a non-vanishing fine-scale field. In fact, this discontinuity may be leveraged to obtain information on the fine-scale solution on element interfaces.

The following identity holds based on the definitions of the average and jump operators provided in Table 2.1. The $\pm$ symbol arbitrarily indicates quantities on either side of the discontinuity.

$$u'^{\pm} = \{\!\{u'\}\!\} + \frac{1}{2}[\![u']\!] \cdot n^{\pm} \tag{5.9}$$

Given the multiscale type transmission conditions employed in, for instance, Eq. (3.36), this equals:

$$u'^{\pm} = \{\!\{u'\}\!\} - \frac{1}{2}[\![\bar{u}]\!] \cdot n^{\pm} \tag{5.10}$$

which only leaves $\{\!\{u'\}\!\}$ as an unknown fine-scale quantity.

As extensively shown in the previous section, the choice of fine-scale constraint dictates the resulting split into coarse-scale and fine-scale solutions. It was also shown that for the one-dimensional case the fine-scale constraint leads to pointwise identities on element interfaces. Refer to Tables 4.4 and 4.5 for an overview of these identities for the different

methods. Of specific interest for the current model are the identities that involve $\{\!\{u'\}\!\}$:

For the Bassi-Rebay or the IP method:

$$\{\!\{u'\}\!\} = 0 \tag{5.11}$$

For the Local DG method:

$$\{\!\{u'\}\!\} = \beta \cdot [\![u']\!] = -\beta \cdot [\![\bar{u}]\!] \tag{5.12}$$

Similar expressions exist for the Baumann-Oden method and the NIPG method, but the exact format depends on the types of boundary conditions. They are omitted for simplicity.

These identities may once again be obtained for the advection-diffusion equation if a suitable fine-scale model is introduced, as was argued in Section 4.6. In order to be consistent, the volumetric fine-scale model has to incorporate these equations into the definition of the fine-scale solution on the element boundary. Therefore:

For the Bassi-Rebay or the IP method:

$$u'^{\pm} := -\frac{1}{2}[\![\bar{u}]\!]\, n^{\pm} \tag{5.13}$$

For the Local DG method:

$$u'^{\pm} := -(\frac{1}{2}n^{\pm} + \beta) \cdot [\![\bar{u}]\!] \tag{5.14}$$

The expression of Eq. (5.7) may then be written as:

$$u'(x) = \int_K g(x,y)\, \mathcal{R}_{\bar{u}}\, \mathrm{d}y + \int_{\partial K} \mathbb{H}g(x,y)\, [\![\bar{u}]\!] \cdot N\, \mathrm{d}y \tag{5.15}$$

where:

$$N = \begin{cases} \frac{1}{2}n & \text{For the Bassi-Rebay or the IP method} \\ \frac{1}{2}n + \beta & \text{For the Local DG method} \end{cases} \tag{5.16}$$

and n is the unit normal facing out of the element K.

In the mixed multiscale formulation, in Eq. (3.46), the occurrence of u' is limited to a weighted form:

$$-\int_K a \cdot \nabla \bar{v}\, u'\, \mathrm{d}x = -\iint_{K\,K} a \cdot \nabla \bar{v}\, g(x,y)\, \mathcal{R}_{\bar{u}}\, \mathrm{d}y\, \mathrm{d}x - \int_K \int_{\partial K} a \cdot \nabla \bar{v}\ \mathbb{H}g(x,y)\, [\![\bar{u}]\!] \cdot N\, \mathrm{d}y\, \mathrm{d}x \tag{5.17}$$

This weighted form enables further simplification. When $\bar{v}$ is a piecewise linear function, and when a is constant on an element, then $a\nabla\bar{v}$ becomes constant and may be extracted from the double integral. Similarly, when $\bar{u}$ is piecewise linear, and f is constant on an element, then also $\mathcal{R}_{\bar{u}}$ is piecewise constant and may be extracted from both integrals. Finally, in the one-dimensional case, the surface integral may be split into the sum of values on the element nodes, and also $[\![\bar{u}]\!] \cdot N$ may be extracted from the integrals, leading to:

$$\begin{aligned}
-\int_K a \cdot \nabla\bar{v}\, u' \,\mathrm{d}x &= -a \cdot \nabla\bar{v} \iint_{K\,K} g(x,y)\,\mathrm{d}y\,\mathrm{d}x\,\mathcal{R}_{\bar{u}} \\
&\qquad - a \cdot \nabla\bar{v} \int_K \sum_{F\in\partial K} \int_F \mathbb{H}g(x,y)\,\mathrm{d}y\,\mathrm{d}x\,[\![\bar{u}]\!]\Big|_F \cdot N\Big|_F \\
&= -\int_K a \cdot \nabla\bar{v} \frac{1}{|K|} \iint_{K\,K} g(\hat{x},y)\,\mathrm{d}y\,\mathrm{d}\hat{x}\,\mathcal{R}_{\bar{u}}\,\mathrm{d}x \\
&\qquad - \int_K a \cdot \nabla\bar{v} \sum_{F\in\partial K} \frac{1}{|K|} \int_K \int_F \mathbb{H}g(\hat{x},y)\,\mathrm{d}y\,\mathrm{d}\hat{x}\,[\![\bar{u}]\!]\Big|_F \cdot N\Big|_F \,\mathrm{d}x \\
&= -\int_K a \cdot \nabla\bar{v}\ \tau\,\mathcal{R}_{\bar{u}}\,\mathrm{d}x - \int_K a \cdot \nabla\bar{v} \sum_{F\in\partial K} \gamma_F\ [\![\bar{u}]\!]\Big|_F \cdot N\Big|_F \,\mathrm{d}x
\end{aligned} \tag{5.18}$$

where F denotes a facet (or in this case node) of ∂K. The following parameter definitions may then be identified:

$$\tau = \frac{1}{|K|} \int_K \int_K g(\hat{x},y)\,\mathrm{d}y\,\mathrm{d}\hat{x} \tag{5.19}$$

$$\gamma_F = \frac{1}{|K|} \int_K \int_F \mathbb{H}g(\hat{x},y)\,\mathrm{d}y\,\mathrm{d}\hat{x} \tag{5.20}$$

For the one-dimensional advection-diffusion problem with constant coefficients, they become:

$$\tau = \frac{h}{2\,a} - \frac{\nu}{a^2} + \frac{h}{a\left(e^{\frac{a}{\nu}h}-1\right)} \tag{5.21}$$

$$\gamma_0 = \frac{\nu - a\,h - \nu e^{-\frac{a}{\nu}h}}{-a\,h\,\left(e^{-\frac{a}{\nu}h}-1\right)} \tag{5.22}$$

$$\gamma_1 = \frac{\nu + a\,h - \nu e^{\frac{a}{\nu}h}}{a\,h\,\left(e^{\frac{a}{\nu}h}-1\right)} \tag{5.23}$$

The derivation thereof may be found in the appendix of either [11] or [13].

The last term in Eq. (5.18) is somewhat unusual in a finite element formulation. The volumetric integral involves information that is defined on the element boundary. This illustrates the interpretation of this term; it incorporates the effect of the nonhomogeneous fine-scale boundary solution onto the volume of the element. In practice, however, a different format may be more intuitive:

$$-\int_K a\cdot\nabla\bar{v}\sum_{F\in\partial K}\gamma_F\,[\![\bar{u}]\!]\Big|_F\cdot N\Big|_F\,\mathrm{d}x=-\sum_{F\in\partial K}\int_K a\cdot\nabla\bar{v}\,\mathrm{d}x\;\;\gamma_F\,[\![\bar{u}]\!]\Big|_F\cdot N\Big|_F \tag{5.24}$$

which is a multiplication of two independent terms. Each of these terms can be assembled separately. Consider a typical finite element framework where the coarse-scale solution can be represented by a linear combination of basis functions weighted by their respective coefficients:

$$\bar{u}(x)=\sum_{i=0}^{n}u_iU_i(x)=\underline{u}^{\mathrm{T}}\underline{U}(x)=\underline{U}^{\mathrm{T}}(x)\,\underline{u} \tag{5.25}$$

where $\underline{u}$ represents the vector of coefficients, and $\underline{U}(x)$ the vector of basis function values evaluated at x. An equivalent expression, but with vector of coefficients $\underline{v}$, would describe $\bar{v}$. Since the vectors of coefficients are spatially invariant, they can be extracted from the integral and from the jump operator. Then:

$$-\int_K a\cdot\nabla\bar{v}\,\mathrm{d}x=\underline{v}^{\mathrm{T}}\int_K a\cdot\nabla\underline{U}(x)\,\mathrm{d}x=\underline{v}^{\mathrm{T}}\underline{a} \tag{5.26}$$

$$\gamma_F\,[\![\bar{u}]\!]\Big|_F\cdot N\Big|_F=\gamma_F\,[\![\underline{U}^{\mathrm{T}}(x)]\!]\Big|_F\cdot N\Big|_F\,\underline{u}=\underline{b}_F^{\mathrm{T}}\,\underline{u} \tag{5.27}$$

Assembly of the vectors $\underline{a}$ and $\underline{b}_F$ should be relatively straight forward in any standard finite element code. Finally, the contribution to the stiffness matrix may then be obtained according to:

$$-\int_K a\cdot\nabla\bar{v}\sum_{F\in\partial K}\gamma_F\,[\![\bar{u}]\!]\Big|_F\cdot N\Big|_F\,\mathrm{d}x=\underline{v}^{\mathrm{T}}\left[\sum_{F\in\partial K}\underline{a}\;\underline{b}_F^{\mathrm{T}}\right]\underline{u}=\underline{v}^{\mathrm{T}}\underline{K}_s\,\underline{u} \tag{5.28}$$

5.2 Numerical experiments in the mixed variational multiscale framework

The effect of the residual-based model in the mixed formulation will now be evaluated by means of two example problems. The first involves a one-dimensional 'boundary layer' problem. In this text, a boundary layer is loosely defined as a region near a (sub)domain boundary where the solution locally exhibits steep gradients. Boundary layers occur often in engineering applications, especially in aerodynamics. Heavy refinement would be required to accurately describe the solution in the boundary layer region. Alternative approaches are sought to keep computational expense reasonable. Of particular interest are finite element schemes that manage to retain solution accuracy without excessive mesh refinement.

For the current steady advection-diffusion model problem, a boundary layer may be fabricated by choosing a velocity and a diffusivity such that $|a| \gg \nu$. This is the advection dominated case, which is often a challenging problem to tackle with the finite element method. Consider a case with constant coefficients a, ν and f, and a domain $\Omega = [0, x_r]$ that ranges from zero to x_r. A homogeneous boundary condition $u = 0$ is prescribed on the left side, and a Dirichlet condition $u_{D,r}$ on the right side. Then, the exact solution is:

$$u(x) = \frac{u_{D,r} - \frac{f}{a}x_r}{e^{\frac{a}{\nu}x_r} - 1}\left(e^{\frac{a}{\nu}x} - 1\right) + \frac{f}{a}x \tag{5.29}$$

$$\sigma(x) = \nu\nabla u(x) = \frac{a\,u_{D,r} - f x_r}{e^{\frac{a}{\nu}x_r} - 1}e^{\frac{a}{\nu}x} + \frac{\nu f}{a} \tag{5.30}$$

In the following, the parameters $a = 0.5$, $\nu = 0.005$, $f = 6$, $x_r = 0.9$, and $u_{D,r} = 2$ are used. The exact solution fields for that case are illustrated as dotted lines in Figure 5.1. A boundary layer occurs at the right boundary of the domain.

A Local DG formulation with $\eta = 0.15$ and $\beta = 0.5$ is used to solve the problem. Larger values for these parameters would over-penalize the jumps in the solution fields, leaving nearly continuous solutions. The space $\overline{U}$ is constructed with linear basis functions, and $\overline{\Sigma}$ with third order polynomials. The dashed line in Figure 5.1 is obtained when a coarse mesh of only 3 elements is used. The upper two figures show the solution fields, and the lower two show the absolute errors. Clearly, the boundary layer cannot accurately be described in the coarse-scale function spaces. As a result, the Local DG solution behaves poorly. With the given resolution, the solution is not accurate in any of the elements.

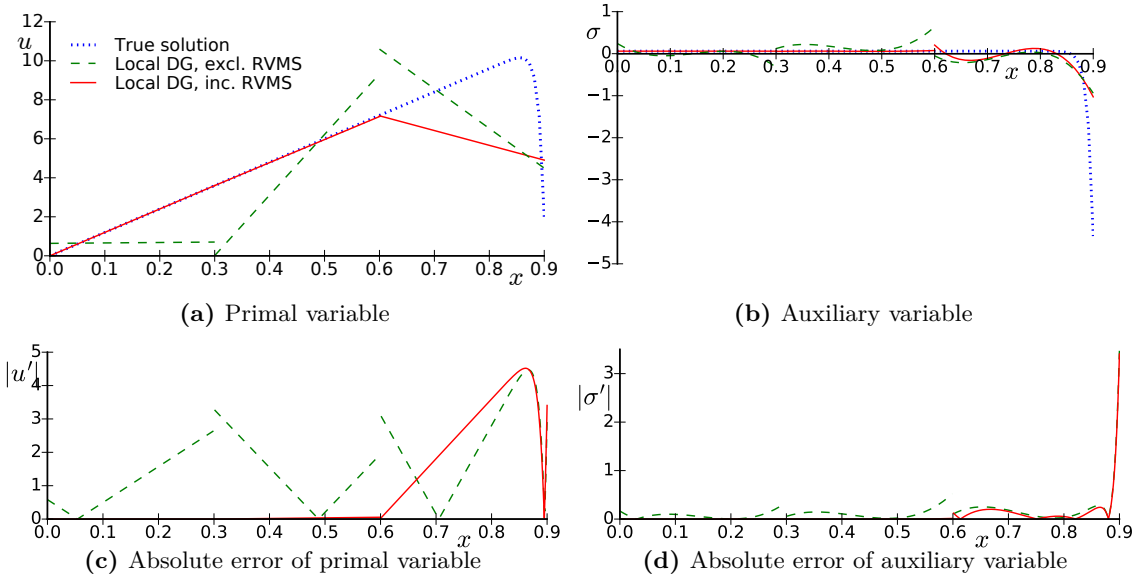

(a) Primal variable

(b) Auxiliary variable

(c) Absolute error of primal variable

(d) Absolute error of auxiliary variable

Fig. 5.1: *Coarse-scale solutions for the boundary layer problem, using 3 elements. With and without the residual-based variational multiscale (RVMS) model in the Local DG formulation.*

If the residual-based fine-scale model is incorporated in the Local DG scheme, then the solid line is obtained. The solution accuracy increases drastically. While the boundary layer is hardly captured by the finite element solution, the far field solution does not suffer from any oscillations or drift. This is illustrated in the error graphs, which show nearly vanishing errors in the first two elements for both the primary and auxiliary variable.

Figure 5.2 shows the obtained solutions when the domain is partitioned with 8 elements. With this mesh refinement, the problem that occurs for the Local DG methods becomes more pronounced. The finite element solution overshoots by a significant margin. This results in strong oscillations throughout the rest of the domain. These artificial oscillations spoil the solution accuracy, even though, in each element, the approximation centers around the true solution. The maximum error hardly reduces compared to Figure 5.1. Again, after the residual-based model is introduced, the finite-element result behaves quite well. The loss of accuracy is once again confined to a single element, and even in that element no excessive overshoot is observed.

An important thing to note is that the fine-scale constraint employed by the finite element formulation that includes the residual-based model does indeed behave as predicted in Section 4.6. By having canceled the advective fine-scale term, the resulting fine-scale

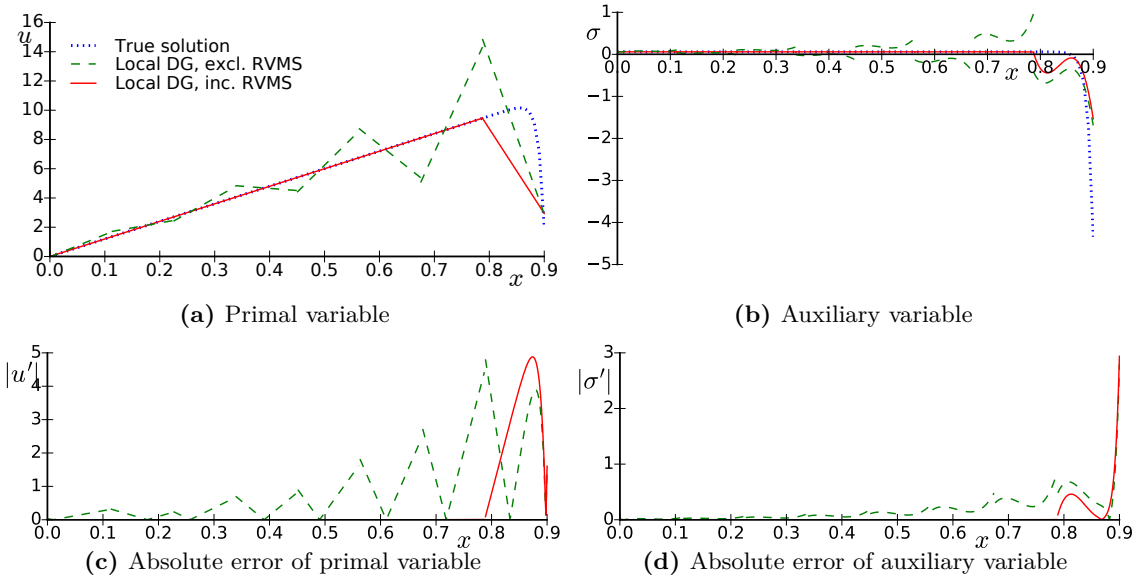

(a) Primal variable

(b) Auxiliary variable

(c) Absolute error of primal variable

(d) Absolute error of auxiliary variable

Fig. 5.2: *Coarse-scale solutions for the boundary layer problem, using 8 elements. With and without the residual-based variational multiscale (RVMS) model in the Local DG formulation.*

constraint equation implies pointwise identities analogous to those described in Table 4.4. This has been verified numerically. One interesting implication is that, through the use of $\sigma' \cdot n - \frac{\eta}{h} u' = 0$, the exact value of σ on the boundary may be retrieved. For fluid mechanics problems this is related to the stress on the surface, which is a key quantity.

For the relatively simple example of Figure 5.2, the coarse-scale solution that is obtained when the RVMS model is included is nearly continuous. To push the boundaries of the proposed fine-scale model, a more complex problem is considered next. This will be a case with piecewise constant, but discontinuous, model parameters:

$$(K, a, f) = \begin{cases} (0.005, \ 0.5, \ \ 0) & \text{for } 0.0 < x < 0.3 \\ (0.05, \ \ 0.5, \ f_2) & \text{for } 0.3 < x < 0.6 \\ (0.15, \ \ 0.5, -80) & \text{for } 0.6 < x < 0.9 \\ (0.0005, 0.5, -25) & \text{for } 0.9 < x < 1.2 \\ (0.05, \ \ 0.5, \ 50) & \text{for } 1.2 < x < 1.5 \\ (0.005, \ 0.5, -75) & \text{for } 1.5 < x < 1.8 \end{cases} \tag{5.31}$$

Only the advective velocity is kept continuous (and constant), such that the proposed upwind formulation remains consistent. The one remaining parameter is f_2, the source

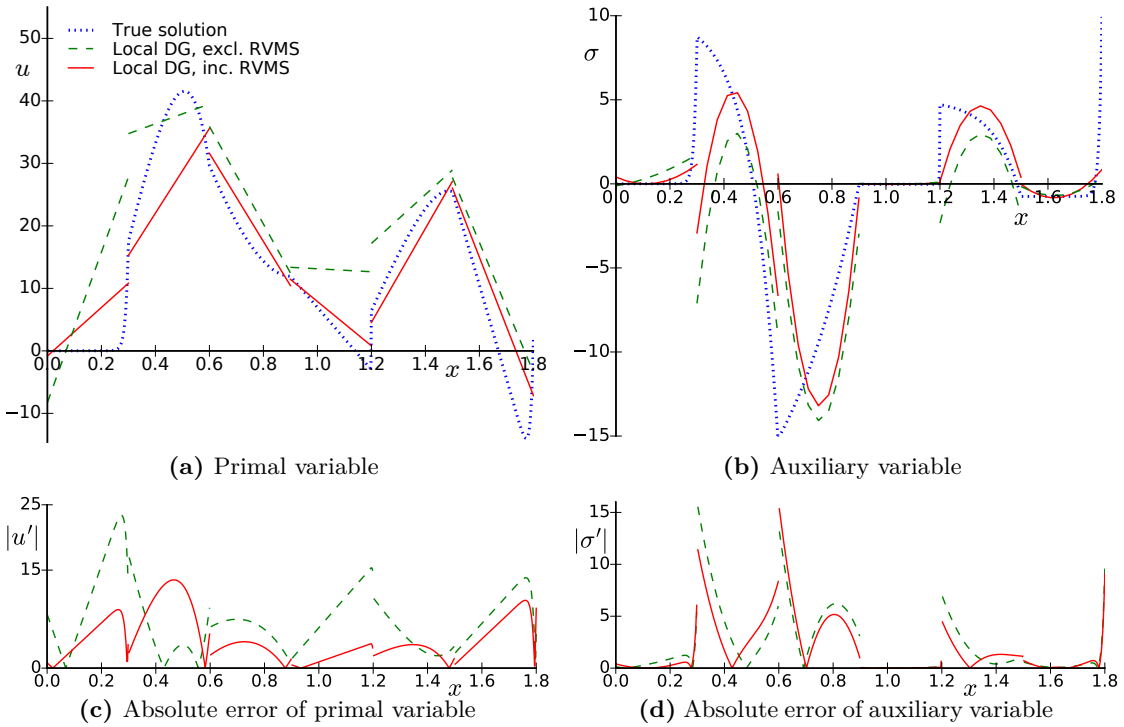

(a) Primal variable

(b) Auxiliary variable

(c) Absolute error of primal variable

(d) Absolute error of auxiliary variable

Fig. 5.3: *Coarse-scale solutions for the model problem with discontinuous model parameters, with $f_2 = 100$. With and without the RVMS model in the Local DG formulation.*

function in the second piece of the domain. Results for the values $f_2 = 100$ and $f_2 = 1000$ are investigated in the following. In both cases Dirichlet conditions are imposed on both sides of the domain: $u_D = 0$ and $u_D = 2$ for the left and right boundary respectively.

Figure 5.3 shows the resulting solutions for $f_2 = 100$. The true solution is obtained by excessive refinement. The residual-based model is added to a Local DG scheme with parameters $\beta = 0.15$ and $\eta = 0.15$. The solution of the Local DG method without the residual-based model is also graphed. The computational mesh consists of 6 elements that match the bounds of the subdomains from the parameter definitions in Eq. (5.31). Linear basis functions are used to construct $\overline{U}$, and quadratics are used for $\overline{\Sigma}$.

Clearly, the simulation result that does include the residual-based model yields a more favorable approximation to the true solution than the results from the Local DG method without the model. This is particularly apparent in the approximation to the primal variable, where the error of the solution that excludes the model is almost consistently higher than those for the solution that includes the model. The values obtained with the

Local DG method without the RVMS model are almost always overpredictions. When the model is incorporated, the coarse-scale solution follows the true solution as well as might be expected, never excessively overshooting or undershooting. The jumps of the coarse-scale solution that includes the model positively impact the solution accuracy, which can not be said for the jumps of the no-model solution.

Similarly, the resulting coarse-scale approximation of the auxiliary variable improves when the model is added, although the effect is not very pronounced in the model problem of Figure 5.3. When, however, the source function value in the second element is increased to $f_2 = 1000$, then the effect becomes more noticeable. The resulting solutions are shown in Figure 5.4. While the approximation to σ in the second element does not improve much, the improvement in the third element is already quite noticeable. The most significant improvement occurs in the fifth element, where error of the Local DG solution is quite large. Also for this case the approximation to u is significantly more accurate when the model is included. Without the model, an offset is observed throughout most of the domain. This offset is completely removed when the model is included.

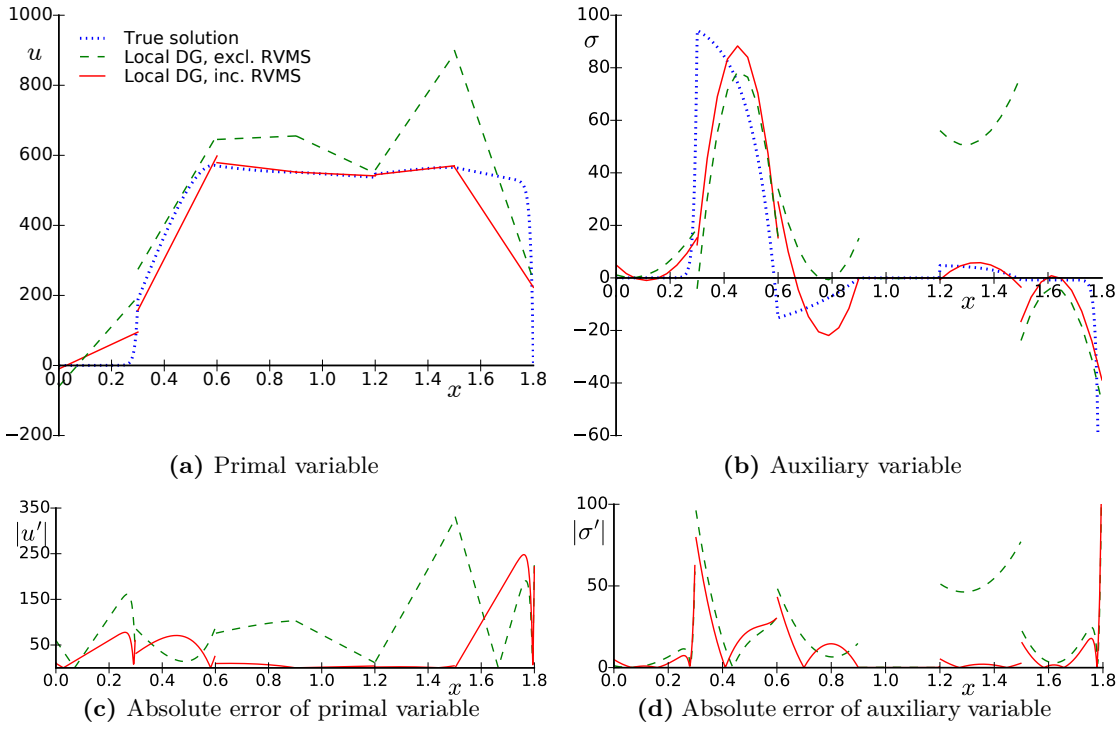

(a) Primal variable **(b)** Auxiliary variable

(c) Absolute error of primal variable **(d)** Absolute error of auxiliary variable

Fig. 5.4: *Coarse-scale solutions for the model problem with discontinuous model parameters, with $f_2 = 1000$. With and without the RVMS model in the Local DG formulation.*

While all these experiments concern a relatively simple set-up, they do indicate the potential improvement that may be achieved by incorporating residual-based fine-scale models in discontinuous Galerkin methods. This is a area of research that has not yet received much scientific attention. The current chapter has aimed to provide a stepping stone for such endeavors, specifically for discontinuous Galerkin methods based on mixed formulations of partial differential equations.

Chapter 6

Summary and conclusion

The objective of this thesis has been to extend the recently introduced domain decomposition variational multiscale method to mixed formulations of partial differential equations. In this work, the approach to derive the multiscale weak formulations for such problem statements has been developed. Both Poisson's equation, and the advection-diffusion model problem have served as examples. Also, the residual-based modeling of the fine scales has been introduced in the new framework. Thereby, this work represents a large step in establishing the DDVMS framework as a general strategy for deriving multiscale weak formulations.

The approach that has been developed may be summarized as follows. The starting point is a domain decomposition formulation of the system of partial differential equations. This means that the partial differential equation is constrained to a subdomain (in this case a single element), and transmission conditions are added that ensure the existence and uniqueness of the solution. Then, a weak form of the problem is proposed, where the associated function spaces may be discontinuous from element to element. Different function spaces are likely required for the primary and the auxiliary variable. These spaces are then decomposed into a discontinuous coarse-scale and a discontinuous fine-scale space. The coarse-scale space is finite dimensional, and will represent the finite element approximation space later on. Integration by parts is performed, whereby many coarse-scale and fine-scale element interface terms are introduced in the equations. A multiscale variant of the transmission conditions is then substituted into the definition of the fine scales on the element interfaces. Thereby, communication between solutions on

neighboring elements is realized. The resulting mixed weak form precisely incorporates the contributions of the fine-scale solution onto the coarse-scale solution via volumetric terms and element interface terms.

If one were to use the obtained multiscale weak formulations as the basis for finite element schemes, then a closure model must be substituted in place of the fine-scale terms. Since, at this stage, the formulation is exact, any fine-scale model that is substituted will also be satisfied exactly. Hence, the closure model becomes a constraint equation for the fine-scale solution. The mixed formulation origin of the derivation leads to two separate constraint equations. When this concept is explored for Poisson's equation, one can observe that the standard discontinuous Galerkin formulations, as well as the Raviart-Thomas method, the Brezzi-Douglas-Marini method and hybridized finite element formulations, can all be interpreted as particular choices of fine-scale constraints. In many cases, these fine-scale constraints correspond to saddle-point problems that capture the projectors that define the scale decomposition. Normally, discontinuous Galerkin formulations are derived by choosing numerical fluxes that couple the elements. These fluxes are often loosely interpreted as numerical approximations to the true fluxes. At the same time, these fluxes must be chosen such that inter-element coupling is achieved. The DDVMS approach developed herein offers a new perspective on the precise meaning of the numerical fluxes, while element coupling is naturally achieved via the use of the transmission conditions in the derivation.

Additionally, the fine-scale constraints have been investigated in more depth for five classical discontinuous Galerkin formulations of Poisson's equation. It could be shown that, in the one-dimensional case, many integral or pointwise expressions involving the finite element solution identically equal zero on element boundaries or element volumes. Refer to Tables 4.4 and 4.5 for an overview of these vanishing quantities.

Similarly, the DDVMS method has been applied to an advection-diffusion equation. The obtained multiscale weak formulation was compared to finite element formulations for the same problem. In the construction of these finite element formulations, it was chosen to use upwind numerical fluxes to treat the advective term, while the diffusive term was treated with the discontinuous Galerkin methods that were investigated earlier. Through the analysis of the implicitly satisfied fine-scale constraints, it was shown that the use of upwind numerical fluxes acts as an increased penalty on the jumps of the primary variable on element interfaces. When one aims to investigate the fine-scale constraints further, the fine-scale advective term clouds the interpretation. For instance, the pointwise identities that could be derived for Poisson's equation no longer hold. In an attempt to mitigate

this issue, a residual-based model was introduced to cancel the problematic fine-scale term. It was shown that the fine-scale constraints obtained after the residual-based model has been included do indeed result in analogous pointwise identities as obtained for Poisson's equation. This led to a considerable accuracy improvement for a number of example problems. The standard Local DG method performed poorly at regions with high gradients where it resulted in a solution with large overshoots and oscillations. Also, the Local DG method resulted in a solution with an offset when highly varying discontinuous model parameters were used. Incorporating the residual-based model completely eliminated these problems. Most of this analysis is only directly applicable for the one-dimensional case and for piecewise constant model parameters. However, extensive research over the last decade has shown that the use of residual-based fine-scale models is beneficial in cases that reach far past these restrictions. To facilitate future research in this area, this work has shown how, and where, the model may be incorporated for mixed formulations of partial differential equations.

The DDVMS methodology has thus far mainly been used as an analysis tool. This has lead to insightful (re-)interpretations of a number of concepts native to discontinuous Galerkin methods. Additionally, analysis of the fine-scale constraint equations has indicated possible points of improvement, e.g. via the use of residual-based models to cancel certain fine-scale terms. However, the potential of the method reaches further. With the newly introduced theory on mixed formulations of the partial differential equation, it has become a general strategy for developing multiscale weak formulations. It is then up to the researcher to substitute a suitable closure model in the form of a fine-scale constraint equation. It is at the level of this fine-scale constraint that new methods may be developed. Given a certain objective that the numerical scheme should be tailored to, one could derive a suitable fine-scale constraint equation. Thereby, the obtained finite element scheme would intrinsically satisfy the conditions that are of primary importance to the researcher. I would strongly like to encourage anyone to explore this avenue of exciting future research.

References

[1] T.J.R. Hughes. Multiscale phenomena: Green's functions, the Dirichlet–to–Neumann formulation, subgrid scale models, bubbles and the origins of stabilized methods. *Computer Methods in Applied Mechanics and Engineering*, 127(1-4):387–401, 1995.

[2] T.J.R. Hughes and J.R. Stewart. A space–time formulation for multiscale phenomena. *Journal of Computational and Applied Mathematics*, 74(1-2):217–229, 1996.

[3] T.J.R. Hughes, G.R. Feijóo, L. Mazzei, and J.-B. Quincy. The variational multiscale method – a paradigm for computational mechanics. *Computer Methods in Applied Mechanics and Engineering*, 166(1-2):3–24, 1998.

[4] Y. Bazilevs, V.M. Calo, J.A. Cottrell, T.J.R. Hughes, A. Reali, and G. Scovazzi. Variational multiscale residual-based turbulence modeling for large eddy simulation of incompressible flows. *Computer Methods in Applied Mechanics and Engineering*, 197(1-4):173–201, 2007.

[5] A.N. Brooks and T.J.R. Hughes. Streamline upwind/Petrov–Galerkin formulations for convection dominated flows with particular emphasis on the incompressible Navier–Stokes equations. *Computer Methods in Applied Mechanics and Engineering*, 32(1-3):199–259, 1982.

[6] T.J.R. Hughes, L.P. Franca, and G.M. Hulbert. A new finite element formulation for computational fluid dynamics: VIII. The Galerkin/least–squares method for advective–diffusive equations. *Computer Methods in Applied Mechanics and Engineering*, 73(2):173–189, 1989.

[7] T.E. Tezduyar. Stabilized Finite Element Formulations for Incompressible Flow Computations. *Advances in Applied Mechanics*, 28(C):1–44, 1991.

[8] K. Takizawa, T.E. Tezduyar, S. McIntyre, N. Kostov, R. Kolesar, and C. Habluetzel. Space–time VMS computation of wind-turbine rotor and tower aerodynamics. *Computational Mechanics*, 53(1):1–15, 2014.

[9] V. Gravemeier and W.A. Wall. Residual-based variational multiscale methods for laminar, transitional and turbulent variable-density flow at low mach number. *International Journal for Numerical Methods in Fluids*, 65(10):1260–1278, 2011.

[10] T.J.R. Hughes, G. Scovazzi, and L.P. Franca. Multiscale and stabilized methods. In E. Stein, R. De Borst, and T.J.R. Hughes, editors, *Encyclopedia of computational mechanics*, chapter 4. John Wiley & Sons, Ltd, 2004.

[11] S.K.F. Stoter. *Residual-based variational multiscale modeling in a discontinuous Galerkin framework*. Master's thesis, Delft University of Technology, 2017.

[12] S.K.F. Stoter, S.R. Turteltaub, S.J. Hulshoff, and D. Schillinger. A discontinuous Galerkin residual-based variational multiscale method for modeling subgrid-scale behavior of the viscous Burgers equation. Submitted to: *International Journal for Numerical Methods in Fluids*, 2017.

[13] S.K.F. Stoter, S.R. Turteltaub, S.J. Hulshoff, and D. Schillinger. Residual-based variational multiscale modeling in a discontinuous Galerkin framework. Submitted to: *Multiscale Modeling and Simulation: A SIAM Interdisciplinary Journal*, arXiv:1709.03934 [math.NA], 2017.

[14] B.M. Fraeijs de Veubeke. Displacement and equilibrium models in the finite element method. In O.C. Zienkiewicz and G.S. Holister, editors, *Stress Analysis*, chapter 9, pages 145–197. John Wiley & Sons, Ltd, 1965.

[15] B.M. Fraeijs De Veubeke and M. Hogge. Dual analysis for heat conduction problems by finite elements. *International Journal for Numerical Methods in Engineering*, 5:65–82, 1972.

[16] B.M. Fraeijs De Veubeke. *Diffusive equilibrium models, Lecture notes*. University of Calgary, Calgary, 1973.

[17] T. Arbogast and S.L. Bryant. A two-scale numerical subgrid technique for waterflood simulations. *Society of Petroleum Engineers Journal*, 7(4):446–457, 2002.

[18] T. Arbogast and K.J. Boyd. Subgrid upscaling and mixed multiscale finite elements. *SIAM Journal on Numerical Analysis*, 44(3):1150–1171, 2006.

[19] J.E. Aarnes. On the use of a mixed multiscale finite element method for greater flexibility and increased speed or improved accuracy in reservoir simulation. *Multiscale Modeling & Simulation*, 2(3):421–439, 2004.

[20] J.E. Aarnes, S. Krogstad, and K.-A. Lie. A hierarchical multiscale method for two-phase flow based upon mixed finite elements and nonuniform coarse grids. *Multiscale Modeling & Simulation*, 5(2):337–363, 2006.

[21] M.G. Larson and A. Målqvist. A mixed adaptive variational multiscale method with applications in oil reservoir simulation. *Mathematical Models and Methods in Applied Sciences*, 19(07):1017–1042, 2009.

[22] A. Masud and J. Kwack. A stabilized mixed finite element method for the first-order form of advection–diffusion equation. *International Journal for Numerical Methods in Fluids*, 57(9):1321–1348, 2008.

[23] F. Brezzi and M. Fortin. *Mixed and hybrid finite element methods*, volume 15. Springer Science & Business Media, 2012.

[24] C.H. Lee, A.J. Gil, and J. Bonet. Development of a stabilised Petrov–Galerkin formulation for conservation laws in Lagrangian fast solid dynamics. *Computer Methods in Applied Mechanics and Engineering*, 268:40–64, 2014.

[25] M. Cervera, M. Chiumenti, L. Benedetti, and R. Codina. Mixed stabilized finite element methods in nonlinear solid mechanics. Part III: Compressible and incompressible plasticity. *Computer Methods in Applied Mechanics and Engineering*, 285:752–775, 2015.

[26] C.A. Felippa. A historical outline of matrix structural analysis: a play in three acts. *Computers & Structures*, 79(14):1313 – 1324, 2001.

[27] J. Donéa and A. Huerta. *Finite element methods for flow problems*. John Wiley & Sons, Ltd, Hoboken, New Jersey, 2003.

[28] T. Gangwar, J. Calder, T. Takahashi, J.E. Bechtold, and D. Schillinger. Robust variational segmentation of 3D bone CT data with thin cartilage interfaces. Submitted to: *Medical Image Analysis*, 2017.

[29] T.J.R. Hughes, L. Mazzei, and K.E. Jansen. Large Eddy Simulation and the variational multiscale method. *Computing and Visualization in Science*, 3(1-2):47–59, 2000.

[30] E.A. Munts, S.J. Hulshoff, and R. De Borst. A Space-Time Variational Multiscale Discretization for LES. In *34th AIAA Aerospace Sciences Meeting and Exhibit*, Portland, Oregon, 2004.

[31] T.J.R. Hughes, V.M. Calo, and G. Scovazzi. Variational and multiscale methods in turbulence. *Mechanics of the 21st Century*, pages 153–163, 2005.

[32] V.M. Calo. *Residual–based Multiscale Turbulence modeling: Finite Volume simulations of bypass transition.* PhD thesis, Stanford University, 2004.

[33] Y. Bazilevs. *Isogeometric analysis of turbulence and fluid-structure interaction.* PhD thesis, The University of Texas at Austin, 2006.

[34] F. Brezzi, L.P. Franca, T.J.R. Hughes, and A. Russo. $b = \int g$. *Computer Methods in Applied Mechanics and Engineering*, (145):329–339, 1997.

[35] T.E. Tezduyar and Y. Osawa. Finite element stabilization parameters computed from element matrices and vectors. *Computer Methods in Applied Mechanics and Engineering*, 190(3-4):411–430, 2000.

[36] F. Xu, D. Schillinger, D. Kamensky, V. Varduhn, C. Wang, and M.-C. Hsu. The tetrahedral finite cell method for fluids: Immersogeometric analysis of turbulent flow around complex geometries. *Computers & Fluids*, 2015.

[37] P. Gamnitzer, V. Gravemeier, and W.A. Wall. Time-dependent subgrid scales in residual-based large eddy simulation of turbulent channel flow. *Computer Methods in Applied Mechanics and Engineering*, 199(13):819 – 827, 2010.

[38] I. Akkerman, Y. Bazilevs, V.M. Calo, T.J.R. Hughes, and S.J. Hulshoff. The role of continuity in residual–based variational multiscale modeling of turbulence. *Computational Mechanics*, 41(3):371–378, 2008.

[39] J.H. Argyris, I. Fried, and D.W. Scharpf. The TUBA Family of Plate Elements for the Matrix Displacement Method. *The Aeronautical Journal*, 72(692):701–709, 1968.

[40] K. Bell. A refined triangular plate bending finite element. *International Journal for Numerical Methods in Engineering*, 1(1):101–122, 1969.

[41] R.W. Clough and J.L. Tocher. Finite element stiffness matrices for analysis of plates in bending. In *Proceedings of the 1st Conference on Matrix Methods in Structural Mechanics*, Wright-Patterson AFB, 1965.

[42] B. Dobronets and V. Shaydurov. Hermitian finite element complementing the Bogner–Fox–Schmit rectangle near curvilinear boundary. *Lobachevskii Journal of Mathematics*, 37(5):527–533, 2016.

[43] T.J.R. Hughes, J.A. Cottrell, and Y. Bazilevs. Isogeometric analysis: CAD, finite elements, NURBS, exact geometry and mesh refinement. *Computer Methods in Applied Mechanics and Engineering*, 194(39):4135–4195, 2005.

[44] J.A. Cottrell, T.J.R. Hughes, and Y. Bazilevs. *Isogeometric analysis: toward integration of CAD and FEA*. John Wiley & Sons, 1st edition, 2009.

[45] D.N. Arnold, F. Brezzi, B. Cockburn, and L.D. Marini. Unified Analysis of Discontinuous Galerkin Methods for Elliptic Problems. *SIAM Journal on Numerical Analysis*, 39(5):1749–1779, 2002.

[46] H. Darcy. *Les fontaines publiques de la ville de Dijon: exposition et application des Principes a Suivre et des Formulesa Employer dans les Questions de Distribution d'Eau*. Dalmont, E., Paris, 1856.

[47] A. Masud and T.J.R. Hughes. A stabilized mixed finite element method for darcy flow. *Computer Methods in Applied Mechanics and Engineering*, 191(39-40):4341–4370, 2002.

[48] S. Zhang. The divergence-free finite elements for the stationary stokes equations. *Preprint University of Delaware*, 2007.

[49] A.F.D. Loula, F.A. Rochinha, and M.A. Murad. Higher-order gradient post-processings for second-order elliptic problems. *Computer Methods in Applied Mechanics and Engineering*, 128(3-4):361–381, 1995.

[50] G. Kanschat and B. Riviere. A strongly conservative finite element method for the coupling of stokes and darcy flow. *Journal of Computational Physics*, 229(17):5933–5943, 2010.

[51] K. Hellan. *Analysis of elastic plates in flexure by a simplified finite element method*, volume 1 of *Acta polytechnica Scandinavica*. Norges tekniske vitenskapsakademi, 1967.

[52] L.R. Herrmann. Finite-element bending analysis for plates. *Journal of the Engineering Mechanics Division*, 93(5):13–26, 1967.

[53] C. Johnson. On the convergence of a mixed finite-element method for plate bending problems. *Numerische Mathematik*, 21(1):43–62, 1973.

[54] P.A. Raviart and J.M. Thomas. A mixed finite element method for second order elliptic problems. In *Proceedings of Symposia in Mathematical Aspects of the Finite*

Element Method (Rome, 1975), volume 606 of *Lecture Notes in Math*, pages 292–315. Springer-Verlag, Berlin, Germany, 1977.

[55] F. Brezzi, J. Douglas, and L.D. Marini. Two families of mixed finite elements for second order elliptic problems. *Numerische Mathematik*, 47(2):217–235, 1985.

[56] F. Brezzi, J. Douglas, R. Durán, and M. Fortin. Mixed finite elements for second order elliptic problems in three variables. *Numerische Mathematik*, 51(2):237–250, 1987.

[57] D.N. Arnold and F. Brezzi. Mixed and nonconforming finite element methods: implementation, postprocessing and error estimates. *ESAIM: Mathematical Modelling and Numerical Analysis*, 19(1):7–32, 1985.

[58] R. Glowinski and M.F. Wheeler. Domain decomposition and mixed finite element methods for elliptic problems. In *First international symposium on domain decomposition methods for partial differential equations*, pages 144–172, 1988.

[59] C.C. Novo, R.C. Leal-Toledo, E.M. Toledo, and L.S. Martins. Discontinuous mixed space-time least-squares formulation for transient advection–diffusion–reaction equations. *Mecánica Computacional*, 25:1113–1125, 2006.

[60] B. Cockburn, B. Dong, J. Guzmán, M. Restelli, and R. Sacco. A hybridizable discontinuous Galerkin method for steady-state convection-diffusion-reaction problems. *SIAM Journal on Scientific Computing*, 31(5):3827–3846, 2009.

[61] N.C. Nguyen, J. Peraire, and B. Cockburn. An implicit high-order hybridizable discontinuous Galerkin method for linear convection–diffusion equations. *Journal of Computational Physics*, 228(9):3232–3254, 2009.

[62] J. Schütz, M. Woopen, and G. May. A hybridized DG/mixed scheme for nonlinear advection-diffusion systems, including the compressible Navier-Stokes equations. In *50th AIAA Aerospace Sciences Meeting including the New Horizons Forum and Aerospace Exposition*, page 729, Nashville, Tennessee, 2012.

[63] W.H. Reed and T.R. Hill. Triangular Mesh Methods for the Neutron Transport Equation. *Proceedings of the American Nuclear Society*, 836:1–23, 1973.

[64] P.G. Ciarlet. A mixed finite element method. In J.L. Lions, G. Papanicolaou, and R.T. Rockafellar, editors, *The finite element method for elliptic problems*, chapter 7, pages 381–424. North Holland publishing company, Amsterdam, 1978.

[65] F. Bassi and S. Rebay. A High-Order Accurate Discontinuous Finite Element Method for the Numerical Solution of the Compressible Navier–Stokes Equations. *Journal of Computational Physics*, 131(2):267 – 279, 1997.

[66] D.N. Arnold. An interior penalty finite element method with discontinuous elements. *SIAM journal on numerical analysis*, 19(4):742–760, 1982.

[67] B. Cockburn and C.-W. Shu. The Local Discontinuous Galerkin Method for Time–Dependent Convection–Diffusion Systems. *SIAM Journal on Numerical Analysis*, 35(6):2440–2463, 1998.

[68] C.E. Baumann and J.T. Oden. A discontinuous *hp*-finite element method for convection-diffusion problems. *Computer Methods in Applied Mechanics and Engineering*, 175(3–4):311–341, 1999.

[69] B. Rivière, M. F. Wheeler, and V. Girault. Improved energy estimates for interior penalty, constrained and discontinuous Galerkin methods for elliptic problems. Part I. *Computational Geosciences*, 3(3):337–360, 1999.

[70] B. Cockburn, J. Gopalakrishnan, and R. Lazarov. Unified hybridization of discontinuous Galerkin, mixed, and continuous Galerkin methods for second order elliptic problems. *SIAM Journal on Numerical Analysis*, 47(2):1319–1365, 2009.